PREPARATION OF ANTIMICROBIAL PLASTIC PACKAGING FROM HYBRID NANO SILVER/EGGSHELL CALCIUM CARBONATE PARTICLES

MOE EI EI ZIN

A Thesis Submitted in Partial Fulfillment of the Requirements for the
Degree of Master of Engineering in Materials Engineering
Suranaree University of Technology
Academic Year 2022

การเตรียมบรรจุภัณฑ์พลาสติกต้านจุลินทรีย์จากอนุภาคไฮบริดระหว่างเงินนาโนและแคลเซียมคาร์บอเนตจากเปลือกไข่

นางสาว โม อิ อิ ซิน

วิทยานิพนธ์นี้เป็นส่วนหนึ่งของการศึกษาตามหลักสูตรวิศวกรรมศาสตรมหาบัณฑิต
สาขาวิชาวิศวกรรมวัสดุ
มหาวิทยาลัยเทคโนโลยีสุรนารี
ปีการศึกษา 2565

PREPARATION OF ANTIMICROBIAL PLASTIC PACKAGING FROM HYBRID NANO SILVER/EGGSHELL CALCIUM CARBONATE PARTICLES

Suranaree University of Technology has approved this thesis submitted in partial fulfillment of the requirements for a Master's Degree.

Thesis Examining Committee

Nitinat Suppakarn
.....
(Assist. Prof. Dr. Nitinat Suppakarn)
Chairperson

.....
(Assoc. Prof. Dr. Wimonlak Sutapun)
Member (Thesis Advisor)

Pranee Chumsamrong
.....
(Assoc. Prof. Dr. Pranee Chumsamrong)
Member

.....
(Assist. Prof. Dr. Supagorn Rugmai)
Member

.....
(Assist. Prof. Dr. Tiraporn Junyusen)
Member

Jirawan Oonmetta-aree
.....
(Assist. Prof. Dr. Jirawan Oonmetta-Aree)
Member

Chatchai Jothityangkoon
.....
(Assoc. Prof. Dr. Chatchai Jothityangkoon)
Vice Rector for Academic Affairs and Quality Assurance

.....
(Assoc. Prof. Dr. Pornsiri Jongkol)
Dean of Institute of Engineering

โม อิ อิ ซิน: การเตรียมบรรจุภัณฑ์พลาสติกต้านจุลินทรีย์จากอนุภาคไฮบริดระหว่างเงินนาโนและแคลเซียมคาร์บอเนตจากเปลือกไข่ (PREPARATION OF ANTIMICROBIAL PLASTIC PACKAGING FROM HYBRID NANO SILVER/ EGGSHELL CALCIUM CARBONATE PARTICLES) อาจารย์ที่ปรึกษา: รองศาสตราจารย์ ดร. วิมลลักษณ์ สุตะพันธ์, 132 หน้า

คำสำคัญ: สารออกฤทธิ์ต้านแบคทีเรีย, อนุภาคเงินนาโน, แคลเซียมคาร์บอเนตจากเปลือกไข่, อนุภาคระหว่างอนุภาคเงินนาโนและแคลเซียมคาร์บอเนตจากเปลือกไข่, การอิเล็กโทรสปิน.

งานวิจัยนี้มีวัตถุประสงค์เพื่อพัฒนาสารตัวเติมหน้าที่เฉพาะที่มีฤทธิ์ต้านจุลชีพสำหรับบรรจุภัณฑ์อาหารพลาสติกที่เป็นอนุภาคไฮบริดขนาดไมโครเมตรระหว่างอนุภาคเงินนาโนและแคลเซียมคาร์บอเนตจากเปลือกไข่เหลือทิ้ง และเตรียมพอลิเมอร์คอมโพสิตจากอนุภาคไฮบริดนี้กับพอลิแลกติกแอซิด ซึ่งเป็นพอลิเมอร์ที่ย่อยสลายในธรรมชาติ และขึ้นรูปโดยใช้เทคนิคอิเล็กโตรสปินนิง

อนุภาคเงินนาโนที่เตรียมจากสารละลายซิลเวอร์ไนเตรต ที่อุณหภูมิ 70 องศาเซลเซียส โดยใช้ไตรโซเดียมซิเตรตเป็นตัวรีดิวซ์และสารทำให้อนุภาคเงินนาโนเสถียร มีรูปร่างทรงกลมและขนาดอนุภาคเฉลี่ย 24.13 ± 2.95 นาโนเมตร การเตรียมอนุภาคไฮบริดระหว่างอนุภาคเงินนาโนและแคลเซียมคาร์บอเนตจากเปลือกไข่ เป็นการตกตะกอนแคลเซียมคาร์บอเนตจากเปลือกในสภาวะที่มีอนุภาคเงินนาโนแขวนลอยในตัวกลางน้ำ (co-precipitating) การตกตะกอนอนุภาคไฮบริดดำเนินการเปรียบเทียบ ณ 25 และ 35 องศาเซลเซียส โดยใช้พอลิ (โซเดียม 4-สไตรีนซัลโฟเนต) เป็นพอลิอิเล็กโทรไลต์ อนุภาคไฮบริดระหว่างอนุภาคเงินนาโนและแคลเซียมคาร์บอเนตจากเปลือกไข่ที่เตรียมที่ 25 องศาเซลเซียส มีสัณฐานวิทยาเป็นทรงกลม มีเส้นผ่านศูนย์กลางเฉลี่ย 3.56 ไมโครเมตร และอนุภาคไฮบริดระหว่างอนุภาคเงินนาโนและแคลเซียมคาร์บอเนตจากเปลือกไข่ที่เตรียมที่ 35 องศาเซลเซียส มีสัณฐานวิทยาเป็นทรงกลม มีเส้นผ่านศูนย์กลางเฉลี่ย 3.19 ไมโครเมตร แต่มีการกระจายขนาดที่กว้าง สำหรับอนุภาคไฮบริดระหว่างอนุภาคเงินนาโนและแคลเซียมคาร์บอเนตทางการค้า ที่เตรียมที่ อุณหภูมิ 25 องศาเซลเซียส มีลักษณะเป็นทรงกลมอย่างสมบูรณ์ มีเส้นผ่านศูนย์กลางเฉลี่ย 5.61 ไมโครเมตร อนุภาคไฮบริดที่เตรียมที่ อุณหภูมิ 25 องศาเซลเซียส อนุภาคไฮบริดระหว่างอนุภาคเงินนาโนและแคลเซียมคาร์บอเนตจากเปลือกไข่มีอนุภาคเงินนาโนร้อยละ 0.78 โดยน้ำหนัก และอนุภาคไฮบริดระหว่างอนุภาคเงินนาโนและแคลเซียมคาร์บอเนตทางการค้ามีอนุภาคเงินนาโนร้อยละ 3.20 โดยน้ำหนัก อนุภาคไฮบริดระหว่างอนุภาคเงินนาโนและแคลเซียมคาร์บอเนตจากเปลือกไข่ และอนุภาคไฮบริดระหว่างอนุภาคเงินนาโนและแคลเซียมคาร์บอเนตทางการค้า แสดงประสิทธิภาพฤทธิ์การต้านแบคทีเรียชัสเพนชั่นจากเนื้อวัวที่ใกล้เคียงกัน โดยโซนการยับยั้งมีเส้นผ่านศูนย์กลางเฉลี่ย 7-10 มิลลิเมตร

ในการเตรียมเส้นใยอิเล็กโทรสปันจาก ๆ พอลิแลกติกแอซิด และพอลิเมอร์คอมโพสิตระหว่างพอลิแลกติกแอซิดและอนุภาคไฮบริด พบว่าระบบสองตัวทำละลายร่วม ระหว่างคลอโรฟอร์มและอะซิโตนในอัตราส่วน 2:1 โดยปริมาตร การใช้สารละลายพอลิแลกติกแอซิดความเข้มข้นร้อยละ 10 และ 15 โดยน้ำหนักต่อปริมาตร ทำให้ได้เส้นใยอิเล็กโทรสปันต่อเนื่องและสัณฐานวิทยาที่ได้ไม่ใช่แบบเม็ดบีดบนเส้นใย แต่เมื่อเส้นใยอิเล็กโทรสปันของพอลิแลกติกแอซิดคอมโพสิตมีปริมาณอนุภาคไฮบริด

ระหว่างอนุภาคเงินนาโนและแคลเซียมคาร์บอเนตจากเปลือกไข่ร้อยละ 3 โดยน้ำหนักต่อปริมาตร จะเกิดการรวมตัวกันแบบบลูมมิ่งของอนุภาคไฮบริด และรูปร่างของเส้นใยอิเล็กโทรสปันไม่สม่ำเสมอ

สำหรับระบบสองตัวทำละลายร่วมระหว่างคลอโรฟอร์มและไดเมทิลฟอร์มาไมด์ และระหว่างไดคลอโรมีเทนและไดเมทิลฟอร์มาไมด์ ในอัตราส่วน 9:1 โดยปริมาตร การใช้สารละลายพอลิแลกติกแอซิดความเข้มข้นร้อยละ 10 โดยน้ำหนักต่อปริมาตร อัตราการไหล 1 มิลลิลิตร/ชั่วโมง และแรงดันไฟฟ้า 20 กิโลโวลต์ เส้นใยอิเล็กโทรสปันที่ได้มีเส้นผ่านศูนย์กลางสม่ำเสมอ เส้นใยอิเล็กโทรสปันจากพอลิแลกติกแอซิดที่มีอนุภาคไฮบริดระหว่างอนุภาคเงินนาโนและแคลเซียมคาร์บอเนตจากเปลือกไข่ ร้อยละ 5 โดยน้ำหนักต่อปริมาตร และใช้ระบบสองตัวทำละลายร่วมระหว่างไดคลอโรมีเทนและไดเมทิลฟอร์มาไมด์ มีเส้นผ่านศูนย์กลางที่ใหญ่ขึ้นและมีสัณฐานวิทยาเส้นใยอิเล็กโทรสปันแบบมีเม็ดบีดบนเส้นใย สำหรับสมบัติความทนแรงดึงนั้น เส้นใยอิเล็กโทรสปันจากพอลิแลกติกแอซิดที่มีอนุภาคไฮบริดระหว่างอนุภาคเงินนาโนและแคลเซียมคาร์บอเนตจากเปลือกไข่ ร้อยละ 5 โดยน้ำหนักต่อปริมาตร และใช้ระบบสองตัวทำละลายร่วมระหว่างไดคลอโรมีเทนและไดเมทิลฟอร์มาไมด์ มีมอดุลัสของยังก์ และความทนต่อแรงดึงสูงสุดที่สูงกว่าเส้นใยอิเล็กโทรสปันพอลิแลกติกแอซิดที่เตรียมจากระบบสองตัวทำละลายร่วมระหว่างคลอโรฟอร์มและไดเมทิลฟอร์มาไมด์

สำหรับแผ่นเส้นใยอิเล็กโตรสปันของพอลิแลกติกแอซิดคอมโพสิตที่มีอนุภาคไฮบริดระหว่างอนุภาคเงินนาโนและแคลเซียมคาร์บอเนตจากเปลือกไข่ และอนุภาคไฮบริดระหว่างอนุภาคเงินนาโนและแคลเซียมคาร์บอเนตทางการค้า ร้อยละ 5 โดยน้ำหนักต่อปริมาตร ที่เตรียมจากระบบสองตัวทำละลายร่วมระหว่างไดคลอโรมีเทนและไดเมทิลฟอร์มาไมด์ ในอัตราส่วน 9:1 โดยปริมาตร และความเข้มข้นของสารละลายพอลิแลกติกแอซิดร้อยละ 10 โดยน้ำหนักต่อปริมาตร พบว่าเฟสของพอลิแลกติกแอซิดเป็นแบบกึ่งผลึก นอกจากนี้ โครงสร้างผลึกของอนุภาคแคลเซียมคาร์บอเนตที่อยู่ในเส้นใยอิเล็กโทรสปันจากพอลิแลกติกแอซิดคอมโพสิต ยังคงเป็นแบบวาเทอร์ไรต์ เส้นใยอิเล็กโทรสปันของพอลิแลกติกแอซิดคอมโพสิตแสดงการเสื่อมสลายทางความร้อน 4 ขั้นตอน และปริมาณอนุภาคไฮบริดในเส้นใยอิเล็กโทรสปันของพอลิแลกติกแอซิด เท่ากับร้อยละ 25 โดยน้ำหนัก แผ่นเส้นใยอิเล็กโทรสปันของพอลิแลกติกแอซิดคอมโพสิตที่มีอนุภาคไฮบริดระหว่างอนุภาคเงินนาโนและแคลเซียมคาร์บอเนตจากเปลือกไข่ มีความแข็ง (hardness) ต่ำกว่า แผ่นเส้นใยอิเล็กโทรสปันของพอลิแลกติกแอซิดคอมโพสิตที่มีอนุภาคไฮบริดระหว่างอนุภาคเงินนาโนและแคลเซียมคาร์บอเนตทางการค้า

แผ่นเส้นใยอิเล็กโทรสปินของพอลแลกติกแอซิดคอมโพสิตไม่มีผลในการยับยั้งแบคทีเรียอีโคไล และแบคทีเรียซัสเพนชั่นจากเนื้อวัวดิบจากตลาดสดและจากที่บรรจุหีบห่อสุญญากาศ

แผ่นเส้นใยอิเล็กโทรสปันของพอลิแลกติกแอซิดที่มีอนุภาคไฮบริดระหว่างอนุภาคเงินนาโนและแคลเซียมคาร์บอเนตจากเปลือกไข่ ร้อยละ 25 มีความเป็นไปได้สูงในการใช้เป็นสารออกฤทธิ์ต้านแบคทีเรียในบรรจุภัณฑ์อาหารสด และสามารถพัฒนาปรับปรุงเพิ่มปริมาณอนุภาคเงินนาโนในอนุภาคไฮบริด และทำให้อนุภาคไฮบริดกระจายตัวอย่างสม่ำเสมอในเมทริกซ์ของพอลิแลกติกแอซิด เพื่อเพิ่มประสิทธิภาพการออกฤทธิ์ต้านแบคทีเรีย

สาขาวิชา วิศวกรรมพอลิเมอร์ ลายมือชื่อนักศึกษา.....

ปีการศึกษา 2565 ลายมือชื่ออาจารย์ที่ปรึกษา.....

MOE EI EI ZIN: PREPARATION OF ANTIMICROBIAL PLASTIC PACKAGING FROM HYBRID NANO SILVER/ EGGSHELL CALCIUM CARBONATE PARTICLES. THESIS ADVISOR: ASSOC. PROF. WIMONLAK SUTAPUN, Ph.D., 132 PP.

KEYWORD: ANTIMICROBIAL AGENT/SILVER NANOPARTICLES/EGGSHELL CALCIUM CARBONATE/SILVER LOADED EGGSHELL CALCIUM CARBONATE/ELECTROSPINNING

The aim of this present research is to develop the functional filler of hybrid silver/calcium carbonate particles from eggshell waste and apply as antimicrobial agent for the plastics food packaging and incorporate into PLA matrix using the electrospinning technique.

Spherical silver nanoparticles (AgNPs) with an average size of 24.13 ± 2.95 nm were successfully prepared by reducing an $AgNO_3$ aqueous solution at 70 °C in the presence of trisodium citrate as a reducing agent and stabilizer. Hybrid particles of AgNPs-loaded eggshell calcium carbonate (AgNPs/e$CaCO_3$) were prepared by co-precipitating the eggshell in the presence of freshly prepared AgNPs. The hybrid particles were comparatively precipitated at 25 °C and 35 °C using poly (sodium 4-styrenesulphonate) as a polyelectrolyte. The AgNPs/e$CaCO_3$ particles prepared at 25 °C had a spherical morphology with a mean diameter of 3.56 μm whereas the particles prepared at 35 °C had a broader size distribution with a mean diameter of 3.19 μm. AgNPs-loaded commercial calcium carbonate particles (AgNPs/$CaCO_3$) comparatively prepared at 25 °C were perfectly spherical with a mean diameter of 5.61 μm. At preparing temperature of 25 °C, the hybrid particles contained AgNPs of 0.78 wt% for AgNPs/e$CaCO_3$ and 3.20 wt% for AgNPs/$CaCO_3$. The AgNPs/e$CaCO_3$ and AgNPs/$CaCO_3$ particles exhibited the same efficiency against bacteria extracted from beef with an average inhibition zone diameter of 7-10 mm.

In preparing electrospun fibers from PLA and PLA filled with the hybrid particles, it was found that with the binary solvent systems of chloroform and acetone (CHL: AC, 2:1 by volume), 10 and 15% (w/v) PLA solutions gave rise to electrospun continuous fibers without beads. PLA electrospun fibers filled with 3 % (w/v) AgNPs/e$CaCO_3$ contained particle blooming and nonuniform shape along the fibers.

For binary solvent systems, by 9:1 by volume, of chloroform and dimethylformamide (CHL: DMF) and dichloromethane and dimethylformamide (DCM: DMF), 10 % w/v PLA solution electrosupn at 1 mL/h flow rate and 20 kV voltage gave uniform diameter fiber for both binary solvent systems. Incorporation of 5% (w/v) AgNPs/e$CaCO_3$ filler into the PLA electrospun fiber, the binary solvent system of DCM: DMF gave rise to larger fiber diameter with bead on the string along the fibers. For tensile properties, PLA with 5% (w/v) AgNPs/e$CaCO_3$ electrospun fibers from the solvent system of DCM: DMF, showed higher Young's modulus and tensile strength.

For PLA electrospun fibers mats filled with 5% (w/v) AgNPs/e$CaCO_3$ and AgNPs/$CaCO_3$ prepared with binary solvent system of dichloromethane and dimethylformamide (DCM: DMF, 9:1 by volume) at 10 % w/v PLA solution, it was found that the XRD patterns showed the semicrystalline structure of PLA. In addition, the crystal structures of calcium carbonate particles incorporated into PLA electrospun fibers were still vaterite polymorph. These filled PLA fibers mats had four stages of thermal degradation. In addition, it was found that approximately 25 wt % hybrid particles were incorporated into the PLA matrix. For mechanical properties, AgNPs/$CaCO_3$ filled PLA had lower hardness than AgNPs/e$CaCO_3$ filled PLA.

For antimicrobial testing, both filled PLA fibers mats had no inhibitory effect against *E. coli*, bacteria extracted from unpacked raw beef from a local fresh market and from vacuum-packed beef ("INCHA BEEF" brand). This was because the amount of 5 % (w/v) AgNPs/e$CaCO_3$ and AgNPs/e$CaCO_3$ filler content inside PLA porous fibers mats was not still enough to kill or inhibit the growth of bacteria.

The electrospun fibers mats of PLA incorporated with approximately 25 wt % AgNPs/e$CaCO_3$ hybrid particles have high potential to be used in antimicrobial fresh food packaging or other biomedical applications in the future. However, more study should be done on the aspect of increasing AgNPs content onto the hybrid particles and make them homogeneously distributed in PLA matrix to magnify antimicrobial activity of the filled PLA film.

School of Polymer Engineering
Academic Year 2022

Student's Signature.....
Advisor's Signature.....

ACKNOWLEDGEMENT

First of all, I would like to express my sincere gratitude to my advisor Assoc. Prof. Dr. Wimonlak Sutapun for the continuous support of my master study and related research, for her patience, motivation, and immense knowledge. I could not have imagined having a better advisor and mentor for my master study.

I am deeply thankful to Assist. Prof. Dr. Tiraporn Junyusen, Pornpimol Moolkaew, Peerawat Taengsopha and Jintaphorn Klinsuk for helping the antimicrobial efficiency testing.

I would like to gratefully acknowledge Thailand Government Scholarship and the SUT Graduate International Students Scholarship (Vithedbundit). I would also like to thank Suranaree University of Technology, Thailand Science Research, and Innovation (TSRI) and the National Science, Research, and Innovation Fund (NSRF) for research funding.

I am grateful to all the faculty members of School of Polymer Engineering, Suranaree University of Technology, Thailand for their kind support throughout my studies. I would like to give special thanks to committee members for their suggestion and advices during examination. I would like to express my gratitude to Miss Thae Thae Min for her suggestion regarding antimicrobial testing and my friends for their kind help throughout my master study.

Moe Ei Ei Zin

TABLE OF CONTENTS

Page

TABLE OF CONTENTS (Continued)

Page

TABLE OF CONTENTS (Continued)

Page

TABLE OF CONTENTS (Continued)

Page

TABLE OF CONTENTS (Continued)

Page

LIST OF TABLES

Table **Page**

LIST OF FIGURES

Figure **Page**

LIST OF FIGURES (Continued)

Figure **Page**

LIST OF FIGURES (Continued)

Figure **Page**

LIST OF ABBREVIATIONS

AC	=	Acetone
AgNPs	=	Silver nanoparticles
Ag^+	=	Silver ions
$AgNPs/CaCO_3$	=	Silver nanoparticles loaded commercial calcium carbonate
$AgNPs/eCaCO_3$	=	Silver nanoparticles loaded eggshell calcium carbonate
AP	=	Antimicrobial Packaging
BET	=	Brunauer-Emmett-Teller surface area analyzer
$CaCO_3$	=	Calcium carbonate
$Ca(NO_3)_2$	=	Calcium nitrate
CHL	=	Chloroform
DCM	=	Dichloromethane
DMF	=	Dimethylformamide
DI	=	Deionized water
DLS	=	Dynamic light scattering analyzer
DNA	=	Deoxyribonucleic acid
ES	=	Eggshells
EPS	=	Eggshell powder
E. coli	=	Escherichia coli
$eCaCO_3$	=	Eggshell calcium carbonate
FESEM	=	Field Emission Scanning Electron Microscope
GCC	=	Ground calcium carbonate
HDF	=	Human dermal fibroblast
MTT	=	3-(4,5-dimethylthiazol-2-yl)-2,5-diphenyl-2H-tetrazolium bromide
$Na_3C_6H_5O_7$	=	Trisodium citrate
Na_2CO_3	=	Sodium carbonate
PCA	=	Plate count agar

LIST OF ABBREVIATIONS (Continued)

PCC	=	Precipitated calcium carbonate
PDI	=	Polydispersity Index
PLA	=	Polylactic acid
PSS	=	Poly (sodium 4-styrenesulfonate)
ROS	=	Reactive oxygen species
SEM	=	Scanning Electron Microscope
TEM	=	Transmission Electron Microscope
TGA	=	Thermogravimetric analyzer
XRD	=	X-ray diffraction analyzer

CHAPTER I

INTRODUCTION

1.1 Background

Nowadays, plastic packaging plays one of the most important roles in food industry because it preserves and prevents food from external contamination. Packaging prevents products in steps of distribution, storage, sale and use. In addition, the packaging promotes shelf-life extension, quality maintenance and food safety. Among several types of packaging materials such as papers, glass, and plastics, plastic packaging is the most mainly used because of its several advantages including cost effective, versatility, processability and water imperviousness. For packaging trays and films from polyethylene (PE) and polypropylene (PP) based packaging are the most common used in food sector because of their low cost and good mechanical properties.

However, nonbiodegradable plastic packaging from PP and PE are causing the problem of waste disposal and staying a long time on earth and in ocean without degradation in short time. This results in pollution problems and this is also responsible for dying wildlife animals because of eating plastics debris. One of the potential solutions for this, is to replace nonbiodegradable plastics packaging with biodegradable plastics and environmental-friendly one. For this reason, biopolymers are getting more attention. Among them, polylactic acid (PLA), polyhydroxyalkanoates (PHAs) are the most popular because they are polymerized from renewable raw materials and also are biodegradable. Moreover, the raw materials for packaging are mostly petro-based polymers, non-renewable resources. In the past decades, non-renewable resources are used without limitation and now it is facing critical condition. Therefore, plastics for societal sustainability have received widespread attention. Due to the increasing health awareness in twenty-first century, conventional food packaging cannot fulfill the consumer's needs because some preservatives which can give negative impacts on human's health, are added into the products to prolong the shelf life.

Preservatives like sodium nitrite/nitrate which are used in processed meats likely to increase cancer and heart disease risk. Additionally, most people with modernized lifestyle are relying on the supermarkets to buy the food products. Therefore, the functions of plastics packaging are very important such as to protect the external contamination, to extend the shelf-life and to be safety enough themselves. Furthermore, the traditional food preservation methods such as freezing, refrigeration, fermentation, drying, salting and canning etc., and new developing methods including irradiation, ionizing radiation are all based on only preventing microbial growth or microbial inactivation.

Therefore, people are trying to look for the packaging systems of which are not only environmental-friendly but also beneficial to human's health. These are the reasons why biodegradable plastics added with new packaging technology called antimicrobial packaging are growing interesting. Antimicrobial (AM) packaging is a type of active packaging that can reduce, inhibit or retard the rapid increase of microorganisms that are contaminating foods by incorporation antimicrobial agents into a polymer film or tray. Due to its outstanding effect on shelf-life extension and food safety, AM packaging is one of the most getting people's notice.

As for antimicrobial agents, they can be divided into two types: natural antimicrobial (AM) agents and synthesis antimicrobial agents. Although natural AM agents which are extracted from plants and animals are safe, they are not enough because of the increasing of food production rate. So, synthesis AM agents which are safe for human are popular in replacing of natural AM agents. Recently, different types of metal nanoparticles such as Ag, Au, TiO_2, CuO, and ZnO are gained attention due to their high antimicrobial activity as well as high surface area per volume. Silver is one of the most well-known synthesis AM agents because of excellent antimicrobial activity and cost effective comparing with Au and TiO_2 antimicrobial agents. With the emerging of nanotechnology, nanosized antimicrobial agents such as silver nanoparticles, gold nanoparticles are introduced to food industry because of their outstanding antimicrobial activity in nano levels.

Moreover, silver nanoparticles with different shapes and sizes have been successfully green synthesized from plants, bacteria, fungi and yeast (Singh, Garg,

Pandit, Mokkapati, & Mijakovic, 2018). AgNPs are nontoxic and safe antimicrobial agent for the human body. In addition, AgNPs are also reported to possess antifungal activity, anti-inflammatory properties, antiviral activity, and antiangiogenic activity (Verma & Maheshwari, 2018). Furthermore, Silver is a safe antimicrobial agent which has a potential to kill 650 different types of diseases-causing organisms in the body (Bapat et al., 2018).

The microorganisms' membrane structure of the cell can be degraded by releasing of silver ions from the surface of silver nanoparticles and it leads to bacterial death (Emamifar, Kadivar, Shahedi, & Soleimanian-Zad, 2010). Furthermore, they can also enter into microbial cells and cause DNA damage (Morones et al., 2005). The silver nanoparticle is antimicrobial agent for *Listeria monocytogenes, Vibrio parahaemolyticus, Escherichia coli O157:H7* and *Salmonella typhimurium* which are the most common foodborne pathogens (Du et al., 2019). Adding nanoparticles into the polymer matrix, the agglomeration of nanoparticles is drawback for nanoparticles to function properly. Using supporter, carrier, vector etc. in micron size for AgNPs will facilitate the homogeneous distribution-dispersion of the nanoparticles (Apalangya, Rangari, Tiimob, Jeelani, & Samuel, 2014; Dlugosz, Bulwan, Kania, Nowakowska, & Zapotoczny, 2012)

Among the functional fillers, calcium carbonate ($CaCO_3$) is the most widely used filler in the plastics industry because it enhances the abilities of heat resistance, stiffness and hardness of the polymer. The commercial $CaCO_3$ is normally derived from sedimentary rocks and these rocks are not renewable in short period of time. Another alternative resource is eggshells which are agricultural wastes containing 95% of $CaCO_3$. Chicken eggshells from household waste are extensively used as a replacement for mineral calcium carbonate in several applications such as plastic and elastomer fillers, heavy metal absorbents, dye removal bio-calcium supplements, concrete replacement and biodiesel oil catalysts (Boyjoo, Pareek, & Liu, 2014).

Incorporating nanosized silver particles into polymer matrix give the excellent antimicrobial effect but they are expensive using in food packaging and also result in particles aggregation. So, using cheap porous calcium carbonate with controllable size, morphology and crystal polymorph as platforms for metallic nanoparticles will reduce

the agglomeration of the silver nanoparticles and enhance their antimicrobial activity by sustainable release active species. To prevent agglomeration and maintain the long-lasting antimicrobial activity of AgNPs, porous micro $CaCO_3$ particles in vaterite polymorph have been used as carriers for metallic nanoparticles (Apalangya et al., 2014; Dlugosz et al., 2012; C. Wang et al., 2006). The vaterite $CaCO_3$ polymorph can be synthesized with a specific size and morphology in the presence of poly (sodium 4-styrene-sulfonate) (PSS) as polyelectrolytes at room temperature (Lei, Tang, Cao, Li, & Yu, 2006).

The main concerns for incorporation of antimicrobial compounds into polymer matrix using the traditional melt processing technique like injection, extrusion, compression etc. are thermal resistance of AgNPs antimicrobial agents and resistance to the melt processing. The incorporation of antimicrobial substances into the polymer matrix through extrusion can be altered the film's barrier, mechanical, and optical properties (Mousavi Khaneghah, Hashemi, & Limbo, 2018). To maintain the efficiency of antimicrobial agents, fiber forming technique like electrospinning is one of the best choices. Due to the controllable fiber morphology such as fiber diameter, high porosity with interconnected voids, large surface area-to-volume ratio, electrospinning has been used in tissue engineering, as scaffolds and/or wound dressings (Rodriguez-Tobias, Morales, & Grande, 2019) and packaging applications (Mousavi Khaneghah et al., 2018). Therefore, electrospinning can be produced with controlled release properties while maintaining their antimicrobial activities. Maliszewska et al. reported that the antimicrobial activity has usually been carried out by diffusion techniques and the electrospun nanofibers loaded with silver nanoparticles exhibited excellent antimicrobial properties against both Gram-positive and Gram-negative bacteria. (Maliszewska & Czapka, 2022).

Electrospinning is a simple technique to prepare nanostructured materials with relatively high manufacturing rate and low cost. There are important factors affecting the electrospinning process such as solvent system, polymer concentration, applied voltage, flow rate, distance between the needle and collector and needle diameter, relativity humidity and temperature (Alven, Buyana, Feketshane, & Aderibigbe, 2021).

Due to the consumers' increased awareness of sustainability and health safety, the products which made from green resources are more favorable in today market. This is also the same for food industry. Therefore, antimicrobial food packaging which based on bio-based plastic will be predominant influence in food sector and that will lead to the sustainable development.

Therefore, this research was aimed to develop hybrid nano silver /eggshell calcium carbonate particles as antimicrobial agent for the plastics food packaging and incorporate into PLA matrix using the electrospinning technique.

This dissertation was written in 6 chapter including Chapters I-IV. Chapter I is the introductory overview. Chapter II is the literature review on antimicrobial packaging and agents, antimicrobial biopolymer composites, eggshell calcium carbonate and electrospinning technique. Chapter III describes about preparation of hybrid particles of Ag nanoparticles and eggshell calcium carbonate and their antimicrobial efficiency against beef extracted bacteria. Chapter IV is about electrospun PLA fibers with silver loaded calcium carbonate filler, effect of solvent systems and mechanical properties of the electrospun PLA and hybrid particles filled PLA fibers. Chapter V focusses on preparation of electrospun PLA fibers with silver loaded calcium carbonate filler as the antimicrobial material. Chapter VI is the conclusions of the whole study.

1.2 Research objectives

1) To prepare hybrid particles of AgNPs/μ$CaCO_3$ from eggshell waste.
2) To apply the hybrid AgNPs/eCaCO3 particles as active antimicrobial agent against beef extracted bacteria for plastic food packaging.
3) To characterize the hybrid particles and PLA filled with the hybrid particles.
4) To test antimicrobial activity and determine cytotoxicity of the hybrid particles and PLA filled with the hybrid particles.

CHAPTER II

LITERATURE REVIEW

2.1 Antimicrobial Packaging (AP)

Traditional food preservation processes like freezing, drying and refrigerating can only prevent food spoilage and contamination caused by microorganisms. The preservation processes cannot reduce or kill the microorganisms. Moreover, in spite of adding preservatives into food can extend the shelf life of the foods, they have negative impact on human health. Antimicrobial packaging is a kind of active packaging which are incorporated with the antimicrobial agents, that can kill the targeted microorganisms by adding into polymeric matrix.

2.1.1 Form of antimicrobial packaging (Appendini, 2002; Sofi et al., 2018)

Antimicrobial packaging can be categorized into five different forms including:

1. Antimicrobial packaging with sachets/pads containing volatile antimicrobial agents into packages
2. The packaging from volatile and non-volatile antimicrobial agents incorporated polymers
3. Coating or absorbing antimicrobials into polymer surfaces
4. Polymers with immobilizable antimicrobials to polymers by ion or covalent linkages
5. Inherently antimicrobial polymers.

Addition of sachets/pads containing volatile antimicrobial agents into packages is the most widely used as commercial applications and these sachets/pads are attached to the inside of the package. These also have different forms such as oxygen and moisture absorbers which are used to prevent oxidation and water condensation in bakery, pasta and meat, and ethanol vapor generator which is advantage of reducing water activity of the products like dried fish (Appendini, 2002).

Incorporation of volatile and non-volatile antimicrobial agents directly into polymers is the most commercial applications of this form, and are medical related applications, household goods and textiles. However, food related applications have been developing in double since last 5 years. Antimicrobial agents which can produce silver ions is the most widely used in food industry because these ions not only can against gram negative and positive bacteria contaminating the foods but also cost effective comparing to other metal nanoparticles like gold.

According to incorporation methods, melt or solvent compounding can be used. Solvent compounding method is suitable for heat sensitive antimicrobial like enzymes and volatile compound and both antimicrobial and polymer need to be soluble in same solvent. Biopolymers are good candidates for this method due to the wide variety of proteins, carbohydrates and lipids involved but also soluble in water, ethanol and many other solvents which are compatible with antimicrobials. Another method is called melt compounding such as extrusion and injection molding which is suitable for thermally stable antimicrobial agents like silver substituted zeolites that withstand very high temperature up to 800 °C and incorporated as a thin co-extruded layer with other polymers (Appendini, 2002).

If antimicrobial agent is non-volatile, it must contact the food's surface and diffuse to surface. Therefore, surface characteristics and diffusion kinetics are important. By using multilayer films, the release system of the antimicrobial agents to the food surface can be controlled (Biji, Ravishankar, Mohan, & Srinivasa Gopal, 2015). The inner layer controls the rate of diffusion of active substance while the matrix layer contains the active substance, and the barrier layer prevents migration of agent towards outside of the package. The theoretical advantage of volatile antimicrobials is that they can penetrate the bulk matrix of the food and so polymer does not need to contact directly with the product. The examples of these release systems are chlorine dioxide, sulfur dioxide, carbon dioxide and allylisothiocyanate. Applications like in ground beef and cut produce, antimicrobial vapor or gases are appropriate, but the disadvantages are off odors, particularly in allylisothiocyanate and high volatility (Appendini, 2002).

Coating or absorbing antimicrobials into polymer surfaces is suitable for Antimicrobials which cannot withstand the high temperature of polymer processing are used these techniques after forming or being added to the cast films. Mostly, edible film coating is used on fresh produce surface in order to improve appearance, reduce bruising during handling and shipping, reduce weight loss. As examples, nisin/methylcellulose coatings for polyethylene films (Quintavall, 2002) and nisin/zein coatings for poultry (Appendini, 2002).

Immobilization of antimicrobials to polymers by ion or covalent linkages need to have functional groups on both polymer and antimicrobial, and peptides, enzymes, polyamines and organic acids are the examples of antimicrobials with functional group. Moreover, apart from the functional group presence, "spacer" molecules are required to connect between the polymer and bioactive agent and give enough motion of active agent that can kill microorganisms on the food surface. Dextran, polyethylene glycol (PEG), ethylenediamine and polyethyleneimine are some examples of spacer used for food application because of low toxicity and common use in foods (Appendini, 2002; Sofi et al., 2018).

Lastly, polymers with inherently antimicrobial efficiency are cationic polymers such as chitosan and poly-L-lysine. Mostly, chitosan is used as film coating in fresh vegetables and fruits because it can reduce fungal degradation (Appendini, 2002).

2.1.2 Antimicrobial Packaging film

The most crucial parameters for antimicrobial packaging films are: (1) films should not be dangerous when handling or release poisonous particles into foods; (2) processing technologies should be easy and cost effective ways; (3) films should maintain their antimicrobial properties along the packaging period , be chemically stable and act as a water barrier; (4) films should be used minimal concentration of antimicrobials which is enough to inhibit the growth of microorganisms and bacteria of the foods [3].

2.1.3 Migration process in Antimicrobial Packaging

The antimicrobial properties of the packaging films depend on the migration of the antimicrobial agents from the packaging to the surface or to the headspace of the products. These substances reduce or inhibit the growth of the microorganisms and bacteria, suspend the food spoilage and extend the shelf life of the products. The most important fact in migration of antimicrobial packaging is that a slow and gradual release of antimicrobial agents into the food. It maintains the effective antimicrobial concentration in the product thought the extended period (Biji et al., 2015; Quintavall, 2002).

The migration is the transfer of low molecular weight compounds from packaging materials to packaged food (Gnanasekharan & Floros, 1997). Although migration in polymer packaging are mainly dependent on the interaction between the packaging materials and the surface of the food (Arvanitoyannis & Kotsanopoulos, 2013), the migration mechanism can commonly be separated into four main stages: (1) diffusion of migrants through the polymer; (2) desorption from the polymer surface; (3) sorption of the compounds in the interface; (4) desorption into the food. However, the condition when the packaging and the food surface has no direct contact, more steps are required to complete the migration mechanism. Firstly, the diffusion of migrants through the polymer in the interface, the interface to the headspace that surrounds the food, and the mass transference in the interface from the headspace to the food (Bhunia, Sablani, Tang, & Rasco, 2013).

2.2 Antimicrobial Packaging for fresh meat produce

Nowadays, ready-to-eat and ready-to-cook meats are very popular because of busy lifestyle of the 21st century. Moreover, microbial contamination is one of the biggest concerns in meat and meat products where microorganism's contamination occurs mostly in surface of the food during processing and subsequent handling. In addition to this, microbial contamination reduces shelf life and cause foodborne illness. A variety of methods have been trying to solve these issues. Antimicrobial packaging incorporating with antimicrobial agents in the packaging matrix can reduce

or inhibit the microbial contamination that results in shelf-life extension (Barros-Velazquez, 2016).

2.2.1 Spoilage or Pathogenic Microorganisms in Meat

Meat and meat products are highly perishable food because of nutritious nature as well as high water content and almost neutral pH, which is an excellent growth media for microorganisms. Yeast, molds, and bacteria, both spoilage and pathogens are mostly found in meat products. Microorganisms normally found on the surface of fresh meat stored aerobically at low temperature include *Arthrobacter spp*., *Acinetobacter spp., Aeromonas spp., Staphylococcus spp., Brochothrix thermosphacta, Enterococcus spp., Moraxella spp., Lactobacillus spp., Leuconostoc spp*., and *Pseudomonas spp.*

Microbes contamination in meat could be either spoilage or pathogenic. The spoilage microbes are responsible for shelf life while foodborne pathogens relate with the risk of food safety. Predominant pathogens causing meat-associated outbreaks include Shiga toxin-producing *E. coli O157, Salmonella spp., Clostridium perfringens, and Campylobacter jejuni.* Salmonella strains include *Sal. heidelberg, Sal. typhimurium, Sal. en- teridis, Sal. bareilly, Sal. nchanga, Sal. anatum, Sal. stanley, Sal. corvallis, and Sal. Hadar* (Bodhidatta, 2013).

2.2.2 Action mode of Antimicrobial Packaging in Meat Products

Two types of mode, direct contact and noncontact mode, can be classified for AM packaging in meat products. Direct contact between the packaging layer and the food surface gives antimicrobial effect onto the microorganisms on the food (nonmigratory mode) or delivery of antimicrobials on the food surface, where diffusion and dissolution occur. In noncontact mode, a volatile antimicrobial compound should be volatilized from the package surface to the headspace where it is absorbed onto the food surface. The transfer of the antimicrobial compound works through the thermodynamics of phase equilibrium and kinetics of diffusion (Barros-Velazquez, 2016).

2.3 Antimicrobial Agents

The activities of antimicrobial packaging depend on the antimicrobial agents which can be divided into natural antibacterial agents and synthetic antibacterial agents. Natural antimicrobial agents are safe because they are obtained from plants and animals, but some extraction procedures are quite complex. Moreover, increasing the production of food, natural antimicrobial agents are not enough. Therefore, organic or inorganic synthesis antimicrobial agents which cannot harm human health have been introduced. As an emergence of nanotechnology, inorganic compounds (silver, copper, zinc and gold) are gaining interest because the nanosized level of these particles show excellent properties in inhabitation of microbial growth. The mechanism of antimicrobial agents in food packaging includes (1) destruction of cell wall or cell membrane, (2) inhabitation of various enzymes in the microbial cell, or (3) destruction of the genetic structure of the protoplasm (Radusin, 2013). These metal nanoparticles are incorporated directly into the polymeric films or embedded into films and use in food related applications.

Several types of metal and metal oxide nanoparticles such as Ag, Au, TiO_2, CuO, and ZnO, have gained attention owing to their antimicrobial efficiency. Ag nanoparticles (AgNPs) are less expensive than Au and TiO_2. TiO_2 nanoparticles are effective antifungal agent against fluconazole-resistant strains and are suitable for photocatalytic activity. Ag, CuO, and ZnO nanoparticles show antibacterial activity against Gram-negative and Gram-positive bacteria. However, Ag nanoparticles (AgNPs) are the most popular antimicrobial agents because of their high activity against drug-resistant bacteria, high stability, and nontoxicity (Dizaj, Lotfipour, Barzegar-Jalali, Zarrintan, & Adibkia, 2014).

2.3.1 Silver nanoparticles

Silver particles are one type of antimicrobial agents which is commonly used in antimicrobial food packaging because of their high stability and high toxicity against a wide range of microorganisms including gram negative and positive bacteria, fungi and mold which are caused food spoilage and contamination. The concentration of silver used in food packaging is very low and effective in against microbes, but this effect can neglect and cause any negative effect for human cell (Humberto H Lara,

2010; Nocchetti et al., 2013). Comparing with the organic antimicrobial agents, using inorganic antimicrobial agents in packaging have many advantages such as low volatility and high stability (Dutta, Nenavathu, Gangishetty, & Reddy, 2012).

2.3.1.1 Antimicrobial activity of AgNPs

The cytotoxicity of AgNPs is highly dependent on several factors such as size, shape, surface chemistry, stability, surface charge, capping agent, pH, ionic strength, degree of agglomeration, and silver content and the interaction of silver surface with the polymer (Chen, Li, Luo, Wang, & Ding, 2016; Kim et al., 2007; Marambio-Jones & Hoek, 2010; Xiu, Zhang, Puppala, Colvin, & Alvarez, 2012). The presence of ligands, divalent cations, and macromolecules are also play a key role on the cytotoxicity (Chen et al., 2016; Marambio-Jones & Hoek, 2010; Xiu et al., 2012). Size-dependent cytotoxicity of AgNPs has been demonstrated in many studies. Smaller particles have a larger specific surface area, which can expose a large number of atoms on the surface for redox, photochemical, and biochemical reactions, as well as physicochemical interactions with cells (Marambio-Jones & Hoek, 2010). Recently, silver nanoparticles have been developed, and these particles are more effective antimicrobial effect than ionic silver because of their small size that can penetrate through the cell membrane of the microorganisms and kill them by releasing silver ions locally from silver nanoparticles (J. L. Castro-Mayorga et al., 2014; Grigor'eva et al., 2013; Marambio-Jones & Hoek, 2010). Although the mechanisms underlying the activity of AgNPs against bacteria have not yet been fully clarified, various antibacterial mechanisms have been proposed. Yin et al. proposed the following possible mechanisms: (1) disruption of the cell wall and membrane by Ag^+, (2) denaturation of ribosomes by Ag^+, (3) interruption of adenosine triphosphate (ATP) production by Ag^+, (4) disruption of the cell membrane by reactive oxygen species (ROS), (5) interference of DNA replication by AgNPs, Ag^+ and ROS, (6) denaturation of the cell membrane by AgNPs and (7) perforation of the membrane by AgNPs (Yin et al., 2020). A diagram of the antibacterial mechanisms of AgNPs drawn using BioRender is shown in Fig. 2.1.

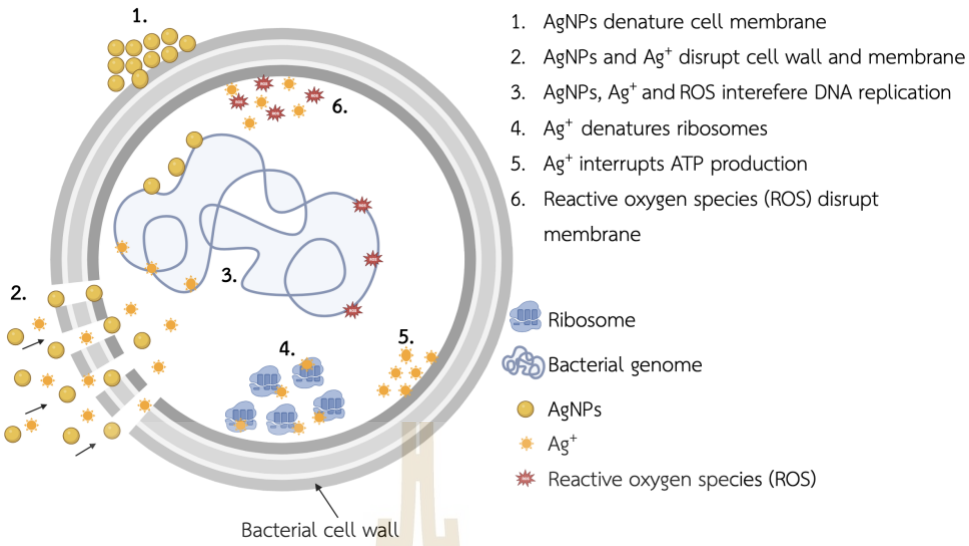

Figure 2.1 The antibacterial mechanism of silver nanoparticles (AgNPs) modified from (Yin et al., 2020)

By using chemical, physical and biological methods, silver nanoparticles can be synthesized; but the most common one is chemical reduction method in which silver salt dissolved in water by using reducing agent. The chemical reduction of a silver salt in aqueous media is a common method for producing AgNPs with reducing compounds such as sodium borohydride ($NaBH_4$) (Banne, Patil, Kulkarni, & Patil, 2017; Kandarp Mavani, 2013; S. M. Lee, Song, & Lee, 2010), trisodium citrate ($Na_3C_6H_5O_7$) (Ahari et al., 2018; Kamat*, 2004; Mamun Ur Rashid, 2013; Pinto et al., 2012), ascorbate ($C_6H_7O_6$) (Marambio-Jones & Hoek, 2010; Valodkar, Modi, Pal, & Thakore, 2011), glucose ($C_6H_{12}O_6$), and hydrazine (N_2H_4) (Marambio-Jones & Hoek, 2010). Trisodium citrate was used as a stabilising and reducing agent for silver nitrate to produce AgNPs (Dlugosz et al., 2012). The citrate reduction of gold and silver colloids serves the dual role of a reductant and stabiliser and silver particles prepared by the citrate reduction method produce relatively large-sized (50-100 nm) silver crystallites with well-defined facets (Kamat*, 2004).

After reduction of metal ions, capping agents are used to coat in order to be stable the synthesized nanoparticles. The major concerns for using metal nanoparticles in antimicrobial packaging is to prepare a dispersed system with the required stability and resistance to the action of external factors, such as high processing temperature of plastics. Additionally, due to the fact that, the release

kinetics of silver nanoparticles in polymer matrices depend on the water uptake capacity of the materials and the release of silver can be modified by the degree of crystallinity of the polymer (Kumar, Howdle, & Munstedt, 2005). If the polymer matrix has a high degree of crystallinity, nanoparticles need to diffuse out through the dense crystalline region that can cause a slow release of silver. So, amorphous films are easier to diffuse than crystalline and a higher crystallinity degree also mean lower water sorption (Kumar et al., 2005).

2.3.2 Calcium carbonate

Calcium carbonate ($CaCO_3$) is the most widely used filler in the plastics industry because of low cost and increased modulus with minimal effect on impact strength. For polypropylene nanocomposites, adding calcium carbonate increased the flexural strength and modulus of PP nanocomposites and the yield strength depended on calcium carbonate content (Yang, Yang, Li, Sun, & Feng, 2006).

The commercial $CaCO_3$ is normally derived from sedimentary rocks by using standard mining procedures. There are two types of $CaCO_3$ which are used as functional fillers in plastic processing. Natural ground calcium carbonate (GCC) and precipitated calcium carbonate (PCC), produced chemically, which have finer and higher purity than natural one, but also more expensive.

2.3.2.1 Production methods

More than 90% of calcium carbonate used in plastic processing are produced by conventional grinding methods. Different kind of grinding methods are as followed (M., 2009).

1. Dry grinding with single stage milling can be obtained the finest ground powder with particle size nearly in diameter of 12 um and this is suitable for inexpensive dark floor tiles and vinyl foam carpet backing. By using multiple stage milling with air classifier, 3 um range particle size can be produced which is used in high-end applications.
2. Wet grinding process give higher purity and a much finer medium particle size in 1 um range for demanding applications. In wet

grinding – high solids process, a dispersant is added to ease deagglomeration, that can reduce the moisture resistance but can be obtained the particle range as low as 0.7 um whereas low solids process, no dispersant is added and slightly bigger particle size about 1 um can be produced. The material needs either flash or spray dried after wet grinding and classification steps.

2.3.2.2 Alternative sources of calcium carbonate

There are many alternative sources that can exact calcium carbonate instead of using sedimentary rocks because these rocks are hard to renewable. Among them, eggshells which are agricultural wastes and contain 95% of $CaCO_3$. Chicken eggshells from household waste are extensively used as a replacement for mineral calcium carbonate in several applications such as plastic and elastomer fillers, heavy metal absorbents, dye removal bio-calcium supplements, concrete replacement and biodiesel oil catalysts (Boyjoo et al., 2014). Eggshell waste can be used as an alternative and green precursor for hybrid particles of AgNPs and $CaCO_3$. The number of patents on eggshell application has exponentially increased in the last seven years, from 150 in 2014 to 250 in 2020, emphasising biotechnological application involving biomedical, chemical, engineering and environmental technology (Ahmed, Wu, Younes, & Hincke, 2021). One of the biotechnological applications of eggshell calcium carbonate is as a hybrid particle. The ceramic-ceramic and ceramic-metal hybrid particles exploit the advantages of the synergistic function of the compositions of the hybrid particles. For example, TiO_2/SiO_2, as ceramic-ceramic hybrid particles, can be applied as a functional filler for elastomers and possesses the advantages of photocatalytic properties and antimicrobial biomaterials by TiO_2, as well as high thermal stability and excellent mechanical strength by SiO_2 (Teamsinsungvon, Ruksakulpiwat, Amonpattaratkit, & Ruksakulpiwat, 2022). For ceramic-metal hybrid particles, $AgNPs/CaCO_3$, could be utilized as an antimicrobial agent with $CaCO_3$ acting as an AgNPs carrier and AgNPs as an active antimicrobial agent. The $CaCO_3$ carrier also improves the distributive of AgNPs (Apalangya et al., 2014; Dlugosz et al., 2012).

2.3.3 Silver nanoparticles/Calcium carbonate hybrid Particles

Owing to growing concerns about antibiotics resistance, incorporating AgNPs into different matrices/supporters/carriers has emerged as an effective way to produce materials with high antimicrobial efficiency. AgNPs incorporated into polymer matrices are currently a popular type of nanocomposite with excellent antimicrobial properties. One of the main challenges in producing this type of antimicrobial is the synthesis of stable nanoparticles, as their antimicrobial effectiveness greatly depends on their size, size distribution, and agglomeration state (J. L. Castro-Mayorga et al., 2014). Notably, the most common application problem involves the agglomeration and diffusion of these nanoparticles into a polymer matrix, which reduces antibacterial activity. To prevent agglomeration and maintain the long-lasting antimicrobial activity of AgNPs, porous micro $CaCO_3$ particles in vaterite polymorph have been used as carriers for metallic nanoparticles (Apalangya et al., 2014; Dlugosz et al., 2012; C. Wang et al., 2006). Using porous micro $CaCO_3$ particles as carriers or supporters, the antimicrobial activity of the active AgNPs can be prolonged owing to reduced agglomeration of the nanoparticles as well as limiting contact of AgNPs with the human body (Dlugosz et al., 2012).

2.4 Antimicrobial Packaging from AgNPs/Biopolymer Composites

As a consequence of using synthesis polymer in packaging, several environmental problems are occurred including landfill and plastic pollution. So, biopolymers which can be degradable and compostable are alternative ways to solve above mention concerns. Using biopolymers as polymer matrix can get stabilized and dispersed nanoparticles because of embedding these metal compounds into the matrix. Polylactydes, polyhydroxyalkanotes, cellulose and chitosan are mostly used to incorporate with silver and the main function of these antimicrobial biopolymer films is to extend the shelf life of the products by reducing the targeted microorganisms. Cellulose-derived polymers such as methylcellulose has been used to synthesize silver nanoparticles to yield good mechanical properties and barrier properties, offering the nanocomposites highly interesting antimicrobial activity (J. L. Castro-Mayorga, Martínez-Abad, A., Fabra, M. F., Lagarón, J.M., Ocio, M.J. and. Sánchez, G.).

2.4.1 Biodegradable Poly(lactic acid) Packaging

One of the most promising biopolymer is the poly(lactic acid) (PLA) obtained from the controlled depolymerization of the lactic acid monomer obtained from the fermentation of sugar feedstock, corn, etc., which are renewable resources and biodegradable (Siracusa, Rocculi, Romani, & Rosa, 2008). Depending on the ratio and distribution of L- and D-LA in the polymer chains, the thermal and mechanical properties of PLA would be justified. L-lactide would produce semicrystalline polymer (PLLA), while poly (DL-lactide) (PDLLA) is an amorphous polymer (Taib et al., 2022). Tg for both semicrystalline and amorphous PLAs are between 50 and 70 °C (Storz, 2013). The degradation half-life is dependent on the PLAs' stereochemistry, and the molecular weight typically ranges from six months to two years. Among the rigid bioplastics, one of the most commercially and successfully used bioplastics is poly lactic acid (PLA) because it has good processability and mechanical properties, and transparency compared to the other biodegradable products (Taib et al., 2022).

Compared to other aliphatic polyesters, PLA has shown many excellent properties such as high mechanical strength and modulus, biodegradability, biocompatibility and easy processing. The increment of PLA application is also related to enhancing its properties as heat-resistance modification, copolymerization and blending modification. PLA has been used in different industries such as Medical and biomedical, food packaging, agriculture and automotive industries (Taib et al., 2022).

2.5 Egg and Eggshell

The egg contains three main parts: eggshell with eggshell membrane, albumen and yolk as shown in Fig. 2.2. It comprises approximately 30 wt.% yolk, 60 wt.% albumen and 10 wt.% shell. The yolk is covered by albumen which is surrounded by eggshell membrane and eggshell (M. T. Hincke, Nys, Y., Gautron, J., Mann, K., Rodriguez-Navarro, A.B. and McKee, M.D, 2012).

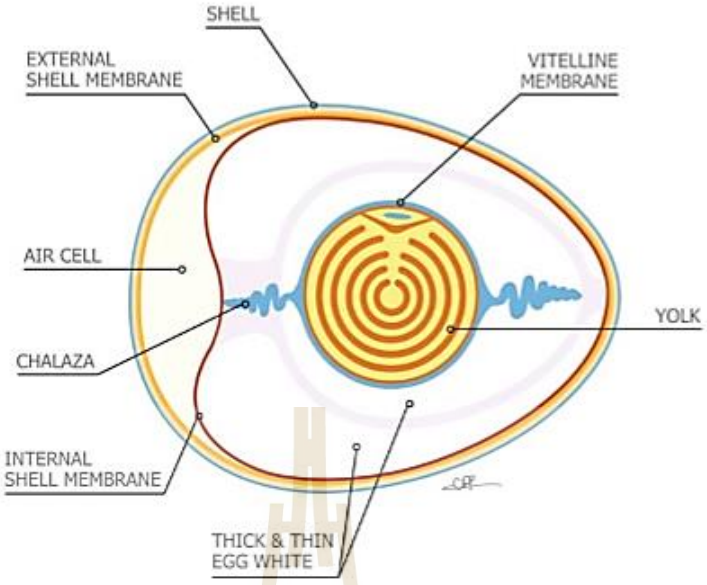

Figure 2.2 Schematic of different parts of egg structure (M. T. Hincke, Nys, Y., Gautron, J., Mann, K., Rodriguez-Navarro, A.B. and McKee, M.D, 2012)

2.5.1 Structure of eggshell

The eggshell is composed of eggshell membrane and calcified eggshell matrix. The eggshell membrane consists of two layers which are called inner membrane which contact directly to the albumen and the outer membrane which is attached to calcified eggshell matrix as shown in Fig. 2.3.

The calcified eggshell is the combination of both inorganic and organic components which are mainly found in palisade and mammillary layers. Calcium carbonate in the form of calcite is the main component of eggshell about 94 wt.%, 1 wt.% magnesium carbonate, 1 wt.% calcium phosphate, and organic materials such as type X collagen, sulfated polysaachrides, and other proteins about 4 wt.%.

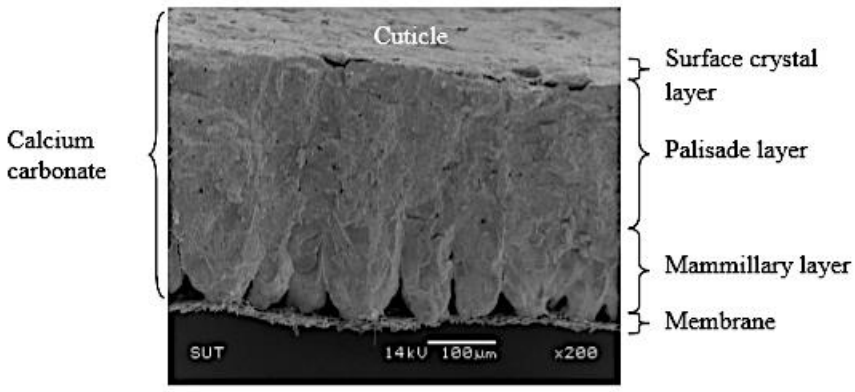

Figure 2.3 SEM micrograph of a cross-fractured chicken eggshell structure (M. Hincke, Gautron, J., Rodriguez-Navarro, A. B. and McKee, M. D. , 2011).

Mammillary layer (~100 um) is the innermost layer of the calcite and represents as calcitic columns/ cones in which the fibers of the outer shell membrane embedded. Mammillae is the major source of calcium and contains microcrystals calcite with spherulitic textures. Palisade layer which is the thickest part (~200 um) of the eggshell and can be found above mammillary layer. The top layer is the vertical layer (~5-8 um) covered by the organic cuticle and crystalline structure of calcite is higher density than the palisade layer. Moreover, the numerous pore canals are distributed at the outer eggshell surface about 7000-17000 pores per egg (M. Hincke, Gautron, J., Rodriguez-Navarro, A. B. and McKee, M. D. , 2011) and the smallest pore size of 3-13 µm (Kinayturk, Tunali, & Turkoz Altug, 2021; Rahn, Paganelli, & Ar, 1987).

2.5.2 Crystalline form

Calcium carbonate can be found three crystalline form: calcite, aragonite and vaterite. Calcite is the most stable form of calcium carbonate whereas aragonite and vaterite are not stable in ambient temperature and atmospheric pressure, and vaterite can be found during high temperature precipitation of $CaCO_3$. Aragonite and vaterite can transform readily into calcite by heating (Sutapun, Pakdeechote, Suppakarn, & Ruksakulpiwat, 2013). Eggshells are readily available with a high $CaCO_3$ content (94 wt%), in the form of calcite polymorph (Hassan, Rangari, Rana, & Jeelani, 2013; M. T. Hincke, Nys, Y., Gautron, J., Mann, K., Rodriguez-Navarro, A.B. and McKee, M.D, 2012).

2.5.3 Eggshell matrix proteins

Eggshell matrix proteins are the organic matrix composed of proteins, glycoproteins and proteoglycans. Their function is to participate in its antimicrobial defenses. Eggshell matrix proteins can be divided into three groups (M. Hincke, Gautron, J., Rodriguez-Navarro, A. B. and McKee, M. D. , 2011).

1. Eggshell specific - Ovocleidin-17, ovocleidin-116, ovocalyxin-32, Ovocalyxin-36
2. Bone protein - Osteopontin
3. Egg white protein - Ovalbumin, ovotransferrin, lysozyme

Table 2.1 Occurrence of proteins in eggshell (M. Hincke, Gautron, J., Rodriguez-Navarro, A. B. and McKee, M. D. , 2011)

1.	ovocleidin-17	in entire calcified part of the shell
2.	ovocleidin-116	in the palisade layer of the eggshell
3.	ovocalyxin-32	external part of the shell (palisade, vertical and cuticle)
4.	ovocalyxin-36	shell membrane and inner the calcified shell
5.	ovocalyxin-36	shell membrane fibers in mammillae, outermost of palisade
6.	osteopontin	Mammillae cores and outermost part of palisade layer
7.	ovalbumin	in shell
8.	ovotransferrin and lysozyme	eggshell membrane and mammillae

2.6 Preparation of Vaterite Calcium carbonate

2.6.1 Factors Effecting Preparation of $CaCO_3$ particles (Vaterite)

Chicken eggshell mainly composed of calcite crystalline form. To incorporate into polymer matrix as carrier for nanoparticles antimicrobial agent, rough surface and spherical shape morphology are required. The morphology and size of $CaCO_3$ particles can be controlled by using different polyelectrolytes such poly

(sodium 4-styrenesulphonate) (PSS), sodium polyacrylate (PAA), sodium polyvinyl sulfonate (PVSA), sodium poly (maleic acid-co-olefin) (PMACO), ethylene glycol (EG), polyethylene glycol (PEG, 600 and 6000) (Azarian & Sutapun, 2022; Jada & Jradi, 2006).

Moreover, $CaCO_3$ concentration on the crystallization of $CaCO_3$, PH and crystallization temperature are also affected on morphology and size of $CaCO_3$ particles (Lei et al., 2006; Matahwa, Ramiah, & Sanderson, 2008).

2.7 Preparation Technique of AgNPs/$CaCO_3$ hybrid particles

There are two types techniques for preparation of nAg/u$CaCO_3$ particles. The first technique used $CaCO_3$ particles while the second one used Ca $(NO_3)_2$ to prepare the hybrid nano silver/ calcium carbonate particles.

2.7.1 Mechanochemical Technique using eggshell and $AgNO_3$

Two grams of the eggshell powder was magnetically stirred into a uniform dispersion in 20 ml of deionized water and ethanol (1:2 v/v) mixture for 10 min. Two grams of silver nitrate was dissolved in 10 ml of distill water. The dissolved silver nitrate solution is then added at a rate of 1.0ml per minute into the eggshell mixture while the content was being stirred at 150 rpm for a total time of 10 min. The dispersed mixture was divided into two and each part added to 5 ml of PPG and ball milled for 2 h using 6 mm stainless balls each as shown in the scheme. The product was washed with 20 ml of distilled water and each time the supernatant was removed by centrifuging at 12,000 rpm for 5 min. In the last step the product was washed with 10 ml of ethanol and then dried in vacuum overnight (Apalangya et al., 2014).

2.7.2 Preparation Technique using AgNPs/$CaCO_3$ particles

Firstly, 45mg of silver nitrate will be dissolved in 250 ml of deionized water and then 5ml of 1% trisodium citrate will be added into the silver nitrate solution. The reaction mixture will be placed in ultrasonic bath which will be heated to75°C for 60 min. Then, 20 ml of the obtained nAg colloid will be simultaneously mixed with 50ml of 0.03 M Ca $(NO_3)_2$ solution and 50 ml of 0.03 Na_2CO_3 with addition of 4.8 g/L of poly (sodium 4-styrenesulfonate). The mixture will be sonicated for 5 min at 25 °C. The obtained white colloid will be washed with deionized water and

centrifuged at 4,000 rpm for 5 min to remove excess of silver. The washing process will be repeated three times and the obtained product will be dried under vacuum (Dlugosz et al., 2012).

2.8 Electrospinning Technique for Preparing Polymer Film

Electrospinning is a simple but versatile and facile technique to prepare nanostructured materials with relatively high manufacturing rate and low cost. The obtained fibers possess advantages of nanoscale, high porosity, and high surface-to-volume ratio, making it easy to obtain a high encapsulation efficiency of bioactive substances, achieving controlled release system of drugs (Wu et al., 2022). Electrospun nanofibers and their nanowebs have also shown some potential in biotechnology and active food packaging, because active additives such as antibacterial, antioxidants, essential oils, or even probiotics can be effectively encapsulated into an electrospun nanofibrous matrix (Kayaci, Umu, Tekinay, & Uyar, 2013).

2.8.1 Effects of parameters on electrospinning

There are several factors affecting the electrospinning process. These factors are classified as electrospinning parameters, solution and environmental parameters. The electrospinning parameters include (1) the applied electric field, (2) distance between the needle and collector, (3) flow rate, and (4) needle diameter. The solution parameters include (1) the solvent, (2) polymer concentration, (3) viscosity and (4) solution conductivity. The environmental parameters include relativity humidity and temperature (Haider, Haider, & Kang, 2018). All of these parameters directly affect the generation of smooth and bead-fee electrospun fibers.

2.8.1.1 Effect of applied voltage

The strength of the applied electric field controls formation of fibers from several microns in diameter to tens of nanometers. The formation of smaller-diameter nanofibers with an increase in the applied voltage is attributed to the stretching of the polymer solution in correlation with the charge repulsion within the polymer jet (Sill & von Recum, 2008). An increase in the applied voltage beyond

the critical value will result in the formation of beads or beaded nanofibers (Haider et al., 2018).

2.8.1.2 Effect of flow rate

The flow of the polymeric solution through the metallic needle tip determines the morphology of the electrospun nanofibers. Uniform beadless electrospun nanofibers could be prepared via a critical flow rate for a polymeric solution (Haider et al., 2018). Increasing the flow rate beyond a critical value not only leads to increase in the pore size and fiber diameter but also to bead formation (due to incomplete drying of the nanofiber jet during the flight between the needle tip and metallic collector) (Silke Megelski, Jean S. Stephens, D. Bruce Chase, & Rabolt, 2002). Due to increases and decreases in the flow rate affect the nanofiber formation and diameter, a minimum flow rate is preferred to maintain a balance between the leaving polymeric solution and replacement of that solution with a new one during jet formation (Haider et al., 2018).

2.8.1.3 Effect of needle to collector distance and needle diameter

The distance between the metallic needle tip and collector plays an essential role in determining the morphology of an electrospun nanofiber. Similar to other electrospinning parameters such as applied voltage and flow rate, the distance between needle to collectors also varies with the polymer system (Haider et al., 2018). The nanofiber morphology could be easily affected by the distance because it depends on the deposition time, evaporation rate, and whipping or instability interval (Matabola & Moutloali, 2013). Matabola et al. (Matabola & Moutloali, 2013) and Wang et al. (T. Wang & Kumar, 2006) studied and concluded that defective and large-diameter nanofibers are formed when this distance is kept small, whereas the diameter of the nanofiber decreased as the distance was increased.

2.8.1.4 Role of solvent in electrospinning

The selection of the solvent or binary solvent system to dissolve the polymer is one of the main factors influencing the solution properties and consequently the electrospinnability of the solution (Casasola, Thomas, Trybala, & Georgiadou, 2014). The selection of the solvent is one of the key factors for the

formation of smooth and beadless electrospun nanofiber. Two important steps needed to be considered for choosing solvents are (1) polymers are completely soluble in the preferred solvents for electrospinning process and (2) the solvent should have a moderate boiling point because boiling point gives an idea about the volatility of a solvent (Haider et al., 2018). Generally volatile solvents are recommended as their high evaporation rates encourage the easy evaporation of the solvent from the nanofibers during their flight from the needle tip to collector. However, neither highly volatile solvents nor less volatile solvents should be avoided. Due to their highly volatile solvents, it can cause the drying of the jet at the needle tip and will block the needle tip which will hinder the electrospinning process. Formation of beaded nanofiber can be resulted from less volatile solvents because their high boiling points prevent their drying during the nanofiber jet flight (Sill & von Recum, 2008). Moreover, solubility parameters are also used to aid the search for suitable solvents and solvent systems for polymers used in electrospinning (Sato, Gondo, Wada, Kanehashi, & Nagai, 2013).

2.8.1.5 Binary solvent systems

Solvents are selected to produce binary solvent systems that have solvent parameters close to a good single solvent for electrospinning of the polymer solution (Luo, Nangrejo, & Edirisinghe, 2010). The highly porous fiber can be formed when a polymer is dissolved in two solvents: one of the solvents will act as a non-solvent. The different evaporation rates of the solvent and non-solvent will lead to phase separation that was the main reason to cause surface porosity in electrospun fibres (Haider et al., 2018; Luo et al., 2010; Sill & von Recum, 2008). Casasola et al. (Casasola et al., 2014) studied that Smooth defect-free nanofibres with a narrow diameter distribution were collected using the binary solvent systems of acetone /dimethylformamide and acetone /dimethylacetamide. It was found that the nanofibre diameter decreases as the boiling point of the second solvent in the mixed-solvent system increases.

2.8.1.6 Effects of polymer concentration

To produce nanofibres, one of the most influential variables to consider is polymer solution concentration (Luo et al., 2010). The electrospinning process relies on the phenomenon of the uniaxial stretching of a charged jet. The stretching of the charged jet is significantly affected by changing the concentration of the polymeric solution (Haider et al., 2018). Casasola et al (Casasola et al., 2014) reported that few nanofibres with many beads were collected using the 5% ((w/v)) PLA solution in the binary solvent system of acetone/dimethylformamide. The beads formation indicates insufficient chain entanglements. When the concentration of the polymeric solution is low, the applied electric field and surface tension cause the entangled polymer chains to break into fragments before reaching the collector. These fragments cause the formation of beads or beaded nanofibers (Haider et al., 2018; Pillay et al., 2013). Increasing the concentration of the polymeric solution will lead to an increase in the viscosity, which then increases the chain entanglement among the polymer chains. These chain entanglements overcome the surface tension and ultimately result in uniform beadless electrospun nanofibers (Haider et al., 2018).

CHAPTER III

PREPARATION OF HYBRID PARTICLES OF AG NANOPARTICLES AND EGGSHELL CALCIUM CARBONATE AND THEIR ANTIMICROBIAL EFFICIENCY AGAINST BEEF EXTRACTED BACTERIA

3.1 Abstract

In this study, hybrid particles of AgNPs-loaded eggshell calcium carbonate (AgNPs/e$CaCO_3$) were prepared by co-precipitating the eggshell in the presence of freshly prepared AgNPs with a mean particle size of 24.13 ± 2.95 nm. The hybrid particles were comparatively precipitated at 25 °C and 35 °C using poly (sodium 4-styrenesulphonate) as a polyelectrolyte. The AgNPs/e$CaCO_3$ particles prepared at 25 °C had a spherical morphology with a mean diameter of 3.56 µm, and BET surface area of 85.08 m^2/g. On the other hand, the particles prepared at 35 °C had a broader size distribution with a mean diameter of 3.19 µm, and a BET surface area of 79.25 m^2/g. AgNPs-loaded commercial calcium carbonate particles (AgNPs/$CaCO_3$) comparatively prepared at 35 °C were perfectly spherical with a mean diameter of 5.61 µm. At preparing temperature of 25 °C, the hybrid particles contain AgNPs of 0.78 wt% for AgNPs/e$CaCO_3$ and 3.20 wt% for AgNPs/$CaCO_3$. The polymorph of precipitated $CaCO_3$ was vaterite. Both AgNPs/e$CaCO_3$ and AgNPs/$CaCO_3$ prepared at 25 °C have four regions of thermal decomposition with the overall weight loss of approximately 55.81% and 47.28% respectively. The AgNPs/e$CaCO_3$ and AgNPs/$CaCO_3$ particles exhibited the same efficiency against bacteria extracted from beef with an average inhibition zone diameter of 7-10 mm according to the modified Kirby–Bauer disc diffusion assay depending on their concentration and beef source. Freshly prepared silver colloids showed comparatively poorer antimicrobial efficiency. Significant human dermal fibroblast (HDF) cells dead were found at 5 mg/mL for AgNPs/e$CaCO_3$ and 25 mg/mL for AgNPs/$CaCO_3$ and no alive HDF cells were resulted at the concentration of 50 mg/mL for both samples.

3.2 Introduction

Several types of metal and metal oxide nanoparticles such as Ag, Au, TiO_2, CuO, and ZnO, have gained attention owing to their antimicrobial efficiency and high surface area per volume. Ag nanoparticles (AgNPs) are less expensive than Au and TiO_2. TiO_2 nanoparticles are effective antifungal agents against fluconazole-resistant strains and are suitable for photocatalytic activity. Ag, CuO, and ZnO nanoparticles show antibacterial activity against Gram-negative and Gram-positive bacteria. However, Ag nanoparticles (AgNPs) are the most popular antimicrobial agents because of their high activity against drug-resistant bacteria, high stability, and nontoxicity (Dizaj et al., 2014). Moreover, AgNPs are highly effective antimicrobial agents against a wide spectrum of *Gram-negative* and *Gram-positive* bacteria; fungi such as *Aspergillus niger* and *Candida albicans*; and viruses including HIV-1, hepatitis B virus, respiratory syncytial virus, herpes simplex virus type 1, and monkeypox virus (Beaudrie, Kandlikar, & Ramachandran, 2016; Chen et al., 2016; Humberto H Lara, 2010; Marambio-Jones & Hoek, 2010). The cytotoxicity of AgNPs is derived from the nanoparticles themselves and Ag^+ released from oxidative dissolution. In aqueous environments, AgNPs suspensions are oxidized in the presence of oxygen and protons, thereby releasing Ag^+ via surface oxidative dissolution (Chen et al., 2016). The oxidative dissolution reaction is shown in Equation (1) (Molleman & Hiemstra, 2015). The release rate of Ag^+ depends on the size, shape, surface properties, capping agent, and colloidal state of AgNPs (S. H. Lee & Jun, 2019).

Equation (1): $Ag^0(s) + ¼\ O_2(aq) + H^+(aq) \leftrightarrow Ag^+(aq) + ½\ H_2O\ (l)$

Although the mechanisms underlying the activity of AgNPs against bacteria have not yet been fully clarified, various antibacterial mechanisms have been proposed. Yin et al. proposed the following possible mechanisms: (1) disruption of the cell wall and membrane by Ag^+, (2) denaturation of ribosomes by Ag^+, (3) interruption of adenosine triphosphate (ATP) production by Ag^+, (4) disruption of the cell membrane by reactive oxygen species (ROS), (5) interference of DNA replication by AgNPs, Ag^+ and ROS, (6) denaturation of the cell membrane by AgNPs and (7) perforation of the membrane by AgNPs (Yin et al., 2020). A diagram of the antibacterial mechanisms of AgNPs drawn using *BioRender* is shown in Fig. 3.1. Durán et al. reported that ROS could be a principal

agent in the induction of cell membrane disruption and deoxyribonucleic acid (DNA) modification. The interaction of Ag^+ with sulphur and phosphorus, which are important DNA compounds, can cause problems in DNA replication and cell reproduction, or even result in the termination of microorganisms. Furthermore, the synthesis of proteins can be inhibited by Ag^+, causing denaturation of ribosomes in the cytoplasm (Duran, Nakazato, & Seabra, 2016).

The cytotoxicity of AgNPs is highly dependent on several factors such as size, shape, surface chemistry, stability, surface charge, capping agent, pH, ionic strength, and degree of agglomeration. Size-dependent cytotoxicity of AgNPs has been demonstrated in many studies. Smaller particles have a larger specific surface area, which can expose a large number of atoms on the surface for redox, photochemical, and biochemical reactions, as well as physicochemical interactions with cells (Marambio-Jones & Hoek, 2010). In addition, the presence of ligands, divalent cations, and macromolecules also play a key role on cytotoxicity (Chen et al., 2016; Marambio-Jones & Hoek, 2010; Xiu et al., 2012).

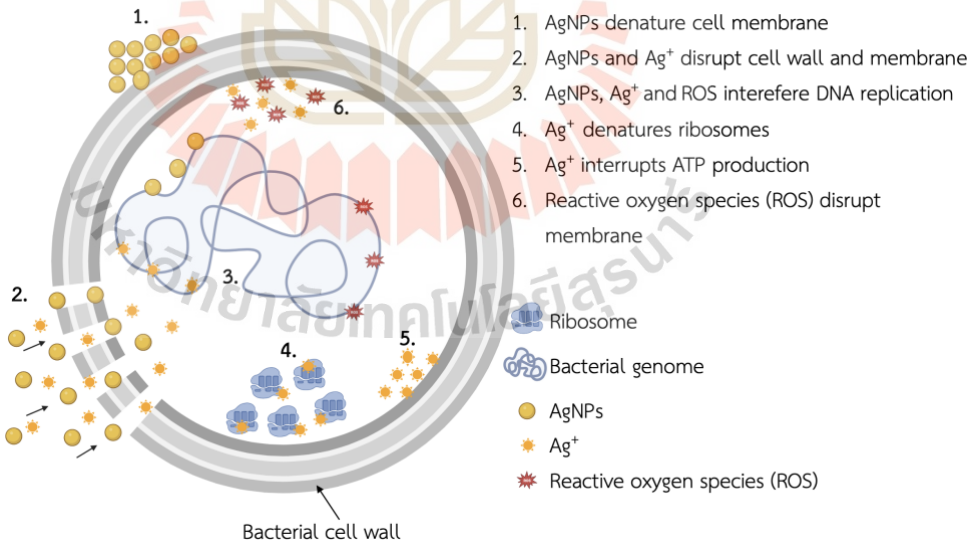

Figure 3.1 The antibacterial mechanism of silver nanoparticles (AgNPs) modified from (Yin et al., 2020)

Silver nanoparticles could be prepared via physical, chemical, green synthetic, and biological methods. The physical methods result in low yields. The chemical

reduction of a silver salt in aqueous media is a common method for producing AgNPs with reducing compounds such as sodium borohydride ($NaBH_4$)(Banne et al., 2017; Kandarp Mavani, 2013), trisodium citrate ($Na_3C_6H_5O_7$) (Ahari et al., 2018; Kamat, 2004 ; Mamun Ur Rashid, 2013), glucose ($C_6H_{12}O_6$), hydrazine (N_2H_4), and ascorbate ($C_6H_7O_6$) (Marambio-Jones & Hoek, 2010). Trisodium citrate was commonly used as a reducing and stabilizing agent for silver nitrate to produce AgNPs (Dlugosz et al., 2012). The citrate reduction of silver colloids serves the dual role of the reductant and stabilizer. The silver particles prepared by the citrate reduction method were relatively large-sized (50-100 nm) with well-defined facets (Kamat, 2004). AgNPs can be also green synthesized from plant-extracted chemicals and biologically obtained from yeast extracts (Barabadi et al., 2021; Talank et al., 2022; Truong et al., 2022). Preferred particle size and distribution, and morphology of the AgNPs can be obtained via the chemical techniques. By utilizing low toxic chemicals as reducing agent, and stabilizing agent in reduction chemical method, the harmful effects on the environment and hazardous by-products will be reduced.

Owing to growing concerns about antibiotics resistance, incorporating AgNPs into different matrices/supporters/carriers has emerged as an effective way to produce materials with high antimicrobial efficiency. AgNPs incorporated into polymer matrices are currently a popular type of nanocomposite with excellent antimicrobial properties. Antimicrobial polymer composites can be applied in food packaging containers (Echegoyen & Nerin, 2013), food packaging films (Omerovic et al., 2021), wound dressing materials (Kalantari et al., 2020; Kwiatkowska et al., 2022), and other antimicrobial applications (Dallas, Sharma, & Zboril, 2011; Zhang, Liu, Shen, & Gurunathan, 2016) owing to their outstanding antimicrobial activity. One of the main challenges in producing this type of antimicrobial is the synthesis of stable nanoparticles, as their antimicrobial effectiveness greatly depends on their size, size distribution, and agglomeration state (J. L. Castro-Mayorga et al., 2014). Notably, the most common application problem involves the agglomeration and diffusion of these nanoparticles into a polymer matrix, which reduces antibacterial activity. To prevent agglomeration and maintain the long-lasting antimicrobial activity of AgNPs, porous micro $CaCO_3$ particles in vaterite polymorph have been used as carriers for metallic

nanoparticles (Apalangya et al., 2014; Dlugosz et al., 2012; C. Wang et al., 2006). Lei et al. synthesized vaterite $CaCO_3$ in the presence of poly (sodium 4-styrene-sulfonate) of a specific size and morphology (Lei et al., 2006). Using porous micro $CaCO_3$ particles as carriers or supports, the antimicrobial activity of the active AgNPs can be prolonged owing to reduced agglomeration of the nanoparticles as well as limiting contact of AgNPs with the human body (Dlugosz et al., 2012). Moreover, chemical, and physical techniques for synthesizing $CaCO_3$ containing AgNPs as hybrid particles must be made greener using either low-toxicity chemicals or raw materials from bioresources for sustainability.

Chicken eggshells from household waste are extensively used as a replacement for mineral calcium carbonate in several applications such as plastic and elastomer fillers, heavy metal absorbents, dye removal bio-calcium supplements, concrete replacement and biodiesel oil catalysts (Boyjoo et al., 2014). Eggshells are readily available with a high $CaCO_3$ content (94 wt%), in the form of calcite polymorph (Hassan et al., 2013; Maxwell T. Hincke1, 2012) with 7000 and 17000 pores (Kinayturk et al., 2021; Rahn et al., 1987) and the smallest pore size of 3-13 μm (Kinayturk et al., 2021; Rahn et al., 1987). In addition, chicken eggshells contain other inorganic compounds including magnesium carbonate (1%), calcium phosphate (1%), and organic matter (4%) (Tsai et al., 2008). Eggshell waste can be used as an alternative and green precursor for hybrid particles of AgNPs and $CaCO_3$.

The number of patents on eggshell applications has increased exponentially in the last seven years, from 150 in 2014 to 250 in 2020, emphasizing biotechnological applications involving biomedical, chemical, engineering and environmental technology (Ahmed et al., 2021). One of the biotechnological applications of eggshell calcium carbonate is as a hybrid particle. The ceramic-ceramic and ceramic-metal hybrid particles exploit the advantages of the synergistic function of the compositions of the hybrid particles. For example, TiO_2/SiO_2, a ceramic-ceramic hybrid particle, can be applied as a functional filler for elastomers and possesses the advantages of photocatalytic properties and antimicrobial biomaterials by TiO_2, as well as high thermal stability and excellent mechanical strength by SiO_2 (Teamsinsungvon et al., 2022). For ceramic-metal hybrid particles, $AgNPs/CaCO_3$, could be utilized as an

antimicrobial agent with $CaCO_3$ acting as an AgNPs carrier and AgNPs as an active antimicrobial agent. The $CaCO_3$ carrier also improves the distribution and distributive of AgNPs (Apalangya et al., 2014; Dlugosz et al., 2012).

The patent filed by Yang et al. disclosed a method to produce hybrid particles of AgNPs and $CaCO_3$ using eggshells as a template. Eggshells were pulverized and loaded with Ag^+, followed by heating at 400—600 °C. The resultant hybrid particles can be utilized for various applications including catalysis, tissue engineering, coatings, and the production of antibacterial agents, pigments, and ceramics (Dapeng, Bin, & Minghuan, 2017). Nevertheless, the proposed method consumes a large amount of energy while heating up to 600 °C. Hassan et al. prepared eggshell $CaCO_3$ platelets using a combination of mechanochemical and sonochemical techniques. The obtained $CaCO_3$ platelets had particle sizes, BET surface areas, and pore volumes of 10 nm, 43.69 m^2/g (Hassan et al., 2013), and 0.164 cm^3/g (Mensah, Abdelmageed, & Shokry, 2022), respectively. Apalangya et al. employed a mechanochemical milling technique to deposit spherical AgNPs with a diameter of 5-20 nm onto the surface of micron-sized ground eggshells with crystal polymorphs of calcite (Apalangya et al., 2014). They also mentioned that macromolecular proteins and functional groups in the eggshells, such as hydroxyl, carboxyl, and amino functional groups could stabilize and immobilize AgNPs onto the surfaces of eggshell particles. However, the morphology of the ground eggshells obtained using the mechanochemical milling technique is platelet-shaped, resulting in the anisotropic properties for the hybrid particles. Zapotoczny et al. prepared hybrid particles of AgNPs and $CaCO_3$, for sustained release applications, using a calcium nitrate and sodium carbonate solution for co-precipitation in the presence of freshly prepared silver colloids (Dlugosz et al., 2012). The particle size of the AgNPs was 10-30 nm. However, crystal polymorphs of the co-precipitated $CaCO_3$ have not yet been reported.

In addition to the above-mentioned techniques involving the preparation of ground eggshell powders, and hybrid particles of AgNPs and eggshell $CaCO_3$; and AgNPs and mineral $CaCO_3$, this article proposes a two-step method using the green raw material of bio-eggshell waste to prepare hybrid particles of AgNPs and $CaCO_3$ as antimicrobial agents. The two-step method comprised silver colloids preparation and

silver colloids/eggshell $CaCO_3$ co-precipitation. Using the two-step method, the specific particle size, size distribution, and morphology of the hybrid particles of AgNPs and eggshell $CaCO_3$ were chemically controllable with a higher BET specific surface area and pore volume.

In this study, AgNPs were used as an active gent against the growth of bacteria contaminating fresh beef due to their highly effective antimicrobial activity against a wide spectrum of Gram-negative and Gram-positive bacteria, biocompatibility, and low production cost. Vaterite calcium carbonate was prepared from eggshell and functioned as the AgNPs carrier due to its, porous structure, isotropic property, and nontoxicity. To prepare the hybrid particles of AgNPs and vaterite calcium carbonate (AgNPs/e$CaCO_3$), AgNPs were freshly synthesized by a chemical reduction method using trisodium citrate, a low toxicity chemical, and then deposited in situ into micro-sized eggshell calcium carbonate particles during precipitation. In addition, hybrid particles of AgNPs loaded with commercial calcium carbonate (AgNPs/$CaCO_3$) were comparatively prepared. Furthermore, the effect of precipitation temperature on the particles size and size distribution of AgNPs/e$CaCO_3$ was investigated. The hybrid particles were characterized using Field Emission Scanning Electron Microscopy (FESEM), Transmission Electron Microscopy (TEM), and Energy Dispersive X-ray Spectroscopy (EDS, EDX) to monitor particle size and size distribution; particle morphology; and silver content, respectively. Dynamic Light Scattering (DLS) technique was also employed to study the hydrodynamic radius of the AgNPs. BET analysis was used to determine the specific surface area, pore volume, and pore diameter of the particles. Finally, the antimicrobial activities of silver colloids, AgNPs/e$CaCO_3$ particles, AgNPs/$CaCO_3$ particles, and precipitated e$CaCO_3$ particles against beef-extracted bacteria were compared using a modified Kirby–Bauer disc diffusion assay. Soon, AgNPs/eCaCO3 particles will be incorporated into a biodegradable poly (lactic acid) using the electrospinning method for antimicrobial food packaging. Using eggshell as a precursor for preparing $Ca(NO_3)_2$ in precipitating vaterite calcium carbonate for carrying AgNPs. has not been previously reported. Effect of the eggshell precipitation temperature has not been studied, as well. This study offers the novel co-precipitation technique for preparing hybrid particles of AgNPs and micron-sized vaterite calcium

carbonate using bio-green source chicken eggshell with the determined mixing step and temperature to control the size of AgNPs, and morphology and size of vaterite calcium carbonate. For the hybrid particles aiming as antimicrobial agents in beef packaging, AgNPs function as active antimicrobial agents and vaterite calcium carbonate as carriers or supporters.

3.3 Materials and Methods

3.3.1 Materials

Chicken eggshells (ES) were obtained from household waste and commercial calcium carbonate particles were obtained from Sand and Soil Industry Co., Ltd. Silver nitrate (≥ 99.0%, ACS reagent), sodium carbonate (≥ 99.5%, ACS reagent), sodium citrate tribasic dihydrate (trisodium citrate) (≥ 99.0%, ACS reagent) and poly (sodium 4-styrenesulphonate) (PSS, average M_w ~ 70,000 g/mole) were obtained from Sigma Aldrich. Nitric acid (65%, AR Grade) was purchased from ANaPURE. Plate count agar (PCA) and peptone were purchased from HiMedia Laboratories Pvt. Ltd and Sisco Research Laboratories Pvt. Ltd, respectively. Unpacked fresh beef and vacuum-packed fresh beef ("MAX BEEF") were purchased from a local fresh market and a Home-Fresh Mart supermarket, respectively.

3.3.2 Preparation of eggshell powder

Household waste eggshells were washed with tap water and boiled in a rice cooker at 100 °C for 4 h. Subsequently, eggshell membranes were peeled off. The eggshells were crushed into small pieces and dried at room temperature for 24 h. To obtain fine eggshells pieces, a grinding machine (Retsch, SR300) was used to reduce the initial size of the dried eggshells. To remove all the remaining biomacromolecules, such as the eggshell membrane, the eggshell powder was washed with water at least five times and then dried in an oven at 60 °C for 24 h. Ball milling with different ball sizes was used for further size reduction. After 24 h of ball milling, the eggshell powder was sieved through No.500 and No.450 sieves, to obtain particle size of 25-32 μm.

3.3.3 Preparation of calcium nitrate solution

To prepare the calcium nitrate solution, 102 g of eggshell powder (ESP) was dissolved in 1000 mL of 2 M nitric acid solution. After the ESP was completely dissolved, titration was performed with a 0.50 M sodium hydroxide solution using phenolphthalein as an indicator to determine the exact molarity of the calcium nitrate solution, after which the pH of the solution was adjusted to neutral using a 0.50 M sodium hydroxide solution. To obtain a molarity equivalent to that of sodium carbonate solution, the calcium nitrate solution was diluted to 0.03 M concentration.

For comparison, 100 g of commercial calcium carbonate was dissolved in a 2 M nitric acid solution. To get 0.03 M calcium nitrate solution from commercial calcium carbonate, the same procedure mentioned in the previous paragraph was performed.

3.3.4 Preparation of silver nanoparticles deposited on eggshell $CaCO_3$ and commercial calcium carbonate

Hybrid particles of silver nanoparticles (AgNPs) deposited on eggshell $CaCO_3$ and commercial calcium carbonate were prepared using a co-precipitation method, as described by Zapotoczny et al. (Dlugosz et al., 2012). First, to prepare the silver colloids, 45 mg of silver nitrate was dissolved in 250 mL of deionised (DI) water, and then 5 mL of 1 (w/v)% trisodium citrate was added. The reaction mixture was placed in an ultrasonic bath and heated at 70-72 °C for 60 min.

At the same time, PSS was dissolved in DI water to get a 4.8 g/L PSS solution and a 0.03 M sodium carbonate solution was prepared. Then, 20 mL of the freshly prepared silver colloids was simultaneously mixed with 50 mL of 0.03 M $Ca(NO_3)_2$ solution prepared from either eggshell calcium carbonate or commercial calcium carbonate and 50 mL of 0.03 M Na_2CO_3 solution with the addition of 15 mL of PSS (4.8 g/L). The mixture was then sonicated for 5 min at 25 °C. The obtained particles were washed with deionized water and centrifuged at 4,000 rpm for 5 min to remove the excess silver. The washing process was repeated thrice, and the obtained particles were dried under vacuum at 40 °C for 24 h. AgNPs/e$CaCO_3$ and precipitated

$eCaCO_3$ were also prepared at a sonication temperature of 35 °C via the same procedure.

3.3.5 Sample characterization

The particle morphology and size of AgNPs, precipitated $eCaCO_3$, AgNPs/$eCaCO_3$, and AgNPs/$CaCO_3$ were determined using a Field Emission Scanning Electron Microscope (FE-SEM, JEOL JSM 7800F) with an accelerating voltage of 3.0 kV. Prior to observation, each sample was coated using a gold sputter coater (Neo-Coater, MP-19020NCTR) for 2 min. The diameter of the particles was measured from the SEM micrographs using an analysis software (Image J) and calculated by randomly selecting 200 particles. MATLAB R2022a was used to obtain the mean diameter, size distribution, and histogram.

Moreover, the morphology and elemental composition of the AgNPs, precipitated $eCaCO_3$, AgNPs/$eCaCO_3$, and AgNPs/$CaCO_3$ were investigated using a Transmission Electron Microscope (TEM, Thermo scientific Talos F200X) coupled with energy dispersive X-ray spectroscopy (EDX). The morphology and size distribution of the nanoparticles from the TEM micrographs were recorded digitally, and the elemental composition of the particles was determined by EDS in the mapping mode using Velox software. Samples for TEM were prepared by depositing a drop of each sample in distilled water on a carbon-coated standard copper grid (200 meshes) and allowed to dry before investigation.

The crystal polymorphs of the ground eggshells, precipitated $eCaCO_3$, and hybrid particles were determined by an X-ray diffraction analyzer (XRD, Bruker D8 ADVANCE). The study was carried out in a 2θ range of 5-80° with a voltage of 40 kV, current of 40 mA, and a Cu Kα (1.5606 Å) radiation source.

To study the decomposition temperature of ground eggshells and precipitated $eCaCO_3$ prepared at 35 °C, a thermogravimetric analyzer (TGA, Mettler Toledo, TGA/DSC1) was employed. The samples were heated from 35 to 1000 °C at a heating rate of 10 °C /min under nitrogen atmosphere.

The hydrodynamic particle size and Polydispersity Index (PDI) of silver colloids and AgNPs, was determined by dynamic light scattering analyzer (DLS, Malvern Instruments Zetasizer Nano ZS). The measurements were carried out in triplicate at 25

°C with laser wavelength of 633 nm, beam back scattering angle of 173° and DI water's refractive index of 1.330.

The BET surface area and porosity of all particles were measured using a BET analyser (Micromeritics 3Flex). All samples were degassed at 40 °C for 24 hunder vacuum before examination.

3.3.6 Antimicrobial test

To examine the antimicrobial efficiency of the hybrid silver nanoparticles/calcium carbonate particles on beef-extracted bacteria, a modified Kirby–Bauer disc diffusion assay was performed as follows. Bacteria were extracted from two types of beef, unpacked beef available at a local market and vacuum-packed beef available at a supermarket ("MAX BEEF" brand). The beef loaf was cut into small pieces and kept at room temperature for 18 h. The powdered forms of precipitated $eCaCO_3$, AgNPs/$eCaCO_3$, and AgNPs/$CaCO_3$ were dispersed in sterile deionized (DI) water and kept at 4 °C overnight. Plate count agar (PCA) powder of 2.35 g was completely dissolved in 100 mL sterile DI water using a hot plate. Next, the PCA solution was sterilized, and then poured into sterile petri dishes after the solution and the dishes were cool down to 45-50 °C. Approximately 25 g of spoiled beef was blended with 225 mL of 0.10% sterile peptone water using a Stomacher laboratory blender for 6 min. The obtained beef extract was smeared onto plate count agar using a sterile cotton swab. Four sterile circular Whatman filter paper discs (6 mm diameter) were placed onto the smeared agar plate and impregnated with 5 µL of precipitated $eCaCO_3$, freshly prepared silver colloids (silver colloids at 0 h), AgNPs/$eCaCO_3$, and AgNPs/$CaCO_3$. The test was performed at particle concentrations of 500 mg/mL, 250 mg/mL, and 125 mg/mL. The plates were incubated at 37 °C for 24 h. After that, each inhibition zone diameter was monitored, and digital images of the antimicrobial zone were taken. The diameters were averaged from the three measurements. The antimicrobial test was performed in triplicate and the average diameter of the inhibition zone with standard deviation was calculated.

3.3.7 Cytotoxicity testing (MTT assay)

First, the initial concentration of polymer film (0.25 g/5mL or 50 mg/mL) for human dermal fibroblast (HDF) treatment were prepared. The powder samples (AgNPs/e$CaCO_3$ and AgNPs/$CaCO_3$) were weighed and placed into sterile petri dishes under individual conditions. Next, these samples were disinfected by UV light sterilization for 15 min. The culture medium DMEM (Dulbecco modified Eagle medium with 4.5 g/L glucose) supplemented with 1% penicillin/streptomycin was added to the polymer and incubated overnight at 25 °C. After incubation, the solution was collected into 15 mL centrifuge tubes prior to treatment.

MTT is a colorimetric assay used to measure the cell viability. The cellular enzymes reduce the tetrazolium dye, MTT (3-(4,5-dimethylthiazol-2-yl)-2,5-diphenyl-2H-tetrazolium bromide), to its insoluble product (formazan) giving a purple color. In this study, MTT assay was used to determine the effect of powder (AgNPs/e$CaCO_3$ and AgNPs/$CaCO_3$) on viability of human dermal fibroblast (HDF) cells. Briefly, HDF cells were seeded on 96-well plates at a density of 7×10^4 cells/well. Cells were then treated with the indicated samples at various concentrations for 24 h. Then, MTT solution was added to each well and incubated at 37°C in the dark for 4 h. After that, the formazan crystals were dissolved with dimethyl sulfoxide (DMSO) and the absorbance of formazan solution was detected at 570 nm using a microplate reader (BMG Labtech, Ortenberg, Germany). The IC50 (50% inhibitory concentration) was calculated from the dose-response curve of percent viability (Y axis) versus concentration tested (X axis) with a linear regression using Microsoft Excel. All experiments were performed in triplicates, and data were expressed as mean ± standard deviation. Statistical analysis was performed using a student's t test (SPSS version 26.0, SPSS Inc., USA) to compare means from two independent sample groups. *$p < 0.05$, **$p < 0.01$ and ***$p < 0.001$ were considered statistically significant.

3.4 Results and Discussion

3.4.1 Characteristic of silver nanoparticles

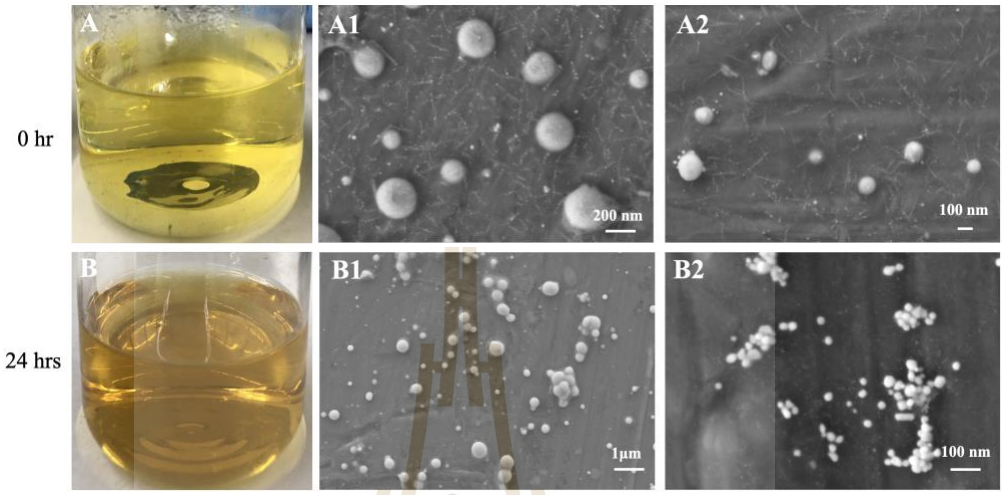

Figure 3.2 The image of freshly prepared silver colloids (silver colloids at 0 h) (A) and SEM micrographs of AgNPs obtained from the silver colloids at 0 hwith a magnification of 50 kX (A1) and 50 kX (A2). The image of silver colloids at 24 h(B) and SEM micrographs of AgNPs obtained from the silver colloids at 24 hwith a magnification of 10 kX (B1) and 100 kX (B2).

The optical micrographs in Fig. 3.2A-B show images of the silver colloids over time. Freshly prepared silver colloids are clear and light-yellow, resulting in both large and exceedingly small silver nanoparticles (AgNPs) of approximately 100-200 nm and 1 nm, respectively, as shown in Fig. 3.2A1 and 3.2A2. However, after being left at room temperature for 24 h, the silver colloids became dark brown (Fig. 3.2B) because the small nanoparticles became larger. The AgNPs began to grow over time, as confirmed by the SEM micrographs shown in Fig. 3.2B1 and 3.2B2. Agglomeration can also be observed in the SEM micrograph shown in Fig. 3.2B2.

TEM micrographs, EDS mapping images and EDX spectrum of AgNPs obtained from freshly prepared silver colloids are shown in Fig. 3.3. The TEM micrographs showed the spherical morphology of AgNPs, as also observed from SEM in Fig. 3.2, and the particle size range of with 9-13 nm with an average size of 24.13 ± 2.95 nm, as illustrated in Fig. 3.3H. Particles with diameters of less than 10 nm were

observed as small white dots. The EDS image mapping and EDX spectrum in Fig. 3.3C-G illustrate that the particles were mainly composed of silver. Large-sized (50-100 nm) silver crystallites were found using trisodium citrate as a reducing and stabilizing agent (Kamat, 2004). Arif et al. also studied the synthesis of silver nanoparticles in the presence of trisodium citrate, resulting in diameters of approximately 40 nm AgNPs (Arif, Ulfiya, Erwin, & Panggabean, 2021). According to the smaller particle size and lesser agglomeration, AgNPs obtained from the freshly prepared silver colloids were further used to prepare AgNPs-loaded calcium carbonate particles as antimicrobial agents.

The freshly prepared silver colloids contained the Z-average (r.nm) of 42.14 nm and PDI of 0.21, as observed from Fig. 3.3I. The hydrodynamic size distribution curve of freshly prepared silver colloids, shown in Fig. 3.3I, shows three peaks at 50.05, 10.34 and 1.20 nm. This distribution curve corresponded well with their TEM micrograph in Fig. 3.3A, showing three different sizes of the particles. In addition, the Z-average size (r.nm) and PDI of AgNPs, obtained from the freshly prepared silver colloids, were 55.07 and 0.19, with two peaks at 69.56 and 11.05 nm as illustrated by the hydrodynamic size distribution curve in Fig. 3.3J. The 1 nm AgNPs might be extracted out during the centrifugal separation as a result there are two particle size ranges observed from the distribution curve. Soliwoda et. al. (Ranoszek-Soliwoda et al., 2017) prepared AgNPs at 100 °C using trisodium citrate as a capping agent. They reported hydrodynamic size (d.nm) of the prepared AgNPs in ranges of 9 ± 2 nm and 58 ± 20 nm, with PDI of 0.50, and the particle size of the AgNPs observed from STEM in ranges of 5-45 nm and larger than 100 nm.

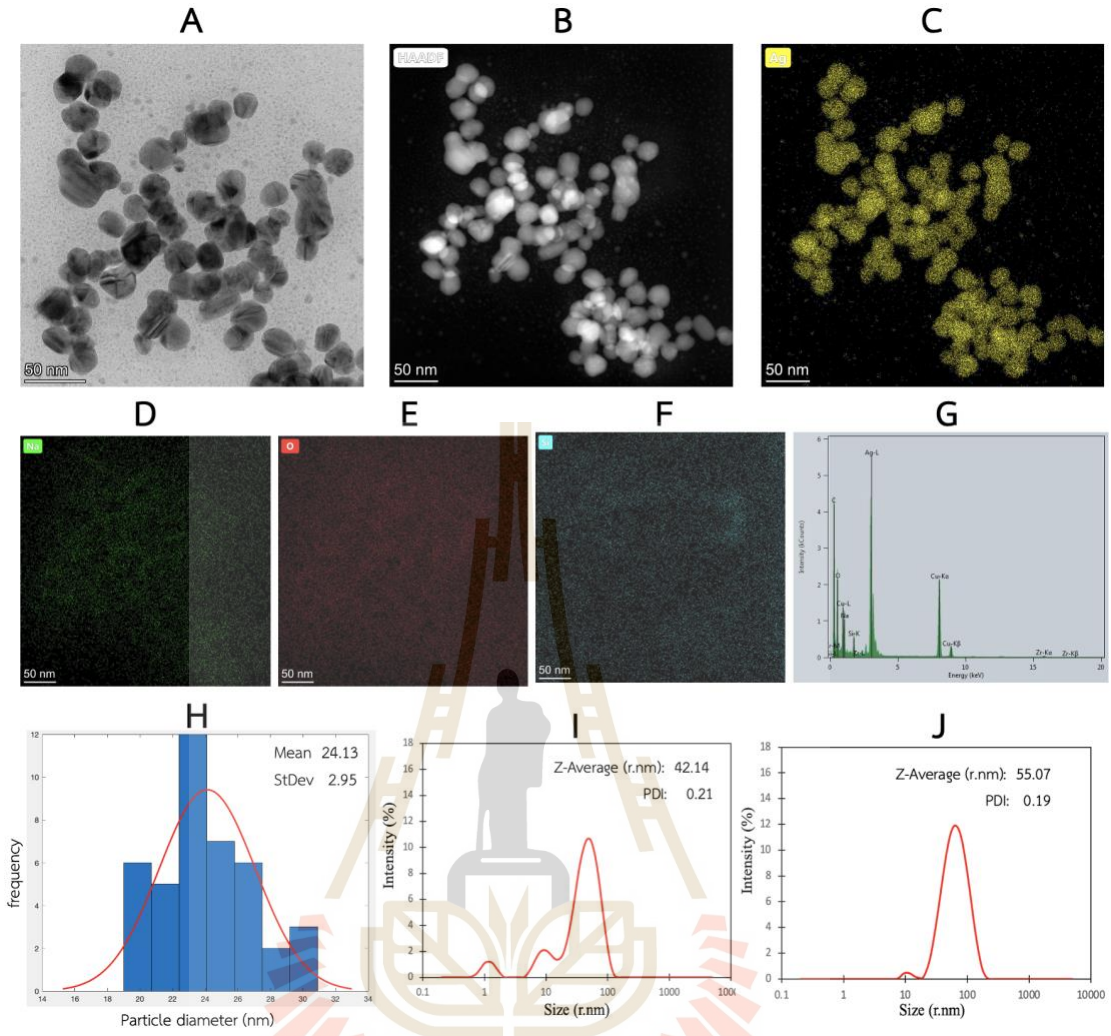

Figure 3.3 TEM micrograph (A), High-angle annular dark-field imaging (HAADF)(B), Silver (Ag) EDS image mapping (C), Sodium (Na) EDS image mapping (D), Oxygen (O) EDS image mapping (E), Silicon (Si) EDS mapping (F), EDX spectrum (G) and a particle size distribution curve (H) of AgNPs obtained from freshly prepared silver colloids, and the hydrodynamic size distribution curves of (H) and AgNPs obtained from (I) freshly prepared silver colloids.

Zeta potential of freshly prepared silver colloids and AgNPs obtained from freshly prepared silver colloids were - 49.30 mV and - 44.10 mV, respectively which were shown in Fig. 3.4A-B. Similar negative zeta potential of - 44.6 mV was observed for chemically synthesized AgNPs using trisodium citrate as reducing agent (Dasaradhudu & Arunachalam Srinivasan, 2020). The presence of negative charge on

the surface of AgNPs cause repulsion among them and prevent the agglomeration, hence provide the stability to the AgNPs (Gola et al., 2021).

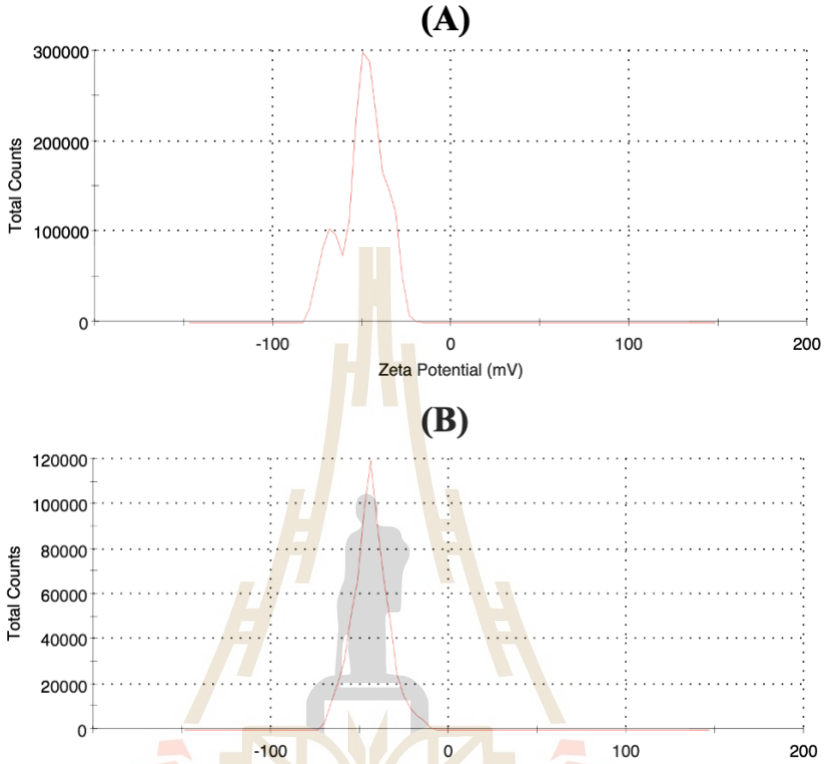

Figure 3.4 Zeta potential distribution of (A) and AgNPs obtained from (B) freshly prepared silver colloids.

3.4.2 Characteristic of precipitated eggshell calcium carbonate ($eCaCO_3$) particles

SEM micrographs in Fig. 3.5A-C show spherical morphology and a broad particle size distribution of precipitated $eCaCO_3$ particles prepared at 35 °C, with a mean diameter of 3.55 ± 1.32 µm. The mechanism of $CaCO_3$ formation involves the creation of nanometre-sized crystallites in the first stage which later aggregate to form micrometer-sized superstructures (Dlugosz et al., 2012). According to the XRD pattern in Fig. 3.5D, crystal polymorphs of the precipitated $eCaCO_3$ prepared at 35 °C was vaterite whereas that of the ground eggshells was calcite. Sutapun et al. also reported that ground eggshells were mainly composed of a calcite crystal structure (Sutapun, Ruksakulpiwat, Suppakarn, Jeencham, & Aontee, 2011). The vaterite crystal structure is

formed when $CaCO_3$ is precipitating in the presence of poly (sodium 4-styrenesulphonate) (PSS) as a polyelectrolyte. Lei et al. studied precipitating vaterite $CaCO_3$ from 0.5 M $CaCl_2$ and 0.5 M Na_2CO_3 and 70,000 g/mole and 1 g/L PSS at pH 10 and the obtained $CaCO_3$ particles were vaterite polymorph with micron-sized spherical shapes. It was deduced that PSS initiated vaterite nucleation through the binding of calcium ions to anionic sulfonate groups, and stabilized the vaterite during crystal growth (Lei et al., 2006). Azarian et al. also found that the crystal structure of precipitated calcium carbonate from calcium nitrate and sodium carbonate in the presence of polyelectrolytes was vaterite with a spherical morphology (Azarian & Sutapun, 2022). The TEM micrographs in Fig. 3.6A-B also show a broad particle size distribution. The EDS image mapping and EDX spectrum in Fig. 3.6C-F illustrated that the particles were rich in calcium carbonate.

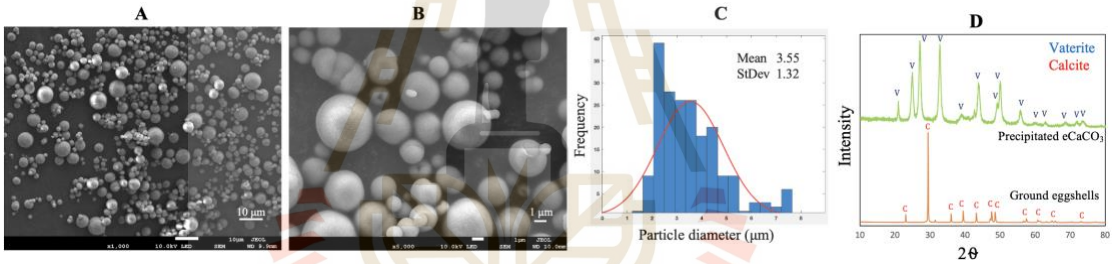

Figure 3.5 SEM micrographs with magnification of 1 kX (A) and 5 kX (B), and a particle size distribution curve (C) of precipitated $eCaCO_3$ particles prepared at 35°C, and XRD patterns of the precipitated $eCaCO_3$ particles and ground eggshells (D).

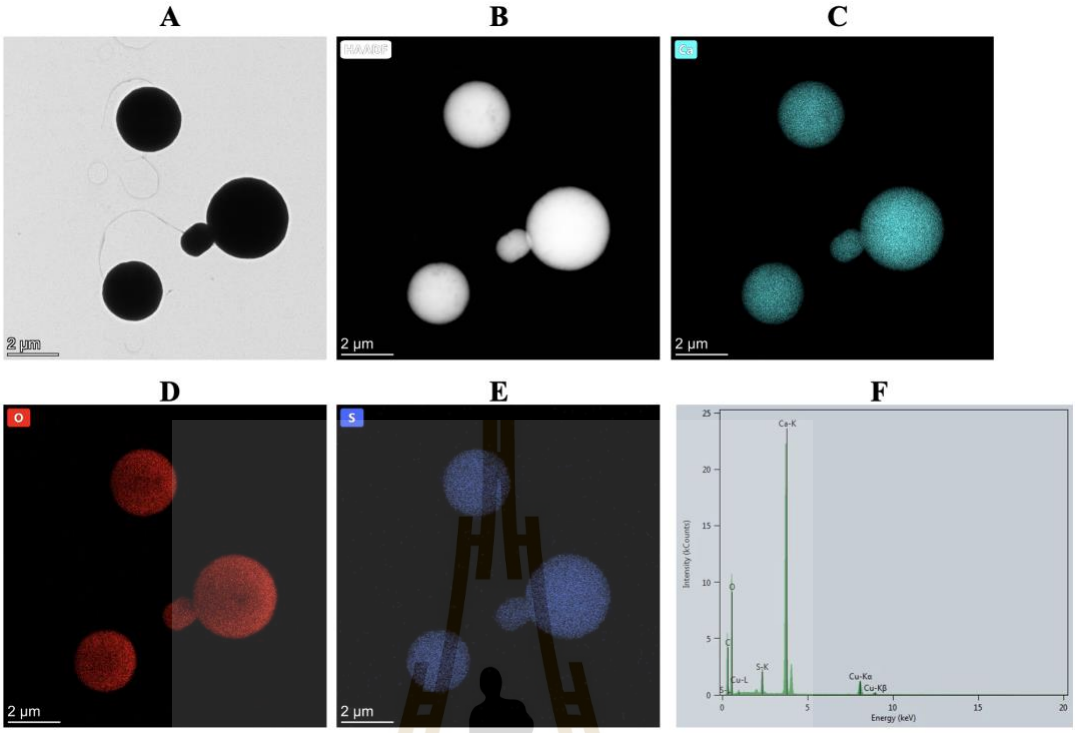

Figure 3.6 TEM micrograph (A), High-angle annular dark-field imaging (HAADF) (B), Calcium (Ca) EDS image mapping (C), Oxygen (O) EDS image mapping (D), Sulphur (S) EDS image mapping (E), and EDX spectrum (F) of precipitated $eCaCO_3$ particles prepared at 35 °C.

3.4.3 Characteristic of silver nanoparticles / eggshell calcium carbonate ($AgNPs/eCaCO_3$) particles

Fig. 3.7A-D show the particle morphology, histogram plot of particle diameter *vs* frequency and XRD spectrum for $AgNPs/eCaCO_3$ particles prepared at 35 °C. The spherical morphology of $AgNPs/eCaCO_3$ particles with a particle size distribution ranging from 1.44 to 7.38 µm and a mean diameter of 3.19 ± 1.20 µm was obtained. Fig. 3.7E-H show the morphology, histogram plot of particle diameter *vs* frequency and XRD spectrum for $AgNPs/eCaCO_3$ particles prepared at 25 °C. The XRD patterns in Fig. 3.7D and 3.7H confirm that the particles prepared at 25 °C and 35 °C were mainly composed of vaterite crystal structures. The obtained $AgNPs/eCaCO_3$ particles also showed a spherical morphology with a narrow size distribution ranging from 2.39 to 4.15 µm and a mean diameter of 3.56 ± 0.26 µm. One of the factors affecting particle size and distribution of precipitated $CaCO_3$ is crystallization temperature. At high

temperature, the crystallization is governed by kinetic factors. Mathawa et al. studied crystallization of $CaCO_3$ at 25 and 80 °C using PAA as a stabilizing agent. They stated that when the crystallization was carried out at high temperature, the dissolution of $CaCO_3$ from the surface of growing particles might be occurred and the secondary crystallization might then be formed. This secondary crystallization resulted in smaller $CaCO_3$ crystals compared to the larger primary crystals (Matahwa et al., 2008).

At an ambient temperature of 25 °C, the precipitated $eCaCO_3$ particles crystallized homogeneously with a narrow particle size distribution, and they did not form perfect spherical structure like precipitated commercial calcium carbonate particles as shown in Fig. 3.9. This is because other compositions of chicken eggshells such as magnesium carbonate (1%) and calcium phosphate (1%) might disturb the crystallization (Tsai et al., 2008).

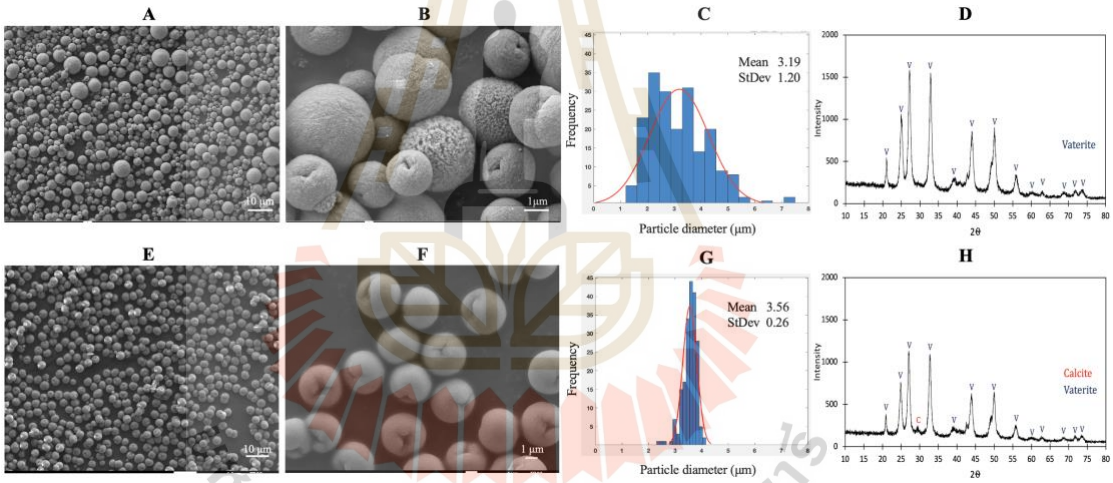

Figure 3.7 SEM micrographs with magnification of 1 kX (A) and 10 kX(B), a particle size distribution curve (C) and an XRD pattern (D) of AgNPs/$eCaCO_3$ particles prepared at 35 °C. SEM micrographs with magnification of 1 kX (E) and 5 kX (F), a particle size distribution curve (G) and an XRD pattern (H) of AgNPs/$eCaCO_3$ particles prepared at 25 °C.

TEM micrographs, EDS image mapping and EDX spectrum of AgNPs/$eCaCO_3$ prepared at 25 °C in Fig. 3.8 show that AgNPs are attached to the eggshell calcium carbonate particles. The TEM micrographs and EDS image mapping in Fig. 3.8A-C confirm the presence of AgNPs on both the surface and inside of $eCaCO_3$. AgNPs are attached to the whole particle of calcium carbonate resulting in silver

content of 0.78 wt% confirmed through EDS mapping element analysis. According to the EDX spectrum shown in Fig. 3.8G, the particles were composed solely of silver and calcium carbonate and no other impurities were observed. So, AgNPs/e$CaCO_3$ particles prepared at 25 °C were further used as antimicrobial agents against food related bacteria due to their smaller size and narrow distribution.

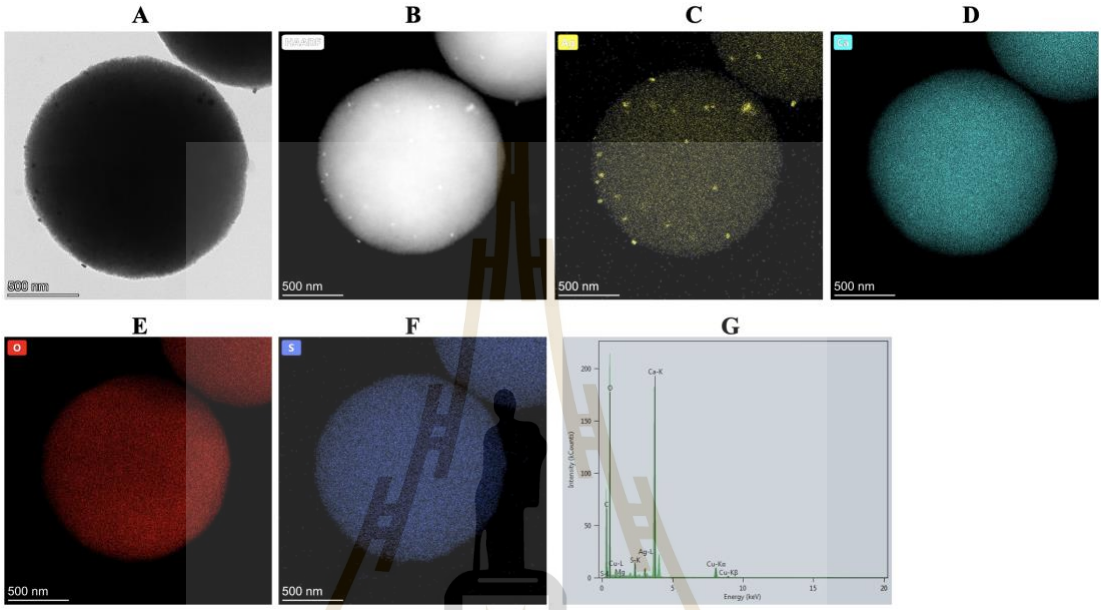

Figure 3.8 TEM micrograph (A), High-angle annular dark-field imaging (HAADF) (B), Silver (Ag) EDS image mapping (C), Calcium (Ca) EDS image mapping (D), Oxygen (O) EDS mapping (E), Sulphur (S) image mapping (F) and EDX spectrum (G) of AgNPs/e$CaCO_3$ particle prepared at 25 °C.

3.4.4 Characteristic of silver nanoparticles / commercial calcium carbonate (AgNPs/$CaCO_3$) particles

The morphology, size distribution and XRD pattern of the AgNPs/$CaCO_3$ particles are shown in Fig. 3.9A-D. According to the SEM micrographs, the AgNPs/$CaCO_3$ particles prepared at 25 °C were spherical microparticles with a particle size distribution ranging from 4.15 to 6.95 µm and a mean diameter of 5.61 ± 0.66 µm (Fig. 3.9C). The particles are dominant in the vaterite crystal structure, as shown in the XRD pattern in Fig. 3.9D. The spherical shape of the precipitated commercial calcium carbonate was loaded with AgNPs on both the surface and inside of the calcium carbonate particles as shown by the TEM micrographs and EDS image mapping in Fig.

3.10A-C with a silver content of 3.20 wt%. The EDX spectrum in Fig. 3.10G confirms that the particles contain only silver and calcium carbonate. Zapotoczny et al. prepared AgNPs loaded calcium carbonate particles at 25 °C using calcium nitrate and sodium carbonate, resulting in a particle size of 2 μm, in approximation (Dlugosz et al., 2012). In this study, AgNPs/e$CaCO_3$ and AgNPs/$CaCO_3$ prepared at 25 °C using eggshell and commercial calcium carbonate as a precursor had a mean particle size of 3.56 ± 0.26 μm and 5.61 ± 0.66 μm, respectively.

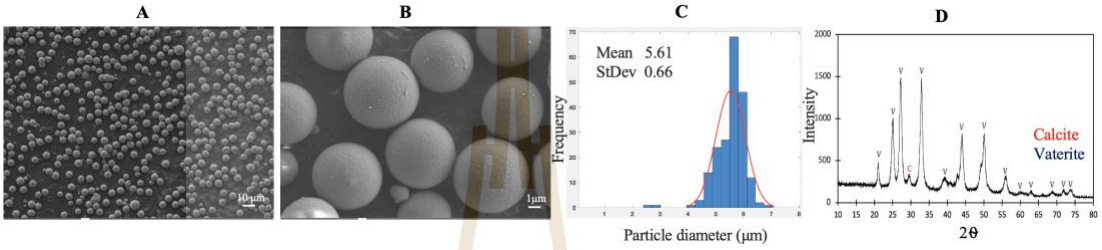

Figure 3.9 SEM micrographs with magnification of 500X (A) and 5kX (B), a particle size distribution curve (C), and an XRD pattern (D) for AgNPs/$CaCO_3$ particles prepared at 25 °C.

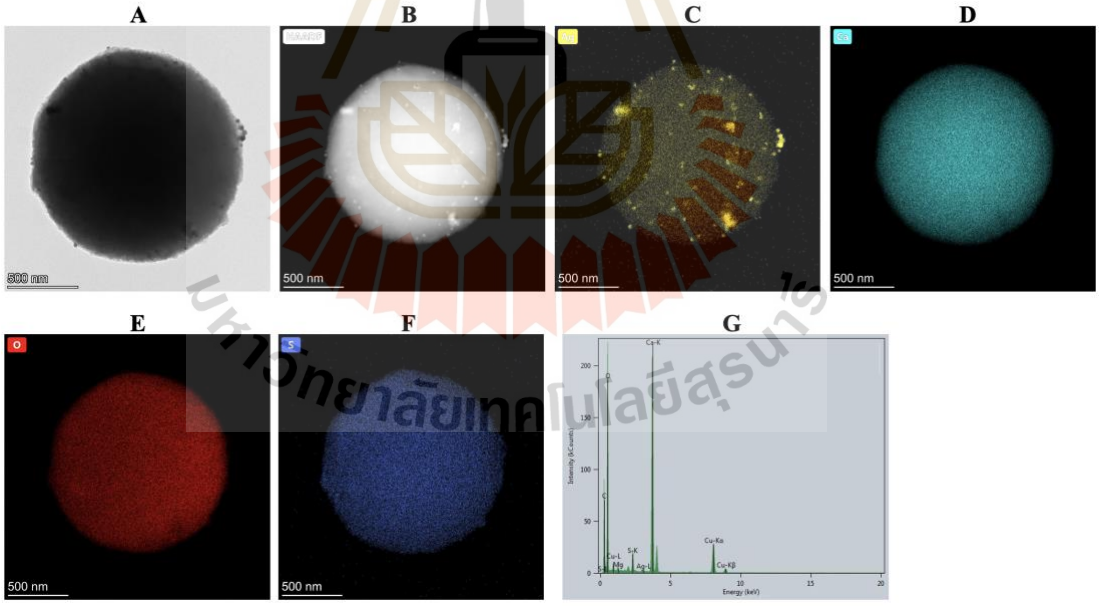

Figure 3.10 TEM micrograph (A), High-angle annular dark-field imaging (HAADF) (B), Silver (Ag) EDS image mapping (C), Calcium (Ca) EDS image mapping (D), Oxygen (O) EDS mapping (E), Sulphur (S) EDS image mapping (F) and EDX spectrum (G) of AgNPs/$CaCO_3$ particle.

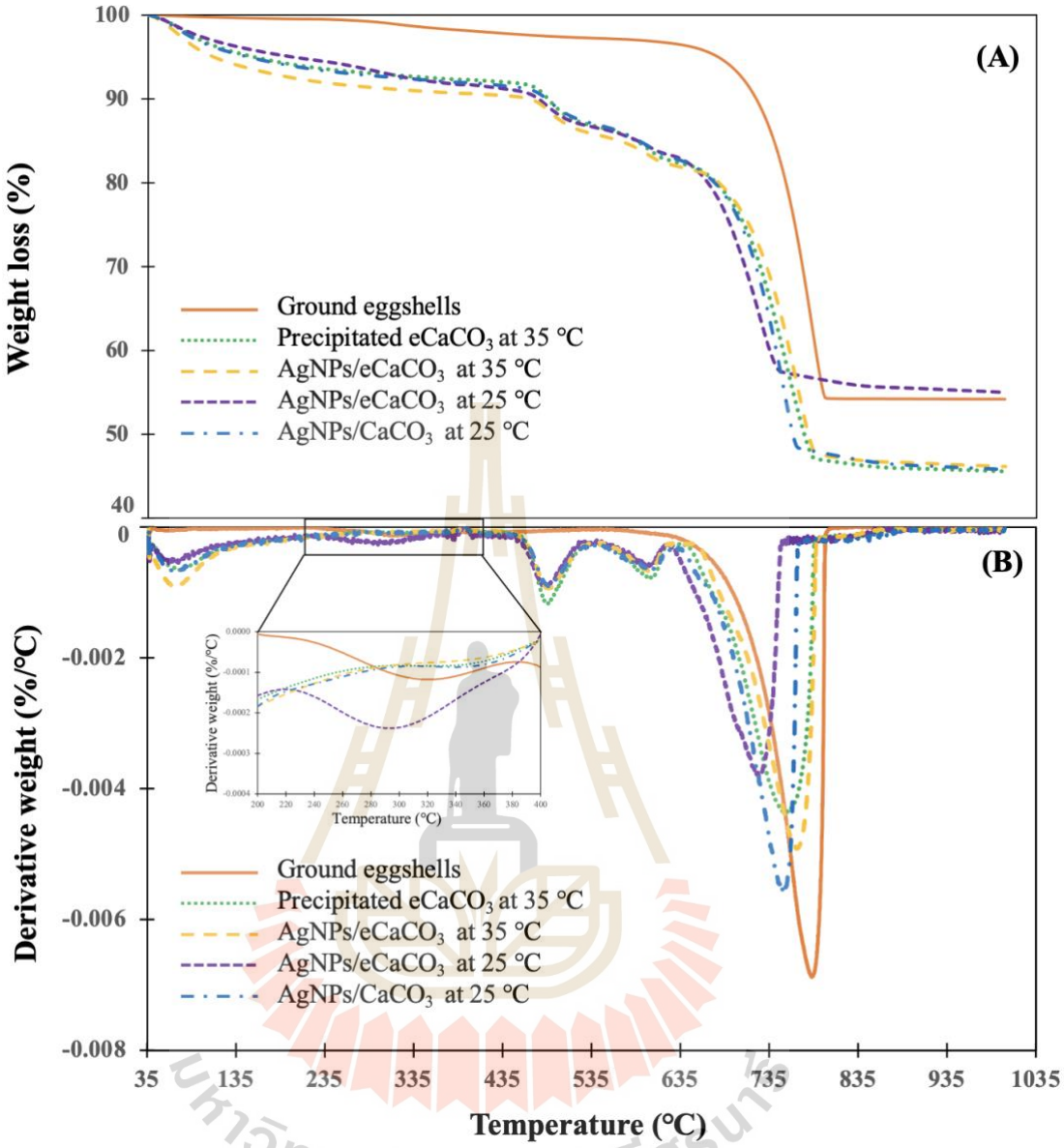

Figure 3.11 TGA curves (A) and DTGA curves (B) of ground eggshells, precipitate $eCaCO_3$ prepared at 35 °C, $AgNPs/eCaCO_3$ prepared at 35 °C, $AgNPs/eCaCO_3$ prepared at 25 °C and $AgNPs/CaCO_3$ prepared at 25 °C.

The TGA and DTGA curves of the ground eggshells, precipitated $eCaCO_3$ prepared at 35 °C, $AgNPs/eCaCO_3$ prepared at 35 °C, $AgNPs/eCaCO_3$ prepared at 25 °C and $AgNPs/CaCO_3$ prepared at 25 °C are shown in Fig. 3.11A-B. Ground eggshells exhibited three thermal transitions of mass loss. The first thermal decomposition occurred in the temperature range of 35–110 °C due to the evaporation of physically adsorbed water. The second transition in the range of 240-350 °C caused by thermal

decomposition of the eggshell matrix left in the ground eggshell. The TGA curve shows overall mass loss of 1.90% from water evaporation and eggshell matrix decomposition. Castro et al. also reported that natural eggshells showed a mass loss of 1.90% between 30-400 °C (Castro, Barañano, Pinheiro, Menini, & Pinheiro, 2019). The third mass loss occurred between 400 and 800 °C, with a DTGA peak at 783 °C and a mass loss of 45.82%. This loss is related to the CO_2 released from $CaCO_3$ decomposition. Decarbonization of chicken eggshells has been reported to occur in the temperature range of 600-850 °C (Nadia Razali1, 2022; Sutapun et al., 2011).

In the cases of precipitated $eCaCO_3$ prepared at 35 °C, AgNPs/$eCaCO_3$ prepared at 35 °C, AgNPs/$eCaCO_3$ prepared at 25 °C and AgNPs/$CaCO_3$ prepared at 25 °C, the TGA and DTGA curves show four regions of thermal decomposition with the overall weight loss of approximately 46.21%, 46.71%, 55.81% and 47.28% respectively. The first weight loss at 35-180 °C was due to the evaporation of physically adsorbed water from $CaCO_3$. The second and third decompositions in the temperature range of 430-520 °C and 550-650 °C, were derived from the thermal degradation of PSS in precipitated $eCaCO_3$. These two thermal decomposition ranges were also reported by Bahrom et al. (Bahrom et al., 2019). They reported that the thermal decomposition of precipitated $CaCO_3$ using PSS as an organic additive at 430-520 °C and 550-650 °C was due to the decomposition of PSS. The fourth thermal decomposition at 720-770 °C corresponded to the decarbonization of vaterite $CaCO_3$. Popescu et al. (Popescu, Isopescu, Matei, Fagarasan, & Plesu, 2014) and Karunadasa et al. (Karunadasa, Manoratne, Pitawala, & Rajapakse, 2019) stated that the transformation temperature range of the $CaCO_3$ into CaO occurred at 600-790 °C with a peak of 750 °C and at 700-800 °C with a peak of 790 °C, respectively. It could be concluded that there was no organic matter left in the precipitated $eCaCO_3$, AgNPs/$eCaCO_3$ and AgNPs/$CaCO_3$ and vaterite polymorph precipitated from eggshell absorbed more water than calcite polymorph of eggshell.

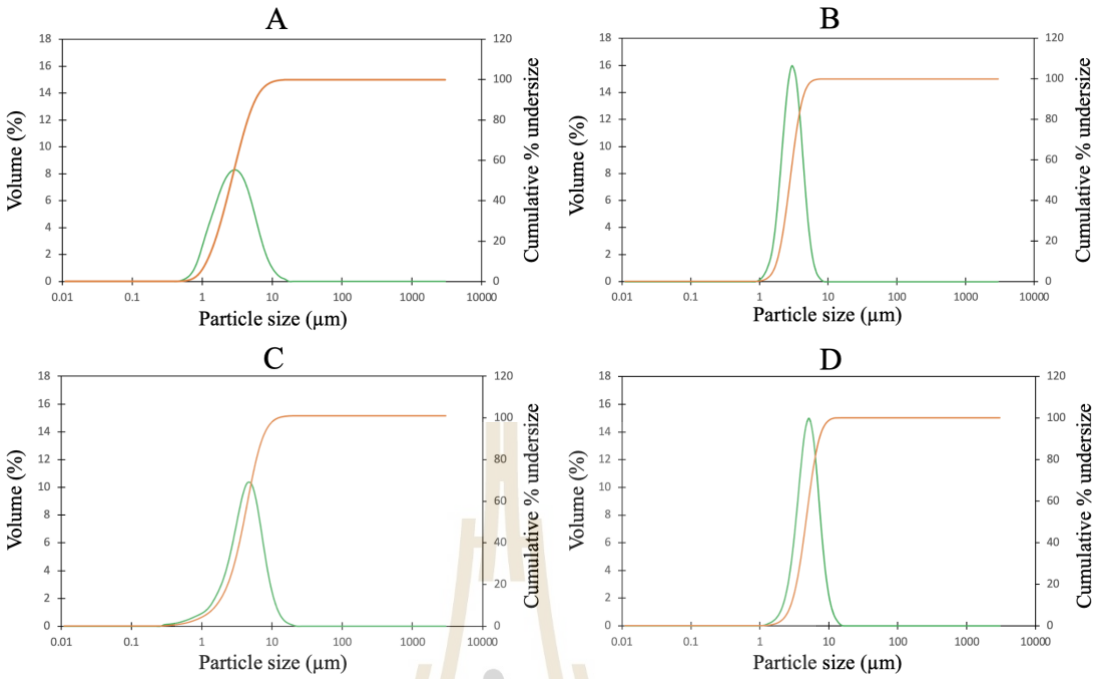

Figure 3.12 Particle size distribution of precipitated $eCaCO_3$ prepared at 35 °C (A), AgNPs/$eCaCO_3$ prepared at 35 °C (B), AgNPs/$eCaCO_3$ prepared at 25 °C (C) and AgNPs/$CaCO_3$ prepared at 25 °C (D).

Particle size distribution curves of precipitated $eCaCO_3$, AgNPs/$eCaCO_3$, and AgNPs/$CaCO_3$ as average size, [D1,0], [D5,0], and [D9,0] are shown in Fig. 3.12. and Table 3.1. The average size and distribution of those particles correspond well with their particle size and distribution observed from SEM micrographs shown in Fig. 3.5A-B, Fig. 3.7A-B, and Fig. 3.9A-B, respectively, except for AgNPs/$eCaCO_3$ prepared at 25 °C. The average particle size of AgNPs/$eCaCO_3$ prepared at 25 °C obtained from DLS technique were larger than those observed from particle morphology shown in Fig. 3.7E-F. In addition, the obtained particle size distribution was broader than that observed from Fig. 3.7E, as well. This might be due to particle agglomeration during DLS characterization.

Table 3.1 Particle size distribution of precipitated $eCaCO_3$, AgNPs/$eCaCO_3$, and AgNPs/$CaCO_3$

Particles	**Average [D3,4] (μm)**	**[D1,0] (μm)**	**[D5,0] (μm)**	**[D9,0] (μm)**
Precipitated $eCaCO_3$ prepared at 35 °C	3.36	1.51	2.60	5.87
AgNPs/$eCaCO_3$ prepared at 35 °C	3.14	1.72	2.60	3.90
AgNPs/$eCaCO_3$ prepared at 25 °C	4.69	1.51	4.47	7.70
AgNPs/$CaCO_3$ prepared at 25 °C	5.20	2.60	4.47	6.72

The specific surface area, total pore volume, and mean pore diameter of precipitated $eCaCO_3$, AgNPs/$eCaCO_3$ prepared at 35 °C, and 25 °C and AgNPs/$CaCO_3$ prepared at 25 °C were remarkably similar as shown in Table 3.2. The specific area of the hybrid particles of AgNPs and $CaCO_3$ prepared at 25 °C was higher than that prepared at 35 °C. At co-precipitation temperature of 25 °C, the specific area of AgNPs/$eCaCO_3$ was approximate the same as that of of AgNPs/$CaCO_3$. However, the mean pore diameter of the hybrid particles of AgNPs and $CaCO_3$ prepared at 25 °C was slightly smaller than that of the particles prepared at 35 °C. All particles mentioned in Table 3.2 have the same total pore volume (V) of around 0.07 m^3/g and a mean pore diameter (d_p) in a range of 3.26 - 3.78 nm.

Table 3.2 Silver content, BET specific surface area (S_{BET}), total pore volume (V), and mean pore diameter (d_p) of precipitated $eCaCO_3$, $AgNPs/eCaCO_3$, and $AgNPs/CaCO_3$

Particles	Silver content (wt%)	S_{BET} (m^2/g)	V (m^3/g)	d_p (nm)
Precipitated $eCaCO_3$ prepared at 35 °C	-	79.77	0.07	3.72
$AgNPs/eCaCO_3$ prepared at 35 °C	-	79.25	0.07	3.78
$AgNPs/eCaCO_3$ prepared at 25 °C	0.78	85.08	0.07	3.26
$AgNPs/CaCO_3$ prepared at 25 °C	3.20	85.85	0.07	3.39

3.4.5 Antimicrobial efficiency

As shown in Fig. 3.13A-C and 3.14A-C, precipitated $eCaCO_3$ (disc a) showed no inhibitory effect against bacteria extracted from unpacked beef purchased from the fresh market and vacuum-packed beef of "MAX BEEF" brand. The freshly prepared silver colloids showed slight antimicrobial activity against the bacteria extracted from the unpacked beef and the vacuum-packed beef with inhibition zone diameters of approximately 7 mm, as observed from disc 'b' in Fig. 3.13A-C and 3.14A-C, respectively. The antimicrobial efficiency of the silver colloids was lower than that of $AgNPs/eCaCO_3$ and $AgNPs/CaCO_3$. This might be caused by the agglomeration of the silver colloids within the disc, in which the dissolution of Ag^0 or Ag^+ was slower than that of the hybrid particles of $AgNPs/eCaCO_3$ and $AgNPs/CaCO_3$ (J. L. Castro-Mayorga et al., 2014). Lee et al. investigated the antimicrobial activity of AgNPs prepared at different molar ratios using the Kirby–Bauer disc diffusion assay and demonstrated a good inhibitory effect against *Escherichia coli* (*E. coli*) and *Staphylococcus aureus* (S. M. Lee et al., 2010). The antimicrobial efficiency depends on the particle size, particle size and concentration (Barabadi et al., 2021; Talank et al., 2022), and the degree of agglomeration of nanoparticles (J. L. Castro-Mayorga et al., 2014). Therefore, the superior antimicrobial activity of $AgNPs/eCaCO_3$ and $AgNPs/CaCO_3$ particles compared to that of the silver colloid was attributed to the reduced agglomeration of AgNPs,

giving rise to a better stabilized and sustained release of AgNPs from the $eCaCO_3$ and $CaCO_3$ carriers (Apalangya et al., 2014). It was reported that 20 nm AgNPs showed antimicrobial against *Escherichia coli* at MIC (minimum inhibitory concentration) of 0.621 mg/mL (Ashmore et al., 2018). In addition, 5 nm and 10 nm AgNPs exhibited MIC at 0.625 mg/mL and 1.35 mg/mL, respectively, against *Staphylococcus aureus* (Parvekar, Palaskar, Metgud, Maria, & Dutta, 2020).

In addition, AgNPs/$eCaCO_3$ and AgNPs/$CaCO_3$ showed concentration-independent antimicrobial activity against bacteria extracted from unpacked beef. The diameters of the inhibition zones at 125, 250, and 500 mg/mL were not significantly different, with an average diameter of 8-9 mm. This suggested that the optimum concentration of AgNPs/$eCaCO_3$ and AgNPs/$CaCO_3$ for inhibiting bacteria growth was 125 mg/mL. In contrast, AgNPs/$eCaCO_3$ and AgNPs/$CaCO_3$ showed concentration-dependent antimicrobial activity against bacteria extracted from vacuum-packed beef. The average inhibition diameter tended to increase with increasing the hybrid particle concentration.

The Laboratory of Cell-Based Assay and Innovation (CBAI), Suranaree University of Technology, reported that the extract from the unpacked beef contained two types of Gram-negative and one type of Gram-positive bacteria whereas the extract from the vacuum-packed beef contained one type of Gram-negative and one type of Gram-positive bacteria. The lesser types of extracted bacteria from vacuum-packed beef might be the main effect of concentration-dependent antimicrobial activity against the bacteria of the hybrid particles. However, it could be concluded that the antimicrobial efficiencies of AgNPs/$eCaCO_3$ and AgNPs/$CaCO_3$ against bacteria extracted from unpacked and vacuum-packed beef were comparable.

For the case of AgNPs/$CaCO_3$, Zapotoczny et al. studied the antimicrobial activity of AgNPs/$CaCO_3$ microparticles against *Staphylococcus* and *Candida* species and reported that the AgNPs/$CaCO_3$ showed inhibitory effects for those species (Dlugosz et al., 2012). Apalangya et al. reported that AgNPs/eggshell particles exhibited superior antimicrobial activity against *Escherichia coli* compared to that of AgNPs (Apalangya et al., 2014). The mentioned reports were in good agreement with the inhibitory effect of the hybrid particles of AgNPs/$eCaCO_3$ and AgNPs against bacteria

extracted from beef, as shown in Table 3.3. In addition, Wang et al. mentioned that *Pseudomonas fragi*, *Myroides phaeus*, and *Brochothrix thermosphacta* were bacteria found in beef (X. Wang et al., 2023) and it was reported that *E. coli* was found in raw beef, as well [56].

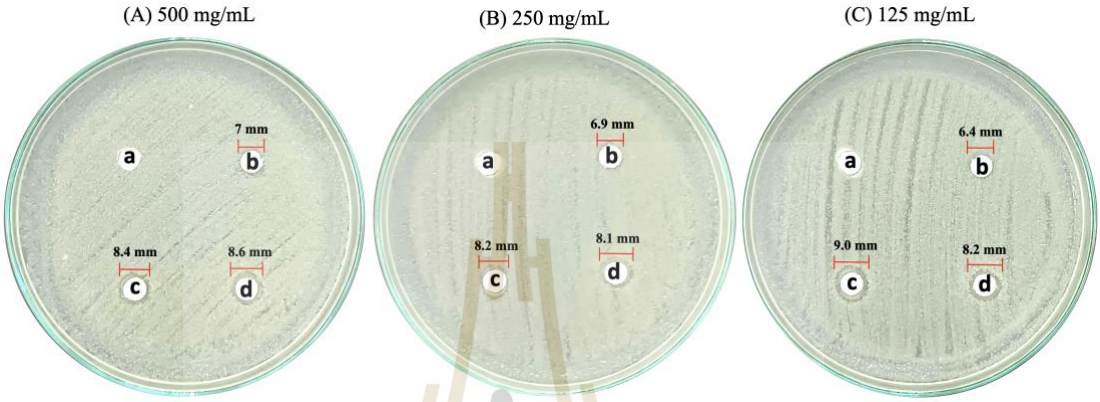

Figure 3.13 Antimicrobial activity against bacteria extracted from unpacked raw beef from a local fresh market. The discs were impregnated with precipitated $eCaCO_3$ (a), freshly prepared silver colloids (b), $AgNPs/eCaCO_3$ (c), and $AgNPs/CaCO_3$ (d), at concentrations of 500 mg/mL (A), 250 mg/mL (B), and 125 mg/mL (C).

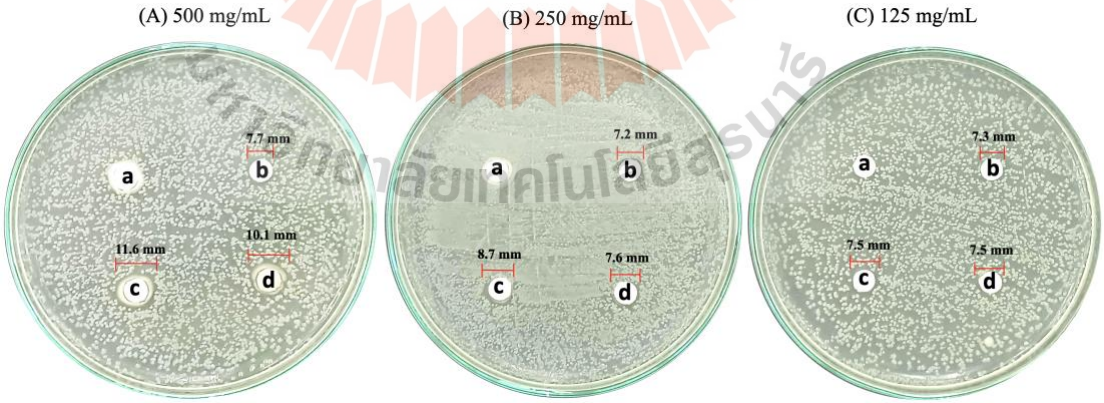

Figure 3.14 Antimicrobial activity against bacteria extracted from vacuum-packed beef (“MAX BEEF” brand). The discs were impregnated with precipitated $eCaCO_3$ (a), freshly prepared silver colloids (b), $AgNPs/eCaCO_3$ (c), and $AgNPs/CaCO_3$ (d), at concentrations of 500 mg/mL (A), 250 mg/mL (B), and 125 mg/mL (C).

The summary of the average inhibition zone diameter with standard deviation obtained from precipitated $eCaCO_3$, freshly prepared silver colloids, $AgNPs/eCaCO_3$, and $AgNPs/CaCO_3$, against extracted bacteria from the unpacked and vacuum-packed beef vs. testing concentrations are shown in Table 3.3.

Table 3.3 Inhibition zone diameter against extracted bacteria from unpacked and vacuum-packed beef using precipitated $eCaCO_3$, freshly prepared silver colloids, $AgNPs/eCaCO_3$ and $AgNPs/CaCO_3$ as antimicrobial agents.

Samples	Inhibition zone diameter (mm)					
	unpacked beef extracted bacteria			vacuum-packed beef extracted bacteria		
	500 mg/mL	250 mg/mL	125 mg/mL	500 mg/mL	250 mg/mL	125 mg/mL
Precipitated $eCaCO_3$	No effect	No effect	No effect	No effect	No effect	No effect
Freshly prepared silver colloids	6.99 ± 0.12	6.77 ± 0.12	6.57 ± 0.19	7.38 ± 0.50	7.17 ± 0.58	7.13 ± 0.33
$AgNPs/eCaCO_3$	8.76 ± 0.26	8.24 ± 0.67	8.98 ± 0.47	10.52 ± 1.06	8.56 ± 0.22	7.44 ± 0.47
$AgNPs/CaCO_3$	8.97 ± 0.49	8.09 ± 0.31	8.27 ± 0.31	10.16 ± 0.80	7.89 ± 0.81	7.45 ± 0.38

3.4.6 Cytotoxicity testing (MTT assay)

The lab report of the cytotoxicity test in Human Dermal Fibroblasts (HDF) of $AgNPs/eCaCO_3$ and $AgNPs/CaCO_3$ were shown in Fig. 3.15 and Fig. 3.16, respectively. According to Fig. 3.15B, starting from the concentration of 5 mg/mL, $AgNPs/eCaCO_3$ showed around 60 % cell viability and no alive cells were observed at 50 mg/mL shown in Fig. 3.15A. Similar results were also found at the 50 mg/mL concentration of $AgNPs/CaCO_3$ which were shown in Fig. 3.16. Significant cells dead were occurred at the concentration of 25 mg/mL (Fig. 3.16B) and no alive cells were found at the morphology of 50 mg/mL concentration of $AgNPs/CaCO_3$ shown in Fig. 3.16A.

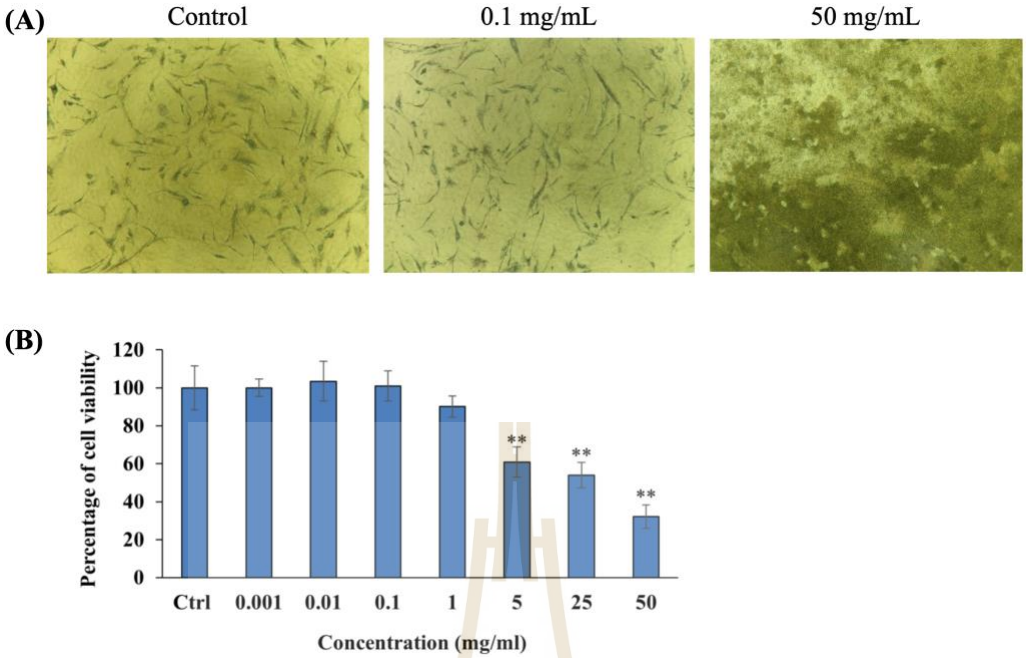

Figure 3.15 *In vitro* cytotoxicity test of AgNPs/eCaCO$_3$. water-insoluble formazan crystals in human dermal fibroblast cells (A) and viability of human dermal fibroblast cells (B).

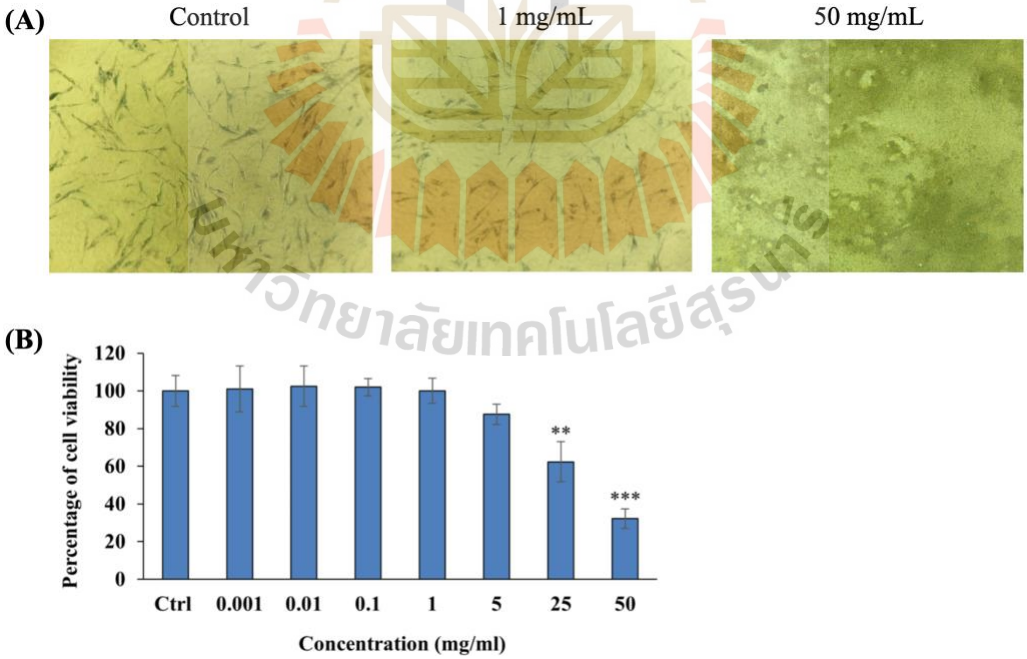

Figure 3.16 *In vitro* cytotoxicity test of AgNPs/CaCO$_3$. water-insoluble formazan crystals in human dermal fibroblast cells (A) and viability of human dermal fibroblast cells (B).

3.5 Conclusion

Spherical AgNPs with an average size of 24.13 ± 2.95 nm were successfully prepared by reducing an $AgNO_3$ aqueous solution at 70 °C in the presence of trisodium citrate as a reducing agent and stabilizer. The Z-average (r.nm) and PDI are 42.14 nm and 0.21, respectively for freshly prepared silver colloids, and 55.07 and 0.19, respectively for AgNPs. Zeta potential of freshly prepared silver colloids and AgNPs obtained from freshly prepared silver colloids were - 49.30 mV and - 44.10 mV, respectively. Novel hybrid antimicrobial microspherical particles of AgNPs/e$CaCO_3$ and AgNPs/$CaCO_3$ were successfully prepared via aqueous precipitation in the presence of freshly prepared silver colloids using poly (sodium 4-styrenesulphonate) as a polyelectrolyte. TEM, EDS and EDX confirmed that AgNPs were incorporated into the spherical precipitated $CaCO_3$ from eggshells and commercial calcium carbonate. The crystal polymorph of the precipitated e$CaCO_3$ and $CaCO_3$ was vaterite. The hybrid AgNPs/e$CaCO_3$ particles prepared at 25 °C had a spherical morphology and a narrow size distribution, with a mean diameter of 3.56 ± 0.26 µm. In contrast, AgNPs/e$CaCO_3$ prepared at 35 °C showed a broader size distribution with a mean diameter of 3.19 ± 1.20 µm. In addition, 0.78 wt% and 3.20 wt% AgNPs were deposited onto and inside the microspherical particles of precipitated eggshells and commercial calcium carbonate, respectively. AgNPs/$CaCO_3$ particles prepared at 25 °C also had a spherical morphology and a narrow size distribution with a mean diameter of 5.61 ± 0.66 µm. Both AgNPs/e$CaCO_3$ and AgNPs/$CaCO_3$ prepared at 25 °C have four regions of thermal decomposition with the overall weight loss of approximately 55.81% and 47.28% respectively. Therefore, eggshells and commercial calcium carbonate can be applied as carriers or supporters for the nanoparticles.

Antimicrobial test showed that both AgNPs/e$CaCO_3$ and AgNPs/$CaCO_3$ particles exhibited the same antimicrobial activity. The hybrid microspherical AgNPs/e$CaCO_3$ and AgNPs/$CaCO_3$ particles inhibited the growth of bacteria extracted from both unpacked and vacuum-packed beef. However, AgNPs/e$CaCO_3$ and AgNPs/$CaCO_3$ showed concentration-dependent antimicrobial activity against bacteria extracted from vacuum-packed beef. Significant HDF cells dead were found at 5 mg/mL for

AgNPs/e$CaCO_3$ and 25 mg/mL for AgNPs/$CaCO_3$ and no alive HDF cells were resulted at the concentration of 50 mg/mL for both samples.

CHAPTER IV

ELECTROSPUN PLA FIBERS WITH SILVER LOADED CALCIUM CARBONATE FILLER: EFFECT OF SOLVENT SYSTEMS AND MECHANICAL PROPERTIES

4.1 Abstract

Silver nanoparticles (AgNPs) are widely used as antimicrobial agent in food packaging applications, wound dressing materials and other antimicrobial applications because of their outstanding antimicrobial activity. AgNPs deposited onto calcium carbonate ($CaCO_3$) particles, have also the antimicrobial activity of which calcium carbonate functions as the agent carrier. Silver nanoparticles loaded eggshell calcium carbonate particles (AgNPs/$CaCO_3$) were prepared by in situ precipitation method and characterized as mentioned chapter III. In this study, antimicrobial composite material from the silver loaded calcium carbonate and poly (L-lactic acid) (PLA) is prepared with electrospinning technique. PLA solution is prepared using binary solvent systems with the solubility parameters close to that of PLA. In this study, three different binary solvent systems were used: chloroform (CHL): acetone (AC) with mixing ratio of 2:1 by volume, and chloroform (CHL): dimethylformamide (DMF) and dichloromethane (DCM): dimethylformamide (DMF) with the mixing ration of 9:1 by volume. Then, the PLA solutions and 1%, 3% and 5% ((w/v)) AgNPs/e$CaCO_3$ were mixed in order to prepare electrospun nanofiber mats. The conditions for fabricating electrospun neat PLA and AgNPs/e$CaCO_3$ filled PLA is a 15 cm of collection distance, 1 and 1.5 mL/hflow rates and 15, 18 and 20 kV of applied voltages. For binary solvent systems of CHL: AC, electrospun continuous fibers without beads were occurred at 10 and 15% (w/v) PLA solution concentrations, 1 mL/hflow rate and 18 kV applied voltage. For binary solvent systems of solvent 1 CHL: DMF and solvent 2 DCM: DMF, incorporation of 5% AgNPs/e$CaCO_3$ filler into the PLA electrospun fiber, solvent system 2 gave rise to larger diameter fiber with bead on the string along the fiber.

4.2 Introduction

Silver nanoparticles (AgNPs) are increasingly used as antimicrobial agent for medical, health care, food, cosmetic applications, and also in industrial purposes like textiles, keyboards. AgNPs can destroy the cell wall of the microorganisms including both Gram-negative and Gram-positive bacteria and have the ability to overcome the bacterial resistance to antibiotics (Zhang, Liu, Shen, & Gurunathan, 2016). Nowadays, several research works have focused on application of AgNPs as antimicrobial agent for plastic food packaging (Casasola, Thomas, Trybala, & Georgiadou, 2014), wound dressing materials and other antimicrobial applications because of their excellent antimicrobial activity. To reduce agglomeration and maintain long-lasting antimicrobial activity of Ag particles, calcium carbonate is one of a good choice as AgNPs carrier for incorporation into polymer matrix (Dlugosz, Bulwan, Kania, Nowakowska, & Zapotoczny, 2012). Chicken eggshell are extensively used as a replacement of commercial calcium carbonate because chicken eggshell is high in $CaCO_3$ content, 95 wt % and plenty available even though it is household waste. Recently, biopolymers have gained much attention as a replacement of petroleum-based synthetic polymer because of increasement of fuel energy utilization and greenhouse gas emission. Poly lactic acid (PLA) is a non-toxic and compostable bio-based material derived from starch and/ or sugar and has high mechanical strength and good barrier properties (Süfer, 2017). PLA has been widely used including biomedical applications and food packaging because of its biodegradability, biocompatibility and ability to be dissolved in common solvents for processing (Pan et al., 2018). The Hildebrand solubility parameter of PLA is around 10.1 $cal^{1/2}$ $cm^{-3/2}$ (20 to 21 $MPa^{½}$) (Su, Duhme, & Kopitzky, 2020).

Electrospinning is simple and the commonly employed technique for the fabrication of nano to microscale fibers. The morphology and fibers diameter during electrospinning influenced by solution properties, processing and ambient factors (Alven, Buyana, Feketshane, & Aderibigbe, 2021). The boiling point, comparative evaporation rate and solubility parameters of AC, CHL, DCM, and DMF are shown in Table 1. For binary solvent system of CHL: DMF and DCM: DMF, CHL and DCM were comparatively employed as the first solvent and DMF, as the second solvent with 1 part out of 10. CHL and DCM as the first solvents would make electrospun PLA fibers

more porous and smaller in diameter as hundred nanometers scale. Whereas DMF would ease fiber forming but the obtained electrospun fibers would be larger in diameter. With binary solvent system in electrospinning, the obtained electrospun fibers will be porous because of phase separation due to the different evaporation rate of the solvents. Casasola et al. (Casasola et al., 2014) found that the fibers diameter decreases as the boiling point of the second solvent in the mixed-solvent system increases. Therefore, DMF was employed as the second solvent due to their boiling points are higher than the boiling point of chloroform and dichloromethane. In addition, the boiling point of chloroform is higher than that of dichloromethane. The aim of this study is to develop the antimicrobial fiber mat for food packaging using electrospinning technique. PLA and PLA filled with AgNPs/eCaCO$_3$ electrospun fiber mat were prepared and the effects of PLA solution concentration, applied voltage, different binary solvent systems and AgNPs/eCaCO$_3$ filler content on morphology of electrospun fibers and distribution of fiber diameter were studied.

Table 4.1 Physical properties of solvents used in this study (Casasola et al., 2014; Haider, Haider, & Kang, 2018)

Solvents	**Boiling point (°C)**	**Evaporation rate at room temp**	**Solubility Parameter δ (cal$^{1/2}$ cm $^{-3/2}$)**
Acetone (AC)	56	5.6 (Butyl acetate =1)	10
Chloroform (CHL)	40	8.8 (Butyl acetate =1)	9.30
Dichloromethane (DCM)	61	14.5 (Butyl acetate =1)	9.70
Dimethylformamide (DMF)	153	0.2 (Butyl acetate =1)	12.10
CHL: AC (2:1)	-	-	9.50*
CHL: DMF (9:1)	-	-	9.58*
DCM: DMF (9:1)	-	-	9.94*

* Calculated solubility parameter

4.3 Materials and Methods

4.3.1 Materials

The commercial poly (L-lactic acid) (PLA grade (4043D)) was purchased from NatureWorks. Chloroform RPE and dichloromethane RPE were purchased form Carlo Erba Reagents, acetone was purchased from Thermo Fisher Scientific and dimethylformamide was purchased from RCI Labscan. Silver nanoparticles loaded eggshell calcium carbonate particles (AgNPs/e$CaCO_3$) were prepared by a coprecipitation method mentioned in chapter III. The particle size range of the AgNPs/e$CaCO_3$ is around 2 to 8 μm with [D0.1] of 1.51 μm, [D0.5] of 4.47 μm and [D0.9] of 7.70 μm.

4.3.2 Sample preparation for binary solvent system of chloroform and acetone (CHL: AC = 2:1 by volume)

Binary solvent system of chloroform and acetone (CHL: AC = 2:1 by volume) was used as solvent for preparing PLA solutions. The PLA solution with different concentrations of 7.5%, 10%, 12.5% and 15% (w/v) were dissolved in the binary solvent system of CHL: AC of 30 mL and were stirred at room temperature for 24 h using a magnetic stirrer. For preparing AgNPs/e$CaCO_3$ filled PLA nanofibers, only 10% (w/v) PLA solution with the binary solvent system of CHL:AC was employed. Firstly, 3.00 g of PLA was dissolved in the binary solvent system of 30 mL for 22 h. Then, 0.30 g or 0.90 g AgNPs/e$CaCO_3$ was slowly added into the 10% PLA solution under stirring condition. After that, the mixtures were magnetically stirred at room temperature for 2 h.

Each PLA solution, unfilled and filled, was loaded into a 10 mL plastic syringe (NIPRO syringe), and the needle (inner diameter 0.9 mm, NIPRO) was used for electrospinning. Two flow rates (1 mL/hand 1.5 mL/h) were varied, and applied voltage of 15 kV and 18 kV were applied. Electrospun fibers were collected on a grounded aluminum collector at a distance of 15 cm from the needle tip. The spinning time for pure PLA solutions and AgNPs/e$CaCO_3$ loaded PLA solutions was 30 min and 15 min, respectively. All experiments were performed at about 30°C and relative humidity around 60%.

4.3.3 Sample preparation for binary solvent systems of chloroform and dimethylformamide (solvent 1 CHL: DMF = 9:1 by volume) and dichloromethane and dimethylformamide (solvent 2 DCM: DMF = 9:1 by volume)

Various concentrations of PLA solution were prepared with different binary solvent systems of chloroform and dimethylformamide (solvent 1 CHL: DMF = 9:1 by volume) and dichloromethane and dimethylformamide (solvent 2 DCM: DMF = 9:1 by volume). PLA solutions were prepared at 7.5%, 10% and 12.5% (w/v) using those binary solvent systems as solvent. The PLA solutions were stirred at room temperature for 12 h using a magnetic stirrer. For preparing AgNPs/eCaCO$_3$ filled PLA fibers, only 10% (w/v) PLA solutions with different binary solvent systems of solvent 1 and solvent 2 were employed.

To prepare AgNPs/eCaCO$_3$ filled PLA, firstly, 3.00 g of PLA was dissolved in both 30 mL binary solvent systems for 10 h and different 0.30 g and 1.50 g of AgNPs/eCaCO$_3$ filler contents were slowly added into the dissolved PLA solutions under stirring condition. Then, the mixtures were further magnetically stirred at room temperature for 2 h and subsequently placed into an ultrasonic bath for 30 min at room temperature to get homogenous dispersion/distribution of the particles along the fibers during electrospinning.

Each PLA solution, unfilled and filled, was loaded into a 10 mL plastic syringe (NIPRO syringe), and the needle (inner diameter of 0.9 mm, NIPRO) was used for electrospinning. Two high applied voltages of 15 and 20 kV, and a flow rate of 1 mL/hwere employed. Electrospun fibers were collected on a grounded aluminum collector at a distance of 15 cm from the needle tip. To select the suitable conditions for electrospun fibers, all the samples were electrospun for 1 hwhile four best conditions, neat PLA at 10% PLA concentration and PLA filled 5% AgNPs/eCaCO$_3$ from both solvent 1 and solvent 2, were selected in terms of fiber size homogeneity and fiber smoothness in order to further investigate their tensile properties. The electrospun fiber mats for mechanical test were prepared with collecting time of 5 h. All experiments were performed at about 30°C and relative humidity around 60%.

4.3.4 Fiber Characterization and Mechanical Test

Morphology of electrospun fibers made of neat PLA and AgNPs/eCaCO$_3$ filled PLA were investigated using a Field Emission Scanning Electron Microscope (FE-SEM, JEOL JSM 7800F) with an accelerating voltage of 3.0 kV. Prior to observation, each sample was coated using a gold sputter coater (Neo-Coater, MP-19020NCTR) for 2 min. For determining average fiber diameters, image analysis software (Image J) was used, and the average diameter was calculated from 100 fibers from the SEM micrographs

Mechanical properties were measured using Instron Universal Testing Machine (Instron 5565, USA) with a crosshead speed of 10 mm/min, a load cell of 1 kN and a gauge length of 50 mm, in an accordance with ASTM 882. The electrospun fiber mat of neat PLA and 5% (w/v) Ag/eCaCO$_3$ filled PLA prepared by solvent 1 CHL: DMF and solvent 2 DCM: DMF with a 1cm x 10 cm dimension were subjected to tensile testing. All 3 samples each were cut with their length aligned to the fiber direction.

4.4 Results and Discussion

4.4.1 Electrospun PLA Fibers using binary solvent system of chloroform and acetone (CHL: AC = 2:1 by volume)

4.4.1.1 Effect of electrospinning parameters and PLA concentration on morphology of electrospun PLA fibers

SEM micrographs in Fig. 4.1 show morphology of the nanofibers electrospun with different PLA concentrations, flow rates and applied voltages. The SEM micrographs show characteristic of porous structure of PLA fibers electrospun from PLA solution with the binary solvent system of CHL: AC. The concentration of PLA solution does affect PLA nanofiber morphology and diameter. The micrographs show that smaller fibers with beads were collected from 7.5% (w/v) PLA solution (Fig. 4.1A-D). The formation of beads indicates insufficient chain entanglements (Sadasivuni et al., 2019). On increasing PLA concentration to 10% (w/v), continuous fibers with various diameter fibers were produced (Fig. 4.1E-H) and uniform fibers were collected at 12.5% (w/v) PLA solution (Fig. 4.1I-L). At the highest PLA concentration of 15% (w/v), electrospun fibers were folded back and forth not randomly oriented as observed from electrospun fiber with lower concentration of PLA solution (Fig. 4.1M-P). Casasola

et al. (Casasola et al., 2014) have mentioned that increasing polymer concentration results in more chain entanglements, an increase in the solution viscosity. As a result, hence an increase in the viscoelastic force will be increased and will counterbalance the Coulombic stretching force. Therefore, it results in continuous fibers with fewer beads.

Uniform electrospun nanofibers in size could be prepared via a critical flow rate of a polymeric solution. At higher flow rate of 1.5 mL/h, fibers with larger diameter were produced comparing to the prepared fiber with lower flow rate of 1 mL/h. Increasing flow rate beyond a critical value not only leads to increase in the pore size and fiber diameter but also bead formation. This might be due to incomplete drying of the nanofiber jet during the flight between the needle tip and metallic collector (Wang et al., 2020). Upon concerning applied voltage, smaller diameter of fibers was produced at higher applied voltage of 18 kV compared to produced fibers at 15 kV, as shown in Fig. 4.1. The formation of smaller diameter nanofibers with an increase in the applied voltage is attributed to the stretching of the polymer solution in correlation with the charge repulsion within the polymer jet (Wang et al., 2020).

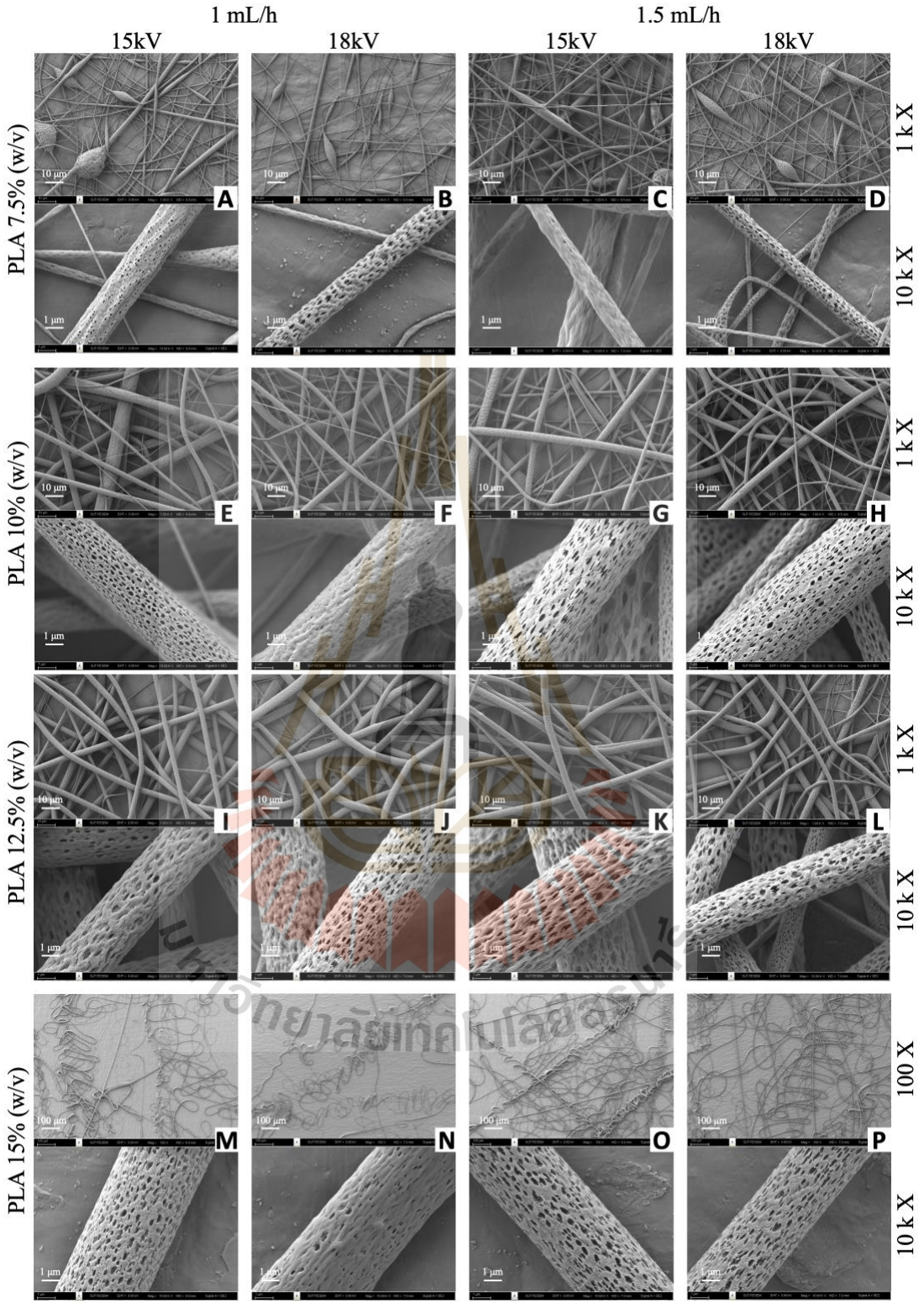

Figure 4.1 SEM micrographs of electrospun PLA fiber prepared from various concentrations, flow rates of 1 and 1.5 mL/h, and applied voltages of 15 and 18 kV

4.4.1.2 Effect of electrospinning parameters and AgNPs/eCaCO$_3$ content on morphology of the electrospun filled PLA fibers

SEM micrographs in Fig. 4.2 show electrospun fibers obtained from PLA solutions filled with 1 and 3% (w/v) AgNPs/eCaCO$_3$ using 1 mL/hflow rate, and 18 and 20 kV applied voltages. At 1% (w/v) AgNPs/eCaCO$_3$ loading, the electrospun filled PLA fibers contained some particles blooming along the fiber, as shown in Fig. 4.2A and 4.2B. However, with 3% (w/v) AgNPs/eCaCO$_3$ loading, the electrospun fiber comparatively contained more particle blooming along the fiber due to higher degree of the local particle agglomeration during electrospinning process, as illustrated in Fig. 4.2C and 4.2D. The local particle agglomeration might be caused by heterogeneous distribution of the particles in PLA solutions during electrospinning.

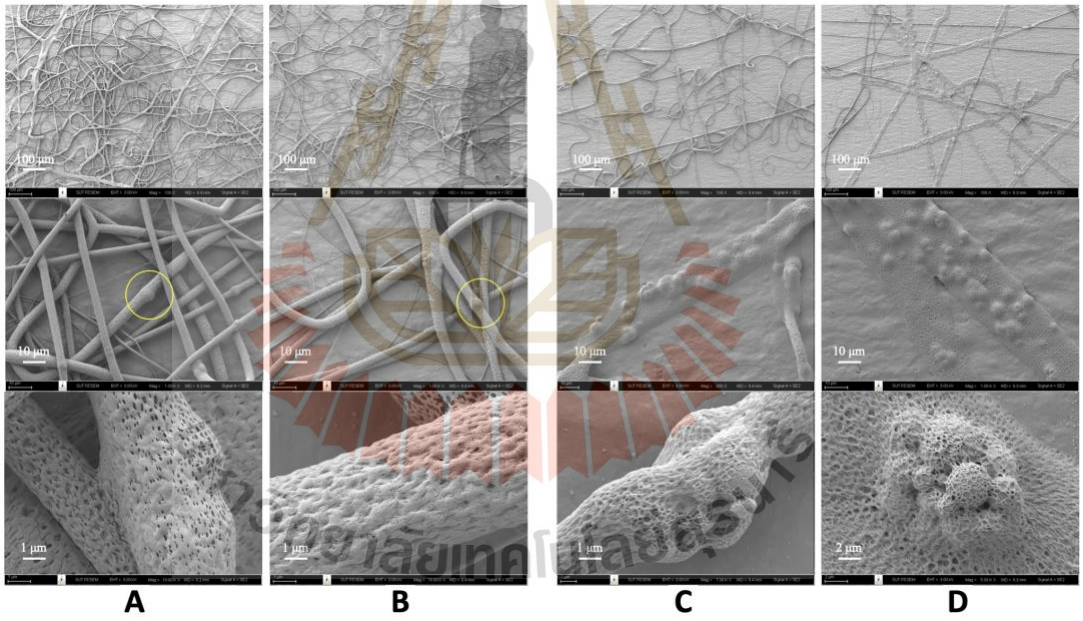

Figure 4.2 SEM micrographs of the electrospun filled PLA fiber with 1% (w/v) AgNPs/eCaCO$_3$ at 1 mL/hand 18 kV (A), and 1mL/hand 20 kV (B); and 3% (w/v) AgNps/eCaCO$_3$ at 1 mL/hand 18 kV (C), and 1mL/hand 20 kV (D).

4.4.2 Electrospun PLA Fibers using binary solvent systems of chloroform and dimethylformamide (solvent 1 CHL: DMF = 9:1 by volume) and dichloromethane and dimethylformamide (solvent 2 DCM: DMF = 9:1 by volume)

4.4.2.1 Effect of binary solvent system, PLA concentration and voltages on morphology of electrospun PLA fibers

SEM micrographs in Fig. 4.3 comparatively show morphology of electrospun PLA fiber prepared from various PLA concentrations, using solvent 1 and solvent 2 with flow rates of 1 mL/h, and applied voltages of 15 kV. The electrospun fibers prepared from both solvent 1 (chloroform: dimethylformamide (CHL: DMF= 9:1 by volume)) and solvent 2 (dichloromethane: dimethylformamide (DCM: DMF = 9:1 by volume)) showed porous structure. The concentration of PLA solution and different binary solvent systems affect PLA nanofiber morphology and diameter. At 7.5% (w/v) PLA solution, the micrographs show that smaller fibers, with more beads were collected from the PLA solution prepared from solvent 1(Fig. 4.3I-A) than from the one prepared from solvent 2(Fig. 4.3II-A). The formation of beads indicates insufficient chain entanglements during electrospinning (Sadasivuni et al., 2019).

On increasing PLA concentration to 10% (w/v), continuous fibers with various diameter fibers were obtained (Fig. 4.3I-B and 4.3II-B). The uniform fiber diameter with no bead on string were collected from 12.5% (w/v) PLA solution (Fig. 4.3I-C and 4.3II-C). Casasola et al. (Casasola et al., 2014) have mentioned that increasing polymer concentration results in more chain entanglements, an increase in the solution viscosity. As a result, an increase in the viscoelastic force will be increased and will counterbalance the Coulombic stretching force. Therefore, it results in continuous fibers with fewer beads.

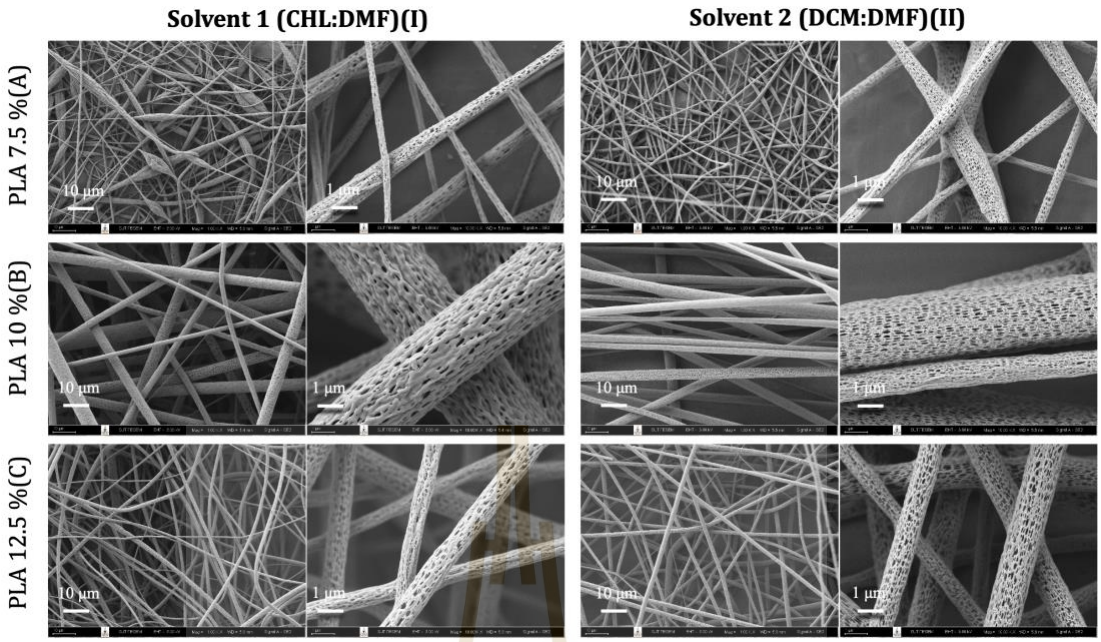

Figure 4.3 SEM micrographs of electrospun PLA fiber prepared from 7.5% (A), 10% (B) and 12.5% (C) PLA solution with flow rates of 1 mL/h, and applied voltages of 15 kV, using Chloroform: Dimethylformamide (CHL: DMF=9:1 by volume) (I) and Dichloromethane: Dimethylformamide (DCM: DMF = 9:1 by volume) (II).

SEM micrographs showing effect of applied voltages on PLA electrospun fiber were illustrated in Fig 4.4 Upon increasing applied voltage from 15 kV to 20 kV, smaller diameter fibers were obtained. In addition, PLA electrospun fibers with uniform diameter are formed at higher applied voltage of 20 kV (Fig. 4.4I-B and 4.4II-B) compared to the fibers obtained from 15 kV applied voltage (Fig. 4.4I-A and 4.4II-A). The formation of smaller diameter electrospun nanofibers with an increase in the applied voltage also observed from (Fig. 4.4I-B and 4.4II-B), is attributed to the stretching of the polymer solution in correlation with the charge repulsion within the polymer jet (Wang et al., 2020).

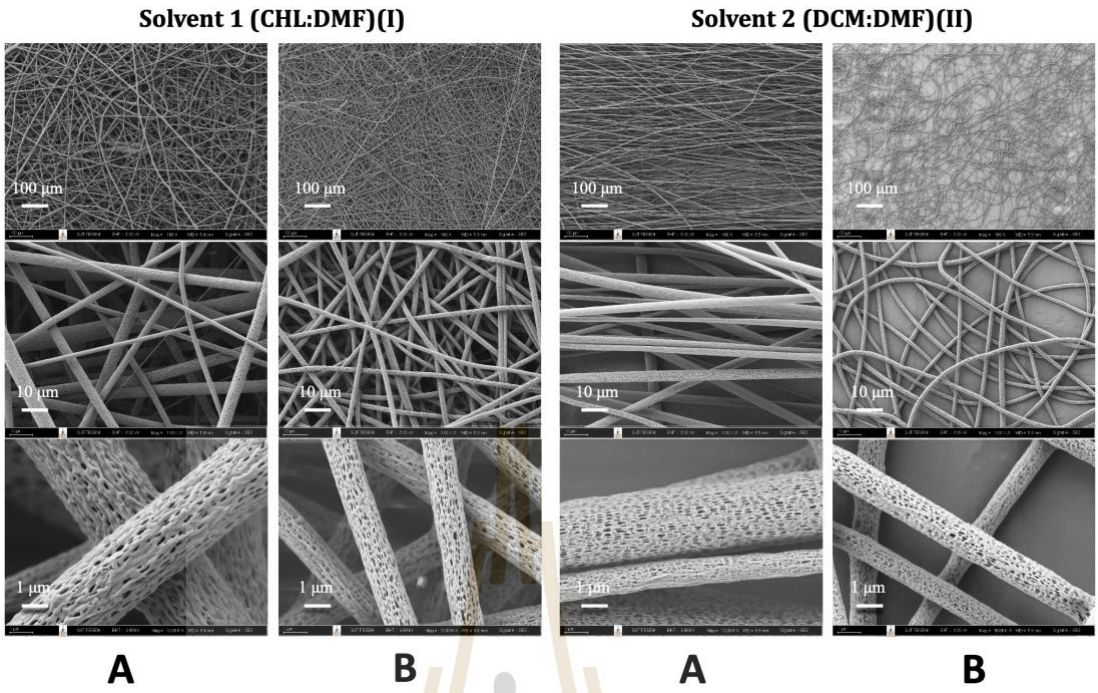

Figure 4.4 SEM micrographs of electrospun PLA fiber prepared from different applied voltages of 15 kV and 20 kV, PLA concentration of 10% ((w/v)), flow rate of 1 mL/h, using Chloroform: Dimethylformamide (CHL: DMF = 9:1 by volume) (I) and Dichloromethane: Dimethylformamide (DCM: DMF = 9:1 by volume) (II).

4.4.2.2 Effect of AgNPs/eCaCO$_3$ content and binary solvent system of solvent 1(CHL:DMF) and solvent 2(DCM:DMF) on morphology of electrospun PLA fibers

SEM micrographs in Fig. 4.5 show electrospun fibers obtained from PLA 10% (w/v) solutions with both binary solvent 1 and 2 filled with 1% and 5% (w/v) AgNPs/eCaCO$_3$ using 1 mL/hflow rate, and 20 kV applied voltage. At 1% (w/v) AgNPs/eCaCO$_3$ loading, the electrospun filled PLA fibers contained some particle beads in string along the fiber, as shown in Fig. 4.5I-A and 4.5II-A. However, with 5% (w/v) AgNPs/eCaCO$_3$ loading, the electrospun fiber comparatively contained more particle beads in string along the fiber due to higher the particles loading causing high degree of the local particle agglomeration during electrospinning process, as illustrated in Fig.

4.5I-B and 4.5II-B. The local particle agglomeration caused heterogeneous distribution of the particles in PLA solutions during electrospinning.

According to fiber morphology and average diameter, porous and uniform diameter fibers were found in neat PLA mat while porous and bead on string fibers for PLA filled with 5% (w/v) AgNPs/eCaCO$_3$ mat. Larger average diameters were occurred in filled PLA fiber mats comparing to neat PLA fiber mats for both binary solvent systems. Moreover, fiber mat prepared from solvent 2 has slightly larger diameter fibers than that prepared from solvent 1.

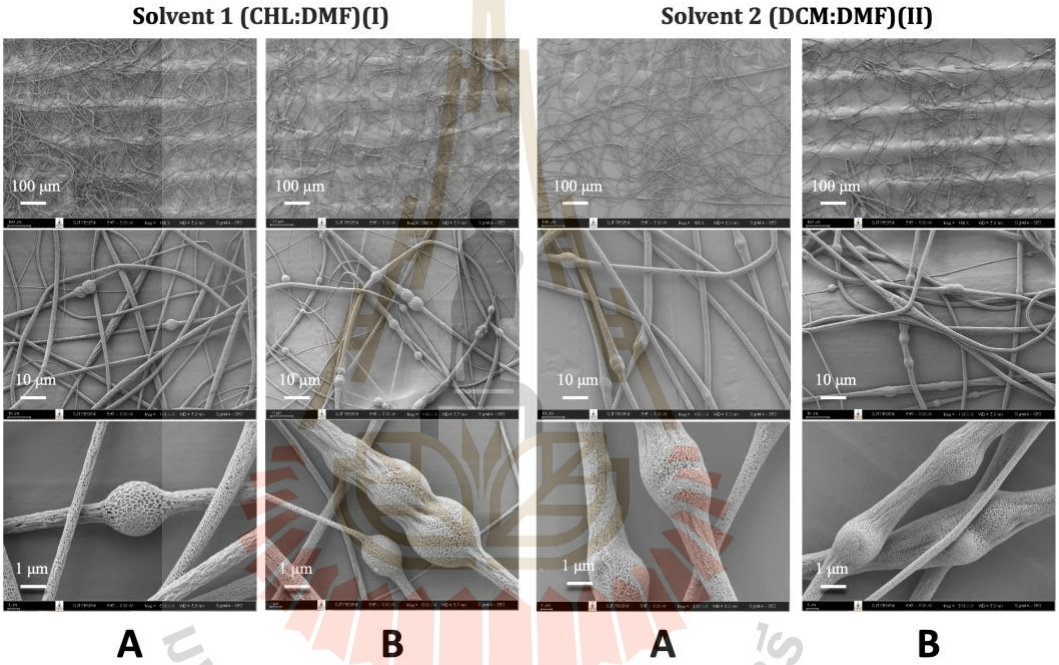

Figure 4.5 SEM micrographs of the electrospun filled PLA fiber with 1% (w/v) AgNPs/eCaCO$_3$ (I-A and II-A), and 5% (w/v) AgNPs/eCaCO$_3$ (I-B and II-B) at PLA 10% (w/v) concentration, 1 mL/h and 20 kV, using Chloroform: Dimethylformamide (CHL: DMF = 9:1 by volume) (I) and Dichloromethane: Dimethylformamide (DCM: DMF = 9:1 by volume) (II).

4.4.2.3 Effect of electrospun PLA fibers filled and unfilled with AgNPs/eCaCO$_3$ particles on mechanical Properties

The effect of AgNPs/eCaCO$_3$ content on tensile properties of electrospun PLA nanofiber sheet prepared using both binary solvent systems, solvent 1 and solvent 2, measured in flow direction was shown in Fig 4.6 and Table 4.2. For

the system using solvent 1, neat PLA sheet exhibited nearly 2-time higher tensile strength than PLA sheet with 5% AgNPs/eCaCO$_3$. In addition, neat PLA sheet from solvent 2 also showed higher tensile strength than the sheet of filled PLA. Local fiber thickness differences between solely fiber and bead on string vicinities caused weak points in electrospun PLA fibers sheet filled with 5% AgNPs/eCaCO$_3$. That resulted in lower tensile strength. By using the solvent system of CHL:DMF, electrospun AgNPs/eCaCO$_3$ filled PLA sheet comparative Young's modulus to that of neat electrospun PLA sheet. However, by using the solvent system of DCM:DMF, the AgNPs/eCaCO$_3$ filled PLA sheet exhibits lower Young's modulus than the neat electrospun PLA sheet does. Neat PLA sheet exhibited nearly 4-time higher elongation at break with solvent 1 and over 2-time higher elongation at break with solvent 2 comparing to filled PLA fiber mat. Apparently, the elongation at break of the PLA filled with 5% AgNPs/eCaCO$_3$ electrospun fiber sheet was decreased due to the particles bead on string acting as weak point under deformation.

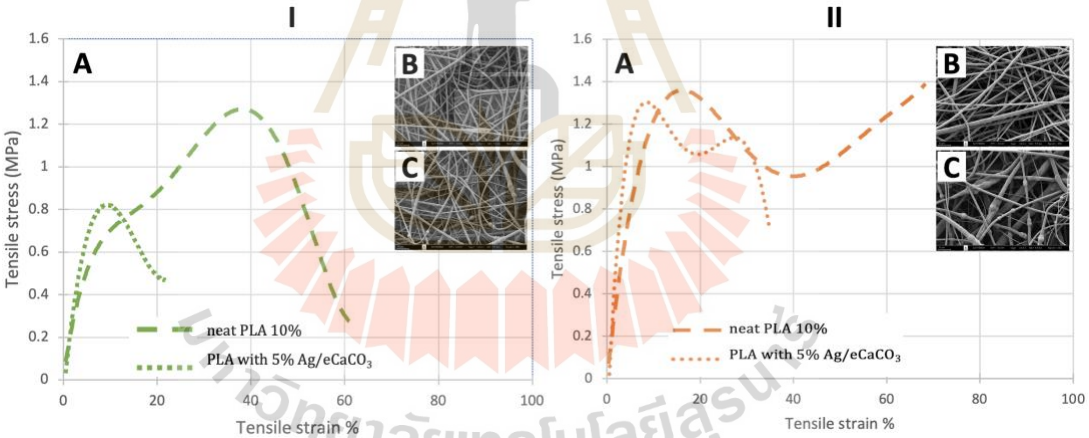

Figure 4.6 Tensile stress-strain curves (I-A and II-A) of PLA and PLA with AgNPs/eCaCO$_3$ using solvent 1 (I) and solvent 2 (II). SEM micrographs of the electrospun neat PLA 10% (I-B and II-B), and PLA with 5% AgNPs/eCaCO$_3$ (I-C and II- C).

The characteristics of PLA electrospun fibers and PLA filled AgNPs/eCaCO$_3$ in term of fiber morphology and diameter, and tensile properties, obtained from different binary solvent systems, applied voltage of 20 kV and 10% (w/v) concentration of PLA solution were comparatively shown in Table 4.2.

Table 4.2 Fiber morphology and diameter, and mechanical properties of PLA electrospun mat unfilled and filled 5% with AgNPs/$eCaCO_3$

Samples		Fiber Morphology	Fiber diameter	Young's Modulus (MPa)	Tensile Strength (MPa)	Elongation at Break (%)
Solvents	PLA					
(CHL:DMF)(9:1)	Neat PLA	Porous, uniform	1.59 ± 0.37	11.18 ± 2.78	1.26 ± 0.12	80.45 ± 3.07
	PLA with 5% AgNPs/$eCaCO_3$	Porous, bead on string	1.87 ± 0.87	11.32 ± 1.52	0.69 ± 0.13	23.95 ± 2.23
(DCM:DMF)(9:1)	Neat PLA	Porous, uniform	1.73 ± 0.52	26.84 ± 5.79	1.50 ± 0.19	70.11 ± 5.67
	PLA with 5% AgNPs/$eCaCO_3$	Porous, bead on string	2.61 ± 1.38	20.12 ± 4.60	1.25 ± 0.29	32.40 ± 3.09

CHL=chloroform, DMF=dimethylformamide, DCM=dichloromethane

4.5 Conclusion

Electrospun PLA fiber with highly porous structure were studied using three different binary solvent systems such as chloroform and acetone (CHL: AC = 2:1 by volume), chloroform and dimethylformamide (solvent 1 CHL: DMF = 9:1 by volume) and dichloromethane and dimethylformamide (solvent 2 DCM: DMF = 9:1 by volume). For binary solvent systems of CHL: AC, PLA solutions of 10 and 15% (w/v) concentrations would give rise to electrospun continuous fibers without beads. Larger diameter electrospun fibers were obtained at higher flow rate of 1.5 mL/hand applying higher voltage of 18 kV resulted in smaller diameter fibers than applying lower voltage. PLA electrospun fibers filled with 1 % (w/v) AgNPs/e$CaCO_3$ contained some particles blooming along the fiber. However, more particle blooming and nonuniform shape were observed from the electrospun fibers filled with 3% (w/v) AgNPs/e$CaCO_3$. The electrospun fibers obtained from 1 % (w/v) AgNPs/e$CaCO_3$ loading with applied voltage of 20 kV were more uniform in shape.

For binary solvent systems of solvent 1 CHL: DMF and solvent 2 DCM: DMF, PLA 10 % (w/v) concentration with 1mL/h flow rate and 20 kV applied voltage gave uniform diameter fiber for both solvent 1 and solvent 2. Incorporation of 5% AgNPs/e$CaCO_3$ filler into the PLA electrospun fiber, solvent system 2 gave rise to larger diameter fiber with bead on the string along the fiber. For tensile properties, PLA with 5% AgNPs/e$CaCO_3$ electrospun fibers from solvent system 2 had higher Young's modulus and ultimate tensile strength than the one prepared from solvent system 1.

CHAPTER V
PREPARATION OF ELECTROSPUN PLA FIBERS WITH SILVER LOADED CALCIUM CARBONATE FILLER AS THE ANTIMICROBIAL MATERIAL

5.1 Abstract

Silver nanoparticles (AgNPs) are widely used as antimicrobial agent in food packaging applications, health care, cosmetic and other antimicrobial applications because of their outstanding antimicrobial activity. AgNPs deposited onto calcium carbonate ($CaCO_3$) particles, have also the antimicrobial activity of which calcium carbonate functions as the agent carrier. Silver nanoparticles loaded eggshell calcium carbonate particles (AgNPs/e$CaCO_3$) and silver nanoparticles loaded commercial calcium carbonate particles (AgNPs/$CaCO_3$) were prepared by *in situ* precipitation method and characterized as mentioned in chapter III. In this study, neat PLA, 5 % (w/v) AgNPs/e$CaCO_3$ filled PLA and 5 % (w/v) AgNPs/$CaCO_3$ filled PLA fibers mats were prepared by electrospinning technique. PLA unfilled and filled fiber mats were prepared using binary solvent system of dichloromethane: dimethylformamide (DCM: DMF with the mixing ration of 9:1 by volume). The conditions for fabricating electrospun neat PLA, AgNPs/e$CaCO_3$ filled PLA and AgNPs/$CaCO_3$ filled PLA fibers mats were PLA solution concentration of 10 % (w/v), flow rate of 1 mL/h, applied voltage of 20 kV and 12 cm of collection distance. It was found that the XRD patterns showed the semicrystalline structure of PLA and the crystal structures of calcium carbonate particles incorporated into PLA electrospun fibers were still vaterite polymorph. In addition, the fibers morphology were showed the beads in strings with the average diameter of 7.10 ± 3.02 μm for AgNPs/e$CaCO_3$ filled PLA and 11.33 ± 3.38 μm for AgNPs/$CaCO_3$ filled PLA.

5.2 Introduction

Silver nanoparticles (AgNPs) are the most popular antimicrobial agents because of their high activity against drug-resistant bacteria, high stability, and nontoxicity (Dizaj, Lotfipour, Barzegar-Jalali, Zarrintan, & Adibkia, 2014). AgNPs have been used in medical, health care, food, cosmetic applications, and also in industrial purposes like textiles, keyboards. AgNPs can destroy the cell wall of the microorganisms including both Gram-negative and Gram-positive bacteria and have the ability to overcome the bacterial resistance to antibiotics (Zhang et al., 2016). To reduce agglomeration and maintain long-lasting antimicrobial activity of AgNPs particles, porous micro $CaCO_3$ particles have been used as carriers for incorporation into polymer matrix (Apalangya, Rangari, Tiimob, Jeelani, & Samuel, 2014; Dlugosz et al., 2012).

Recently, biopolymers have gained much attention as a replacement of petroleum-based synthetic polymer because of increasement of fuel energy utilization and greenhouse gas emission. Poly lactic acid (PLA) has shown many excellent properties such as high mechanical strength and modulus, biodegradability, biocompatibility and easy processing. PLA has been used in different industries such as Medical and biomedical, food packaging, agriculture and automotive industries (Süfer, 2017; Taib et al., 2022).

Electrospinning is a simple technique to prepare nanostructured materials with relatively high manufacturing rate and low cost. There are important factors affecting the electrospinning process such as solvent system, polymer concentration, applied voltage, flow rate, distance between the needle and collector and needle diameter, relativity humidity and temperature (Alven et al., 2021; Haider et al., 2018). The aim of this study is to develop the antimicrobial fiber mats for food packaging using electrospinning technique.

In this study, AgNPs loaded with calcium carbonate particles from eggshell (AgNPs/e$CaCO_3$) and commercial calcium carbonate (AgNPs/$CaCO_3$) were incorporated into PLA polymer using electrospinning technique. PLA and PLA filled with 5 % (w/v) AgNPs/e$CaCO_3$ and AgNPs/$CaCO_3$ electrospun fiber mats were prepared at PLA concentration of 10 % (w/v), flow rate of 1 mL/h, and 20 kV applied voltage using binary solvent system of dichloromethane and dimethylformamide (DCM: DMF = 9:1

by volume). The morphology of neat PLA, AgNPs/eCaCO$_3$ filled PLA and AgNPs/CaCO$_3$ filled PLA electrospun fibers were characterized using Field Emission Scanning Electron Microscopy (FESEM). The crystal polymorphs and thermal degradation of those electrospun fibers mats were determined by X-ray diffraction analyzer and thermogravimetric analyzer. The mechanical properties of elastic modulus and hardness were measured Nanoindentation were studied by NanoTest indenter. Cytotoxicity and antimicrobial testing were also measured using MTT assay and modified Kirby–Bauer disc diffusion assay.

5.3 Matereials and Methods

5.3.1 Materials

The commercial poly (L-lactic acid) (PLA grade (4043D)) was purchased from NatureWorks. Dichloromethane (RPE) was purchased form Carlo Erba Reagents and dimethylformamide was purchased from RCI Labscan. Silver nanoparticles loaded calcium carbonate particles from eggshell and commercial calcium carbonate were prepared by a coprecipitation method mentioned in chapter III. The particle size of silver nanoparticles loaded eggshell calcium carbonate (AgNPs/eCaCO$_3$) and silver nanoparticles loaded commercial calcium carbonate (AgNPs/CaCO$_3$) are mean diameter of 3.56 ± 0.26 um and 5.61 ± 0.66 um, respectively. Plate count agar (PCA) and peptone were purchased from HiMedia Laboratories Pvt. Ltd and Sisco Research Laboratories Pvt. Ltd. Unpacked fresh beef and vacuum-packed fresh beef (“INCHA BEEF”) were purchased from a local fresh market and a Home-Fresh Mart supermarket, respectively. *E. coli* was kindly provided by Ms. Jintaphorn Klinsuk.

5.3.2 Sample Preparation

PLA solution of 10% (w/v) concentration was prepared with binary solvent system of dichloromethane and dimethylformamide (solvent 2 DCM: DMF = 9:1 by volume). PLA of 3.00 g was dissolved in the binary solvent system of DCM: DMF of 30 mL and was stirred at room temperature for 12 h using a magnetic stirrer. Then, the solution was subsequently placed into an ultrasonic bath for 30 min at room temperature. For preparing PLA solution filled with AgNPs/eCaCO$_3$ and AgNPs/CaCO$_3$, firstly, 3.00 g of PLA was dissolved in the binary solvent system of 30 mL for 10 h.

Then, 1.5 g AgNPs/eCaCO$_3$ or AgNPs/CaCO$_3$ was slowly added into the 10% PLA solution under stirring condition. After that, the mixtures were further magnetically stirred at room temperature for 2 h and subsequently placed into an ultrasonic bath for 30 min at room temperature to get homogenous dispersion/distribution of the particles along the fibers during electrospinning.

The unfilled and filled PLA fibers were prepared via electrospinning technique using NANON-01B (MECC CO., LTD, Fukuoka, JAPAN). Each PLA solution, filled and unfilled, was loaded into a 10 mL plastic syringe (NIPRO syringe) with hypodermic needle (inner diameter of 0.9 mm, NIPRO). High applied voltages of 20 kV, and a flow rate of 1 mL/h were employed. The electrospun fibers were collected on a grounded aluminum collector at a distance of 12 cm from the needle tip. All electrospun fiber mats were obtained at spinning time of 5 h and the width of the fibers were fixed to 3 mm. All experiments were performed at about 30°C and relative humidity around 60%.

5.3.3 Materials Characterization

Morphology of electrospun fibers made of neat PLA, and PLA filled with 5% ((w/v)) of AgNPs/eCaCO$_3$ and AgNPs/CaCO$_3$ were investigated by the Field Emission Scanning Electron Microscope (FE-SEM, JEOL JSM 7800F) with an accelerating voltage of 3.0 kV. Prior to observation, each sample was coated using a gold sputter coater (Neo-Coater, MP-19020NCTR) for 2 min. For determining average fiber diameters, image analysis software (Image J) was used, and the average diameter was calculated from 50 fibers from the SEM micrographs.

The crystal polymorphs of neat PLA fiber mat, PLA filled with 5% (w/v) of AgNPs/eCaCO$_3$ and AgNPs/CaCO$_3$ fiber mats were determined by an X-ray diffraction analyzer (XRD, Bruker D8 ADVANCE). The study was carried out in a 2 θ range of 5-80° with a voltage of 40 kV, current of 40 mA, and a Cu K α (1.5606 Å) radiation source.

The decomposition temperature of neat PLA fiber mat and PLA filled fiber mats with 5% (w/v) of AgNPs/eCaCO$_3$ and AgNPs/CaCO$_3$ were determined using a thermogravimetric analyzer (TGA, Mettler Toledo, TGA/DSC1) under nitrogen atmosphere. The samples were heated from 35 to 900 °C at a heating rate of 10 °C/min.

5.3.4 Materials Testing

To determine nanomechanical properties, thickness of all electrospun fiber mats were measured at five points that were evenly distributed through the width of the fiber mats (3 mm) using dial gauge. The average of those five data was taken as the thickness of the sheet that was shown in Table 5.2.

The nanomechanical measurements were carried out with NanoTest indenter (Micro Materials, Wrexham, UK) platform 3 with a Berkovich triangular diamond pyramid indenter. A loading rate of 0.8 mN was held for 10 s before the indenter was unloaded. Ten different indents were performed on each sample in randomly selected to obtain average hardness and elastic modulus values.

5.3.5 Cytotoxicity testing (MTT assay)

For cytotoxicity testing (MTT assay), firstly the initial concentration of polymer film of 0.25 g/5 mL or 50 mg/mL) were prepared for human dermal fibroblast (HDF) treatment. The polymer films were weighed and cut into sterile petri dishes under individual conditions. Next, these films were disinfected by UV light sterilization for 15 min. The culture medium DMEM (Dulbecco modified Eagle medium with 4.5 g/L glucose) supplemented with 1 % penicillin/streptomycin was added to the polymer and incubated overnight at 25 °C. After incubation, the solution was collected into 15 mL centrifuge tubes prior to treatment.

MTT assay is a colorimetric assay used to measure the cell viability. The cellular enzymes reduce the tetrazolium dye, MTT (3-(4,5-dimethylthiazol-2-yl)-2,5-diphenyl-2H-tetrazolium bromide), to its insoluble product (formazan) giving a purple color. In this study, MTT assay was used to determine the effect of polymer (Neat PLA, PLA/AgNPs/e$CaCO_3$ and PLA/AgNPs/$CaCO_3$) on viability of human dermal fibroblast (HDF) cells. Briefly, HDF cells were seeded on 96-well plates at a density of 7×10^4 cells/well. Cells were then treated with the indicated polymers at various concentrations for 24 h. Then, MTT solution was added to each well and incubated at 37°C in the dark for 4 h. After that, the formazan crystals were dissolved with dimethyl sulfoxide (DMSO) and the absorbance of formazan solution was detected at 570 nm using a microplate reader (BMG Labtech, Ortenberg, Germany). The IC50 (50% inhibitory concentration) was calculated from the dose-response curve of percent viability (Y

axis) versus concentration tested (X axis) with a linear regression using Microsoft Excel. All experiments were performed in triplicates, and data were expressed as mean ± standard deviation. Statistical analysis was performed using a student's t test (SPSS version 26.0, SPSS Inc., USA) to compare means from two independent sample groups. *p < 0.05, **p < 0.01 and ***p < 0.001 were considered statistically significant.

5.3.6 Antimicrobial testing

To examine the antimicrobial efficiency of neat PLA fibers and PLA fibers filled with 5% (w/v) of AgNPs/eCaCO$_3$ and AgNPs/CaCO$_3$ on beef-extracted bacteria and *Escherichia coli (E coil)*, a modified Kirby–Bauer disc diffusion assay was performed as follows. Beef extracted bacteria were extracted from two types of beef, unpacked beef available at a local market and vacuum-packed beef ("INCHA" brand) available at a supermarket. The beef loaf was cut into small pieces and kept at room temperature for 18 h. Plate count agar (PCA) powder of 2.35 g was completely dissolved in 100 mL sterile DI water using a hot plate. Next, the PCA solution was sterilized, and then poured into sterile petri dishes after the solution and the dishes were cool down to 45-50 °C. Approximately 25 g spoiled beef was blended with 225 mL of 0.10% (w/v) sterile peptone water using a Stomacher laboratory blender for 6 min. The obtained beef extract or *E coli* was smeared onto plate count agar using a sterile cotton swab. Unfilled and filled PLA fiber mats were cut into a circular shape of 6 mm diameter using sterile paper puncher and then they were placed onto the smeared agar plate. The plates were incubated at 37 °C for 24 h. After that, each inhibition zone diameter was monitored, and digital images of the antimicrobial zone were taken. The diameters were averaged from the three measurements. The antimicrobial test was performed in duplicate and the average diameter of the inhibition zone with standard deviation was calculated.

5.4 Results and Discussion

5.4.1 Morphology of filled and unfilled electrospun PLA fibers

SEM micrographs in Fig. 5.1 comparatively show morphology of electrospun neat PLA fibers, PLA fibers filled with 5% (w/v) AgNPs/eCaCO$_3$ and AgNPs/CaCO$_3$ prepared with flow rate of 1 mL/h and applied voltage of 20 kV. The

electrospun fibers were prepared using binary solvent system of dichloromethane: dimethylformamide (DCM: DMF = 9:1 by volume). For unfilled PLA, continuous and uniform porous PLA fibers were obtained as illustrated in Fig. 5.1A. The porous morphology was initiated by the rapid evaporation of dichloromethane solvent and that led to phase separation of binary solvent system. This is the main reason to occur pores on the fiber surfaces (Luo, Nangrejo, & Edirisinghe, 2010). With 5% (w/v) AgNPs/e$CaCO_3$ and AgNPs/$CaCO_3$ loading, the electrospun fibers comparatively contained more beads of the filled particles in string along the fiber due to high degree of the local particle agglomeration during electrospinning process, as illustrated in Fig. 5.1B and 5.1C. The local particles agglomeration were caused by heterogeneous distribution of the particles during fiber forming and solvent evaporation after electrospinning. However, lesser particles agglomeration along the electrospun fibers were obtained from AgNPs/$CaCO_3$ filled PLA electrospun fibers comparing to the electrospun fibers of AgNPs/e$CaCO_3$ filled PLA. So, larger particles beads were obtained as AgNPs/$CaCO_3$ filled PLA fiber mat showed less particles agglomeration along the fiber comparing to AgNPs/e$CaCO_3$ filled PLA fiber mat because of the larger particle size of AgNPs/e$CaCO_3$. This results in occurring larger particles beads in string along the fiber in AgNPs/e$CaCO_3$ filled PLA.

The average diameter of electrospun fibers were 13.97 ± 2.69 μm, 7.10 ± 3.02 μm and 11.33 ± 3.38 μm for neat PLA, 5% (w/v) AgNPs/e$CaCO_3$ and AgNPs/$CaCO_3$ filled PLA, respectively.

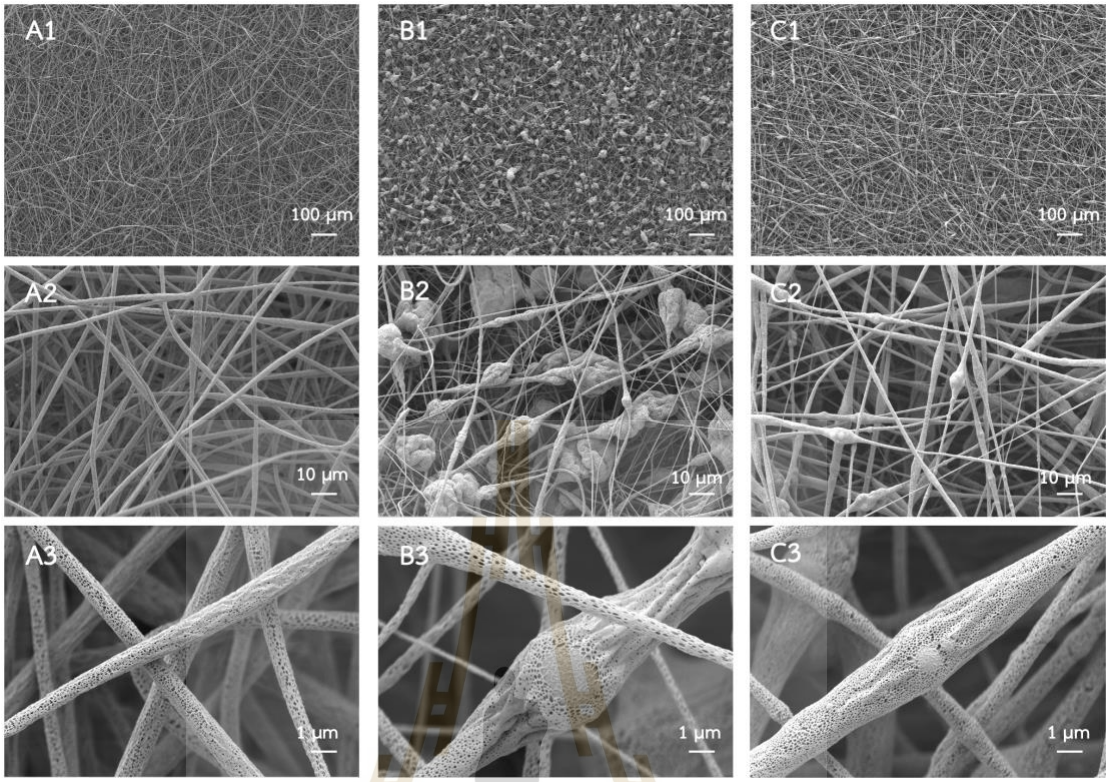

Figure 5.1 SEM micrographs of electrospun neat PLA fibers (A), PLA fiber filled with 5% (w/v) AgNPs/eCaCO$_3$ (B), and PLA fiber filled with 5% (w/v) AgNPs/CaCO$_3$ (C) prepared from PLA 10% (w/v) concentration, 1 mL/h flow rate and 20 kV applied voltage, using dichloromethane: dimethylformamide (DCM: DMF = 9:1 by volume) at magnification of 100 X (1), 800 X (2), and 5 kX (3).

5.4.2 X-ray Diffraction Analysis

The XRD patterns of neat PLA fibers, PLA fiber filled with 5% (w/v) AgNPs/eCaCO$_3$ and AgNPs/CaCO$_3$ are shown in Fig. 5.2. All the electrospun fibers showed the intensity with a broad maximum appearing at approximately 2θ = 15°, indicating semicrystalline structure of PLA. Tanase-Opedal et al. (Tanase-Opedal, Espinosa, Rodriguez, & Chinga-Carrasco, 2019) reported that PLA exhibits a broad peak at 2θ degrees = 10°– 25° associated with the semicrystalline nature of PLA. For the XRD patterns of PLA fibers filled with AgNPs/eCaCO$_3$ and AgNPs/CaCO$_3$, the diffraction peaks at 2θ = 25°, 27°, 33°, 44° and 50° which are corresponding to vaterite crystal

structures of calcium carbonate particles. Azarian et al. (Azarian & Sutapun, 2022) mentioned that XRD peaks appear at 2 θ of 21.07° , 25.05°, 27.20° , 32.94° , 43.33° , 50.15° , and 57.53° , corresponding to the presence and formation of vaterite polymorph crystal structure. Therefore, both AgNPs/eCaCO$_3$ and AgNPs/CaCO$_3$ particles were still maintained as vaterite crystal structures inside PLA electrospun fibers.

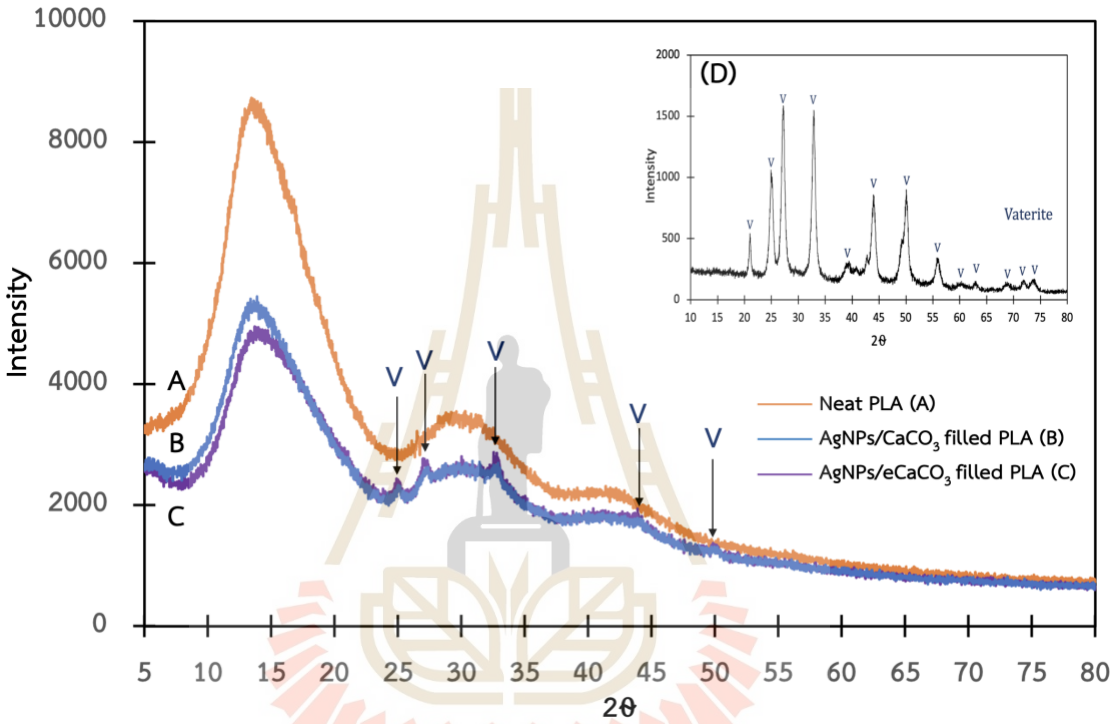

Figure 5.2 XRD patterns of electrospun fiber mats. Neat PLA fibers (A), AgNPs/CaCO$_3$ filled PLA (B), AgNPs/eCaCO$_3$ filled PLA (C) and an XRD pattern of AgNPs/eCaCO$_3$ particles.

5.4.3 Thermal degradation on unfilled and filled PLA

Thermogravimetric analysis has been extensively used to examine the thermal stability and decomposition of PLA and PLA based composites and to determine the amount of inorganic filler incorporated in the electrospun fibers. For PLA pellet and neat PLA fibers, the first thermal decomposition occurred in the temperature range of 35–150 °C due to the evaporation of physically adsorbed water. The second thermal degradation occurred at 363 °C for PLA pellet and 345 °C for neat PLA fibers respectively, as shown in TGA curves of Fig. 5.3A. Pakolpakçıl et al.

(Pakolpakçıl et al., 2021) and Alharbi et al. (Alharbi et al., 2018) stated that PLA thermally degraded at ~ 368 °C and it was completely decomposed at ~ 444 °C, associated with the loss of ester groups by unzipping depolymerization.

On the other hand, 5 % (w/v) AgNPs/e$CaCO_3$ filled PLA and 5 % (w/v) AgNPs/$CaCO_3$ filled PLA electrospun fiber mats showed similar four stages of degradation. The first thermal decomposition occurred in the temperature range of 35–150 °C due to the evaporation of physically adsorbed water. Secondly, PLA degradation peak occurred at 349 °C with the weight loss of 75.20 % for AgNPs/e$CaCO_3$ added PLA and 346 °C with the weight loss of 73.90 % for AgNPs/$CaCO_3$ added PLA, respectively. It is implied that the approximately 25 wt % hybrid particles incorporated into PLA matrix. The third decompositions in the temperature range of 460-505 °C for both PLA composites were derived from the thermal degradation of PSS in precipitated $CaCO_3$ of AgNPs/e$CaCO_3$ and AgNPs/$CaCO_3$. Bahrom et al. (Bahrom et al., 2019) reported that the thermal decomposition of precipitated $CaCO_3$ using PSS as an organic additive at 430-520 °C and 550-650 °C was due to the decomposition of PSS.

The final mass loss occurred between 665 and 742 °C, with DTGA peaks at 728 °C and a mass loss of 86.60 % for AgNPs/e$CaCO_3$ added PLA and at 720 °C and a mass loss of 87.10 %, for AgNPs/$CaCO_3$ added PLA. This final thermal decomposition corresponded to the decarbonization of vaterite $CaCO_3$ incorporated in the electrospun PLA composites. Popescu et al. (Popescu, Isopescu, Matei, Fagarasan, & Plesu, 2014) and Karunadasa et al. (Karunadasa, Manoratne, Pitawala, & Rajapakse, 2019) stated that the transformation temperature range of the $CaCO_3$ into CaO occurred at 600-790 °C with a peak of 750 °C and at 700-800 °C with a peak of 790 °C, respectively.

Table 5.1 Summary of thermal degradation on unfilled and filled PLA

Samples	**Filler content**	**1st thermal decomposition**	**2nd thermal decomposition**	**3rd thermal decomposition**	**4th thermal decomposition**
PLA pellet	-	35–150 °C	363 °C	-	-
Neat PLA fibers	-	35–150 °C	345 °C	-	-
AgNPs/$eCaCO_3$ filled PLA	5 % (w/v) AgNPs/$eCaCO_3$	35–150 °C	349 °C	460-505 °C	665-742 °C
AgNPs/$CaCO_3$ filled PLA	5 % (w/v) AgNPs/$CaCO_3$	35–150 °C	346 °C	460-505 °C	665-742 °C

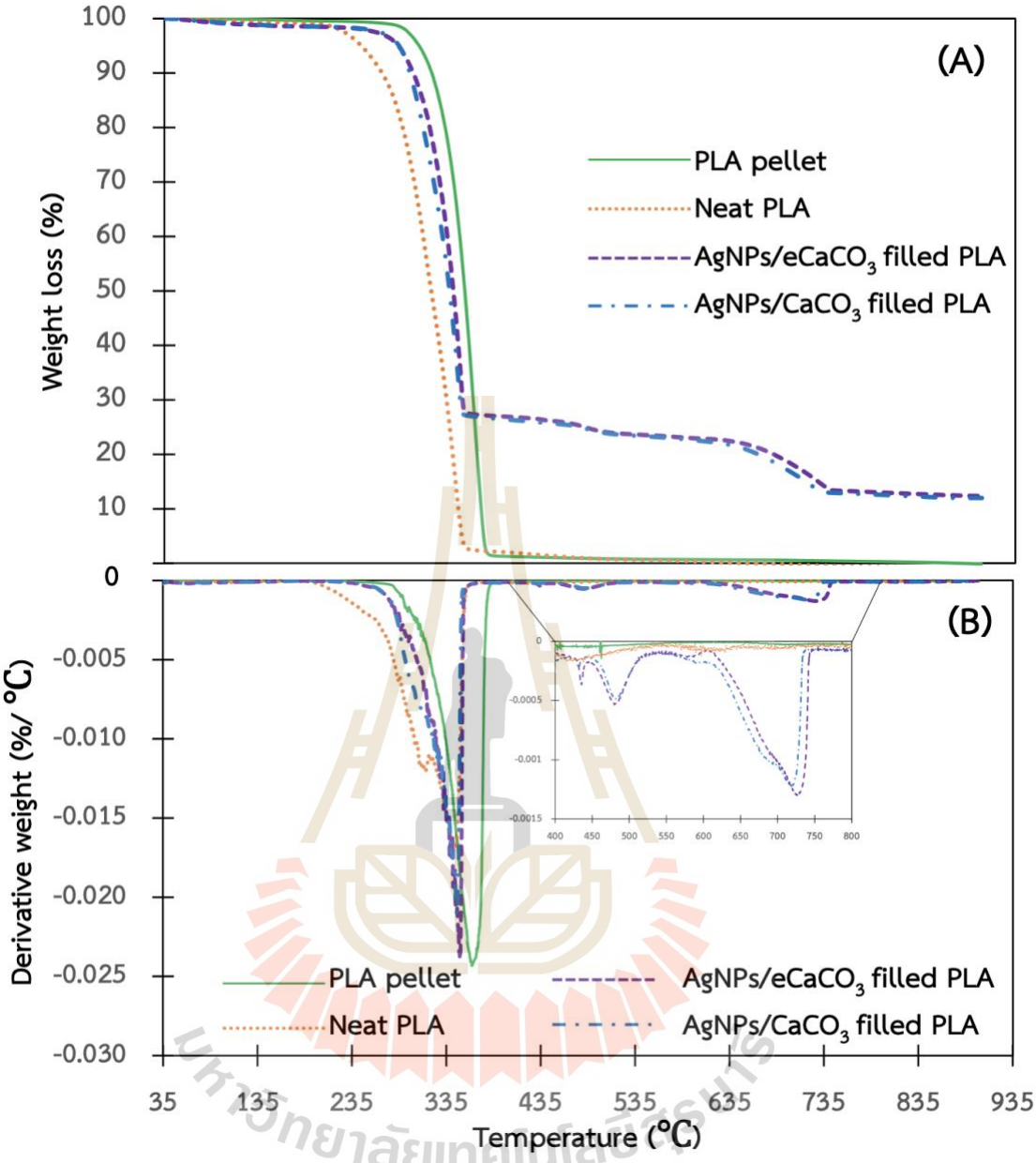

Figure 5.3 TGA curves (A) and DTGA curves (B) of PLA pellet, neat PLA fiber, 5 % (w/v) AgNPs/eCaCO$_3$ filled PLA and 5 % (w/v) AgNPs/CaCO$_3$ filled PLA.

5.4.4 Nanoindentation

The averaged load-depth curves and summary of nanoindentation results of neat PLA, 5 % (w/v) AgNPs/eCaCO$_3$ filled PLA and 5 % (w/v) AgNPs/CaCO$_3$ filled PLA are illustrated in Fig. 5.4 and Table 5.2, respectively. Neat PLA fibers showed the highest value of the maximum depth, followed by AgNPs/CaCO$_3$ filled PLA and AgNPs/eCaCO$_3$

filled PLA. The modulus is the resistance of material to elastic deformation. The initial slope of unloading curve is corresponds to the unloading stiffness and directly related to the elastic modulus (Lutpi, Anuar, Samat, Surip, & Bonnia, 2012). The unloading curve of AgNPs/eCaCO$_3$ filled PLA electrospun fiber mat in Fig. 5.4 showed the increase of unloading stiffness compared with the other electrospun fiber mats. Thus, the elastic modulus for AgNPs/eCaCO$_3$ filled PLA was 4.73 ± 0.84 MPa and highest among all of electeospun fiber mats. The elastic modulus of electrospun neat PLA fibers mat was 1.75 ± 0.19 MPa and AgNPs/CaCO$_3$ filled PLA was 1.66 ± 0.14 MPa.

Hardness is the resistance of material to local plastic deformation. The relation between indentation depth and hardness is inversely proportional as the additional percentage of nanoclay has increased hardness of all the polyamide-12/nanoclay which indicates by the lowest indentation depth (Aldousiri, Dhakal, Onuh, Zhang, & Bennett, 2011). Neat PLA has the highest indentation depth (17736.68 nm) showing that it has the lowest hardness of 0.20 MPa among all of electeospun fiber mats. The indentation depth of AgNPs/CaCO$_3$ filled PLA was 16365.93 nm and AgNPs/eCaCO$_3$ filled PLA was 10536.75 nm as their resulted hardness were 0.40 and 0.64 MPa, respectively.

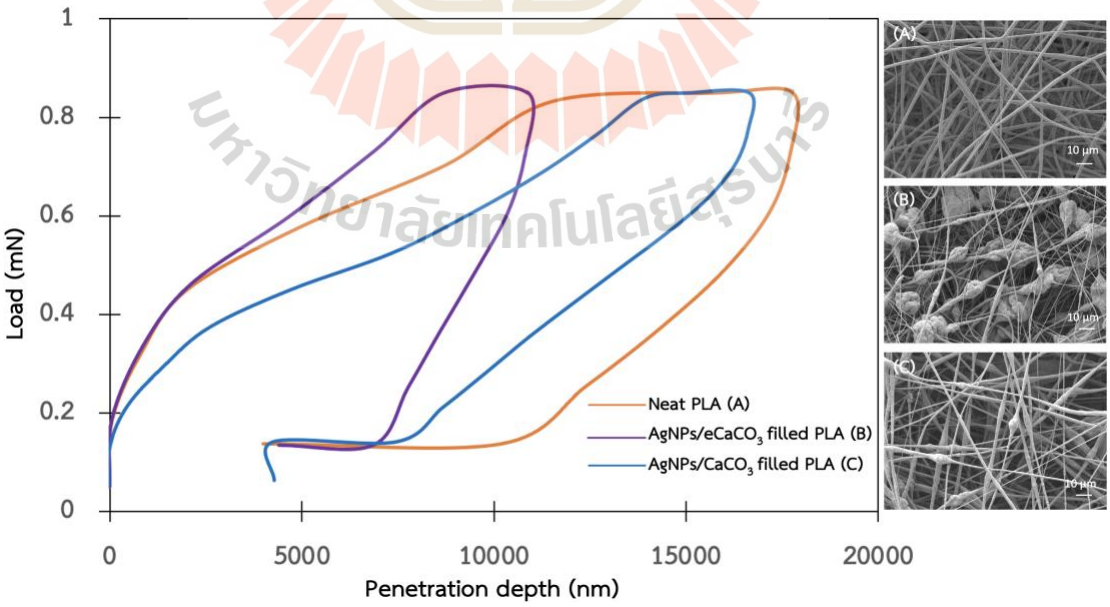

Figure 5.4 Load–depth curves of neat PLA, 5 % (w/v) AgNPs/eCaCO$_3$ filled PLA, 5 % (w/v) AgNPs/CaCO$_3$ filled PLA and their SEM images (A-C, respectively).

Table 5.2 Summary of nanoindentation results

Samples	Fiber mat's thickness (mm) (SD)	Max Depth (nm)(SD)	Hardness (MPa)(SD)	Elastic Modulus (MPa)(SD)
Neat PLA	0.035 ± 0.003	17736.68 ± 632.28	0.20 ± 0.02	1.75 ± 0.19
5 % (w/v) AgNPs/eCaCO$_3$ filled PLA	0.061 ± 0.003	10536.75 ± 809.58	0.64 ± 0.15	4.73 ± 0.84
5 % (w/v) AgNPs/CaCO$_3$ filled PLA	0.058 ± 0.005	16365.93 ± 583.88	0.40 ± 0.08	1.66 ±0.14

5.4.5 Cytotoxicity testing (MTT assay)

The lab report by Laboratory of Cell-Based Assay and Innovation (CBAI), Suranaree University of Technology on the cytotoxicity test in Human Dermal Fibroblasts (HDF) of neat PLA fibers, 5 % (w/v) AgNPs/eCaCO$_3$ filled PLA and 5 % (w/v) AgNPs/CaCO$_3$ filled PLA were shown in Fig. 5.5 and Fig. 5.6, respectively. At the higher concentration of 50 mg/mL for neat PLA fibers, no dead cells were found as shown in Fig. 5.5A-B. According to Fig. 5.6, nearly 100 % cell viability was found at the highest concentration of 50 mg/mL for AgNPs/eCaCO$_3$ filled PLA and AgNPs/CaCO$_3$ filled PLA. These proved that the antimicrobial effect of 5% (w/v) AgNPs/eCaCO$_3$ and AgNPs/CaCO$_3$ were not inhibited the growth of tested bacteria. Therefore, more study should be done on the aspect of increasing the hybrid particle content into PLA matrix in order to magnify antimicrobial activity of the filled PLA film.

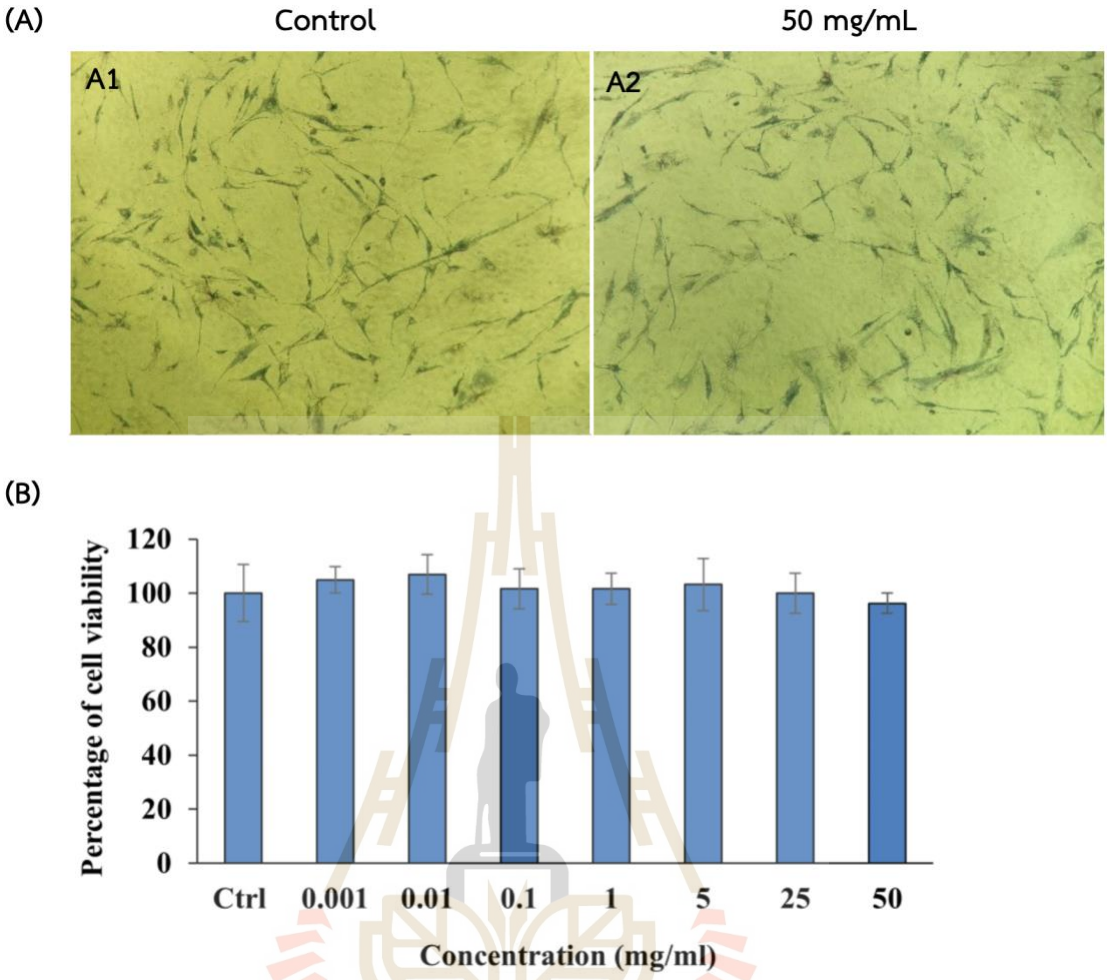

Figure 5.5 *In vitro* cytotoxicity test results of neat PLA fibers: Water-insoluble formazan crystals in human dermal fibroblast cells (A) and plots of cell viability (%) of human dermal fibroblast cells vs concentration (mg/mL) (B).

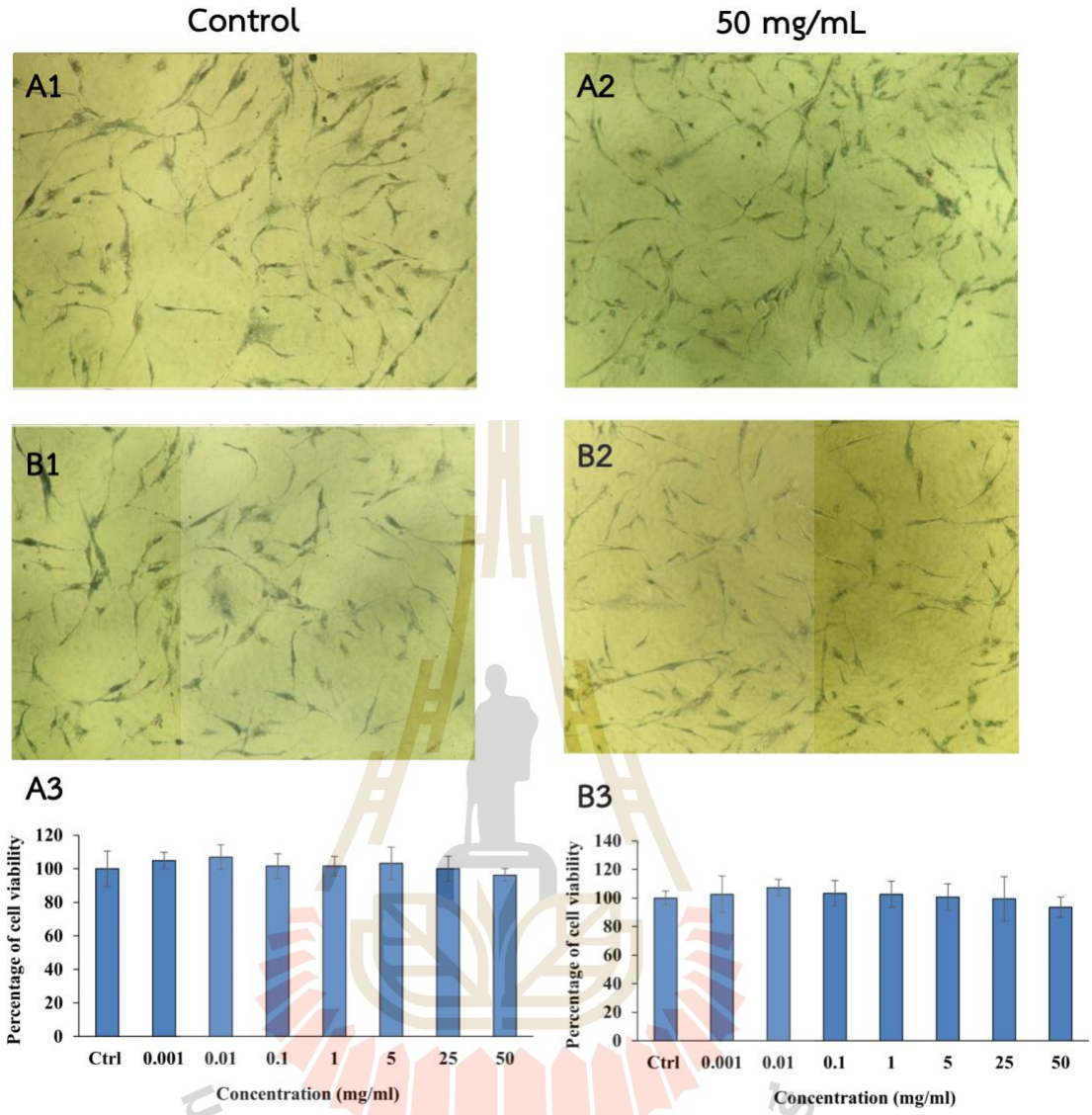

Figure 5.6 *In vitro* cytotoxicity test results of 5 % (w/v) AgNPs/eCaCO$_3$ filled PLA (A) and 5 % (w/v) AgNPs/CaCO$_3$ filled PLA (B): Water-insoluble formazan crystals in human dermal fibroblast cells (A1-2 and B1-B2) and Polts of cell viability (%) of human dermal fibroblast cells vs concentration (mg/mL) (A3 and B3).

5.4.6 Antimicrobial test

The Laboratory of Cell-Based Assay and Innovation (CBAI), Suranaree University of Technology, reported that the extract from the unpacked beef contained two types of Gram-negative and one type of Gram-positive bacteria whereas the extract from the vacuum-packed beef contained one type of Gram-negative and one type of Gram-positive bacteria. The image of the initial condition of *E. coli* smeared agar plate, clear color agar plate, was shown in Fig. 5.7A. As shown in Fig. 5.7A-C, there is no inhibitory effect was found for PLA and filled PLA against *E. coli* (A), bacteria extracted from unpacked raw beef from a local fresh market (B) and bacteria extracted from vacuum-packed beef ("INCHA BEEF" brand). This was proved that the antimicrobial effect of 5 % (w/v) AgNPs/e$CaCO_3$ and AgNPs/$CaCO_3$ were not enough to inhibit the growth of tested bacteria. So, more study should be done on the aspect of increasing the hybrid particle content into PLA matrix in order to magnify antimicrobial activity of the filled PLA film. These results were also well agreed with cytotoxicity testing against Human Dermal Fibroblasts (HDF) cells.

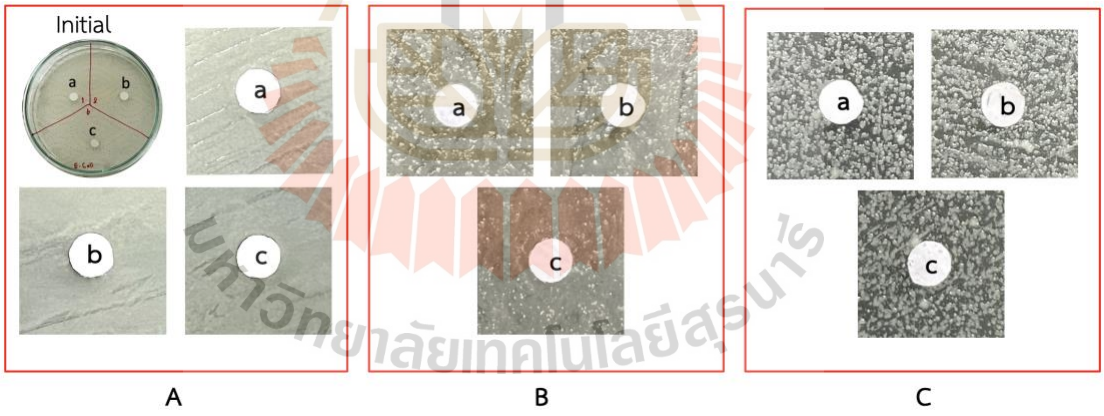

Figure 5.7 Antimicrobial activity against *E. coli* with the image of initial stage (A), bacteria extracted from unpacked raw beef from a local fresh market (B) and bacteria extracted from vacuum-packed beef ("INCHA BEEF" brand) (C). Neat PLA (a), 5 % (w/v) AgNPs/e$CaCO_3$ filled PLA (b), and 5 % (w/v) AgNPs/$CaCO_3$ filled PLA (c).

5.5 Conclusion

Electrospun PLA unfilled and filled fiber with highly porous structure were obtained at PLA 10 % w/v concentration, 1 mL/h flow rate and 20 kV applied voltage using binary solvent system of dichloromethane and dimethylformamide (DCM: DMF = 9:1 by volume). The average diameter of electrospun fiber were 13.97 ± 2.69 μm ,7.10 ± 3.02 μm, and 11.33 ± 3.38 μm for neat PLA, and AgNPs/e$CaCO_3$ and AgNPs/$CaCO_3$ filled PLA, respectively. The XRD patterns of the electrospun PLA and filled PLA fibers showed the semicrystalline structure of PLA. For 5 % (w/v) AgNPs/e$CaCO_3$ filled PLA and 5 % (w/v) AgNPs/$CaCO_3$ filled PLA, the crystal structures of calcium carbonate particles incorporated into PLA electrospun fibers were stilled vaterite polymorph.

The PLA thermal degradation of PLA pellet and neat PLA fibers occurred at 363 °C and 345 °C whereas four stages of degradation were occurred at 5 % (w/v) AgNPs/e$CaCO_3$ filled PLA and 5 % (w/v) AgNPs/$CaCO_3$ filled PLA. The first thermal decomposition occurred in the temperature range of 35–150 °C due to the evaporation of physically adsorbed water. Secondly, PLA degradation occurred at 349 °C with the weight loss of 75.20 % for AgNPs/e$CaCO_3$ added PLA and 346 °C with the weight loss of 73.90 % for AgNPs/$CaCO_3$ added PLA, respectively. The third decomposition were related to thermal degradation of PSS in precipitated $CaCO_3$ which occurred at 460-505 °C. The final thermal decomposition was at 665-742 °C corresponded to the decarbonization of vaterite $CaCO_3$ incorporated into electrospun PLA fibers.

Neat PLA fibers mat had the highest indentation depth of 17736.68 nm showing that it has the lowest hardness of 0.20 MPa among all of electeospun fiber mats. The indentation depth of AgNPs/$CaCO_3$ filled PLA was 16365.93 nm and that of AgNPs/e$CaCO_3$ filled PLA was 10536.75 nm with hardness of 0.40 and 0.64 MPa, respectively. The elastic modulus for AgNPs/e$CaCO_3$ filled PLA of 4.73 ± 0.84 MPa was highest among all of electeospun fiber mats.

No inhibitory effect was found for all samples against *E. coli*, bacteria extracted from unpacked raw beef from a local fresh market and from vacuum-packed beef (“INCHA BEEF” brand). For cytotoxicity testing against Human Dermal Fibroblasts (HDF) cells, no dead cells were found at 50 mg/mL concentration for all tested samples.

CHAPTER VI
CONCLUSION

Spherical AgNPs with an average size of 24.13 ± 2.95 nm were successfully prepared by reducing an $AgNO_3$ aqueous solution at 70 °C in the presence of trisodium citrate as a reducing agent and stabilizer. The Z-average (r.nm) and PDI are 42.14 nm and 0.21, respectively for freshly prepared silver colloids, and 55.07 and 0.19, respectively for AgNPs. Zeta potential of freshly prepared silver colloids and AgNPs obtained from freshly prepared silver colloids were - 49.30 mV and - 44.10 mV, respectively.

Novel hybrid antimicrobial microspherical particles of AgNPs/e$CaCO_3$ and AgNPs/$CaCO_3$ were successfully prepared via aqueous precipitation in the presence of freshly prepared silver colloids using poly (sodium 4-styrenesulphonate) as a polyelectrolyte. TEM, EDS and EDX confirmed that AgNPs were incorporated into the spherical precipitated $CaCO_3$ from eggshells and commercial calcium carbonate. The crystal polymorph of the precipitated e$CaCO_3$ was vaterite. The hybrid AgNPs/e$CaCO_3$ particles prepared at 25 °C had a spherical morphology and a narrow size distribution, with a mean diameter of 3.56 ± 0.26 μm. In contrast, AgNPs/e$CaCO_3$ prepared at 35 °C showed a broader size distribution with a mean diameter of 3.19 ± 1.20 μm. In addition, 0.78 wt% and 3.20 wt% AgNPs were deposited onto and inside the microspherical particles of precipitated eggshells and commercial calcium carbonate, respectively. AgNPs/$CaCO_3$ particles prepared at 25 °C also had a spherical morphology and a narrow size distribution with a mean diameter of 5.61 ± 0.66 μm. Both AgNPs/e$CaCO_3$ and AgNPs/$CaCO_3$ prepared at 25 °C have four regions of thermal decomposition with the overall weight loss of approximately 55.81% and 47.28% respectively. Therefore, eggshells and commercial calcium carbonate can be applied as carriers or supporters for the nanoparticles.

Antimicrobial test showed that both AgNPs/e$CaCO_3$ and AgNPs/$CaCO_3$ particles exhibited the same antimicrobial activity. The hybrid microspherical AgNPs/e$CaCO_3$ and

AgNPs/$CaCO_3$ particles inhibited the growth of bacteria extracted from both unpacked and vacuum-packed beef. However, AgNPs/e$CaCO_3$ and AgNPs/$CaCO_3$ showed concentration-dependent antimicrobial activity against bacteria extracted from vacuum-packed beef. Significant HDF (human dermal fibroblast) cells dead were found at 5 mg/mL for AgNPs/e$CaCO_3$ and 25 mg/mL for AgNPs/$CaCO_3$ and no alive HDF cells were resulted at the concentration of 50 mg/mL for both samples.

In preparing electrospun fibers from PLA and PLA filled with the hybrid particles, it was found that with the binary solvent systems of chloroform and acetone (CHL: AC, 2:1 by volume), 10 and 15% (w/v) PLA solutions gave rise to electrospun continuous fibers without beads. Larger diameter electrospun fibers were obtained at higher flow rate of 1.5 mL/h and higher applied voltage of 18 kV resulted in smaller diameter fibers than lower applied voltage of 15 kV. PLA electrospun fibers filled with 1 % (w/v) AgNPs/e$CaCO_3$ contained some particles blooming along the fibers. However, more particle blooming and nonuniform shape were observed from the electrospun fibers filled with 3% (w/v) AgNPs/e$CaCO_3$. The electrospun fibers obtained from 1 % (w/v) AgNPs/e$CaCO_3$ loading with applied voltage of 18 kV were more uniform in shape.

For binary solvent systems, by 9:1 by volume, of chloroform and dimethylformamide (CHL: DMF) and dichloromethane and dimethylformamide (DCM: DMF), 10 % w/v PLA solution electrosupn at 1 mL/h flow rate and 20 kV applied voltage gave uniform diameter fiber for both binary solvent systems. Incorporation of 5% (w/v) AgNPs/e$CaCO_3$ filler into the PLA electrospun fiber, the binary solvent system of DCM: DMF gave rise to larger fiber diameter with bead on the string along the fibers. For tensile properties, PLA with 5% (w/v) AgNPs/e$CaCO_3$ electrospun fibers from the solvent system of DCM: DMF, showed higher Young modulus and ultimate tensile strength than the one prepared from solvent system of CHL: DMF . Therefore, 5% (w/v) AgNPs/e$CaCO_3$ and AgNPs/$CaCO_3$ filled PLA electrospun fibers mats using dichloromethane and dimethylformamide were electrospun for 5 h in order to use in further characterization such as nanoindentation, XRD, antimicrobial and cytotoxicity testing.

Electrospun PLA unfilled and filled fiber with highly porous structure were obtained at PLA 10 % (w/v) concentration, 1 mL/h flow rate and 20 kV applied voltage

using binary solvent system of dichloromethane and dimethylformamide (DCM: DMF = 9:1 by volume). The average diameter of electrospun fibers were 13.97 ± 2.69 μm ,7.10 ± 3.02 μm, and 11.33 ± 3.38 μm for neat PLA, and AgNPs/eCaCO$_3$ and AgNPs/CaCO$_3$ filled PLA, respectively. The XRD patterns of all the electrospun fibers showed the semicrystalline structure of PLA. For 5 % (w/v) AgNPs/eCaCO$_3$ and AgNPs/CaCO$_3$ filled PLA fibers mats, the crystal structures of calcium carbonate particles incorporated into PLA electrospun fibers were still vaterite polymorph. The PLA thermal degradation of PLA pellet and neat PLA fibers occurred at 363°C and 345 °C whereas four stages of degradation were occurred at 5 % (w/v) AgNPs/eCaCO$_3$ and AgNPs/CaCO$_3$ filled PLA fibers mats. The first thermal decomposition occurred in the temperature range of 35–150 °C due to the evaporation of physically adsorbed water. Secondly, PLA degradation occurred at 349 °C with the weight loss of 75.20 % for AgNPs/eCaCO$_3$ added PLA and 346 °C with the weight loss of 73.90 % for AgNPs/CaCO$_3$ added PLA, respectively. Approximately 25 wt % hybrid particles incorporated into PLA matrix. The third decomposition were related to thermal degradation of PSS in precipitated CaCO$_3$ which occurred at 460-505 °C. The final thermal decomposition was at 665-742 °C corresponded to the decarbonization of vaterite CaCO$_3$ incorporated into electrospun PLA fibers.

Neat PLA fibers mat had the highest indentation depth showing that it has the lowest hardness of 0.20 MPa among all of electeospun fiber mats. AgNPs/CaCO$_3$ filled PLA had higher indentation depth than AgNPs/eCaCO$_3$ filled PLA. The higher indentation depth led to lower hardness of 0.40 MPa for AgNPs/CaCO$_3$ filled PLA and 0.64 MPa for AgNPs/eCaCO$_3$ filled PLA. The elastic modulus for AgNPs/eCaCO$_3$ filled PLA of 4.73 ± 0.84 MPa was highest among all of electeospun fiber mats.

No inhibitory effect was found for all samples against *E. coli*, bacteria extracted from unpacked raw beef from a local fresh market and from vacuum-packed beef (“INCHA BEEF” brand). This was because the amount of 5 % (w/v) AgNPs/eCaCO$_3$ and AgNPs/eCaCO$_3$ filler content inside PLA porous fibers mats was not still enough to kill or inhibit the growth of bacteria. The results showed the same when testing cytotoxicity. For cytotoxicity testing against Human Dermal Fibroblasts (HDF) cells, no dead cells were found at 50 mg/mL concentration for all tested samples. Therefore,

up to 5 to 15 % (w/v) AgNPs/eCaCO$_3$ and AgNPs/eCaCO$_3$ will be needed to incorporate into PLA fibers mats.

Therefore, this study confirmed that hybrid antimicrobial microspherical particles of AgNPs/eCaCO$_3$ and AgNPs/CaCO$_3$ were successfully prepared and incorporated into PLA matrix using electrospinning technique. These electrospun fibers mats have potential to be developed as antimicrobial food packaging in the future. However, more study should be done on the aspect of increasing AgNPs content of the hybrid particles and make them homogeneously distributed in PLA matrix.

REFERENCES

Ahari, H., Karim, G., Anvar, A. A., Pooyamanesh, M., Sajadis, A., Mostaghim, A., & Heydari, S. (2018). *Synthesis of the Silver Nanoparticle by Chemical Reduction Method and Preparation of Nanocomposite based on AgNPS*. Paper presented at the Proceedings of the 4th World Congress on Mechanical, Chemical, and Material Engineering.

Ahmed, T. A. E., Wu, L., Younes, M., & Hincke, M. (2021). Biotechnological Applications of Eggshell: Recent Advances. *Front Bioeng Biotechnol, 9*, 675364. doi:10.3389/fbioe.2021.675364

Aldousiri, B., Dhakal, H. N., Onuh, S., Zhang, Z. Y., & Bennett, N. (2011). Nanoindentation behaviour of layered silicate filled spent polyamide-12 nanocomposites. *Polymer Testing, 30*(6), 688-692. doi:10.1016/j.polymertesting.2011.05.008

Alharbi, H. F., Luqman, M., Khalil, K. A., Elnakady, Y. A., Abd-Elkader, O. H., Rady, A. M., . . . Karim, M. R. (2018). Fabrication of core-shell structured nanofibers of poly (lactic acid) and poly (vinyl alcohol) by coaxial electrospinning for tissue engineering. *European Polymer Journal, 98*, 483-491. doi:10.1016/j.eurpolymj.2017.11.052

Alven, S., Buyana, B., Feketshane, Z., & Aderibigbe, B. A. (2021). Electrospun Nanofibers/Nanofibrous Scaffolds Loaded with Silver Nanoparticles as Effective Antibacterial Wound Dressing Materials. *Pharmaceutics, 13*(7). doi:10.3390/pharmaceutics13070964

Apalangya, V., Rangari, V., Tiimob, B., Jeelani, S., & Samuel, T. (2014). Development of antimicrobial water filtration hybrid material from bio source calcium carbonate and silver nanoparticles. *Applied Surface Science, 295*, 108-114. doi:10.1016/j.apsusc.2014.01.012

Appendini, P. (2002). Review of antimicrobial food packaging. *Innovative Food Science & Emerging Technologies, 3*, 113-126. doi:https://doi.org/10.1016/S1466-8564(02)00012-7

Arif, M. S., Ulfiya, R., Erwin, & Panggabean, A. S. (2021). *Synthesis silver nanoparticles using trisodium citrate and development in analysis method*. Paper presented at the International Conference on Energy and Environment (Icee 2021).

Arvanitoyannis, I. S., & Kotsanopoulos, K. V. (2013). Migration Phenomenon in Food Packaging. Food–Package Interactions, Mechanisms, Types of Migrants, Testing and Relative Legislation—A Review. *Food and Bioprocess Technology, 7*(1), 21-36. doi:10.1007/s11947-013-1106-8

Ashmore, D., Chaudhari, A., Barlow, B., Barlow, B., Harper, T., Vig, K., . . . Pillai, S. (2018). Evaluation of E. coli inhibition by plain and polymer-coated silver nanoparticles. *Rev Inst Med Trop Sao Paulo, 60*, e18. doi:10.1590/s1678-9946201860018

Azarian, M. H., & Sutapun, W. (2022). Tuning polymorphs of precipitated calcium carbonate from discarded eggshells: effects of polyelectrolyte and salt concentration. *RSC Adv, 12*(23), 14729-14739. doi:10.1039/d2ra01673g

Bahrom, H., Goncharenko, A. A., Fatkhutdinova, L. I., Peltek, O. O., Muslimov, A. R., Koval, O. Y., . . . Zyuzin, M. V. (2019). Controllable Synthesis of Calcium Carbonate with Different Geometry: Comprehensive Analysis of Particle Formation, Cellular Uptake, and Biocompatibility. *ACS Sustainable Chemistry & Engineering, 7*(23), 19142-19156. doi:10.1021/acssuschemeng.9b05128

Banne, S. V., Patil, M. S., Kulkarni, R. M., & Patil, S. J. (2017). Synthesis and Characterization of Silver Nano Particles for EDM Applications. *Materials Today: Proceedings, 4*(11), 12054-12060. doi:10.1016/j.matpr.2017.09.130

Bapat, R. A., Chaubal, T. V., Joshi, C. P., Bapat, P. R., Choudhury, H., Pandey, M., . . . Kesharwani, P. (2018). An overview of application of silver nanoparticles for biomaterials in dentistry. *Mater Sci Eng C Mater Biol Appl, 91*, 881-898. doi:10.1016/j.msec.2018.05.069

Barabadi, H., Mohammadzadeh, A., Vahidi, H., Rashedi, M., Saravanan, M., Talank, N., & Alizadeh, A. (2021). Penicillium chrysogenum-Derived Silver Nanoparticles: Exploration of Their Antibacterial and Biofilm Inhibitory Activity Against the Standard and Pathogenic Acinetobacter baumannii Compared to Tetracycline. *Journal of Cluster Science, 33*(5), 1929-1942. doi:10.1007/s10876-021-02121-5

Barros-Velazquez, J. (2016). *Antimicrobial Food Packaging-Elsevier Ltd,Academic Press (2016).pdf*.

Beaudrie, C. E. H., Kandlikar, M., & Ramachandran, G. (2016). Using Expert Judgment for Risk Assessment. In *Assessing Nanoparticle Risks to Human Health* (pp. 91-119).

Bhunia, K., Sablani, S. S., Tang, J., & Rasco, B. (2013). Migration of Chemical Compounds from Packaging Polymers during Microwave, Conventional Heat Treatment, and Storage. *Comprehensive Reviews in Food Science and Food Safety, 12*(5), 523-545. doi:10.1111/1541-4337.12028

Biji, K. B., Ravishankar, C. N., Mohan, C. O., & Srinivasa Gopal, T. K. (2015). Smart packaging systems for food applications: a review. *J Food Sci Technol, 52*(10), 6125-6135. doi:10.1007/s13197-015-1766-7

Bodhidatta. (2013). Bacterial pathogens isolated from raw meat and poultry compared with pathogens isolated from children in the same area of rural thailand. *Southeast Asian J Trop Med Public Health, 44*.

Boyjoo, Y., Pareek, V. K., & Liu, J. (2014). Synthesis of micro and nano-sized calcium carbonate particles and their applications. *J. Mater. Chem. A, 2*(35), 14270-14288. doi:10.1039/c4ta02070g

Casasola, R., Thomas, N. L., Trybala, A., & Georgiadou, S. (2014). Electrospun poly lactic acid (PLA) fibres: Effect of different solvent systems on fibre morphology and diameter. *Polymer, 55*(18), 4728-4737. doi:10.1016/j.polymer.2014.06.032

Castro, L. d. S., Barañano, A. G., Pinheiro, C. J. G., Menini, L., & Pinheiro, P. F. (2019). Biodiesel production from cotton oil using heterogeneous CaO catalysts from eggshells prepared at different calcination temperatures. *Green Processing and Synthesis, 8*(1), 235-244. doi:10.1515/gps-2018-0076

Castro-Mayorga, J. L., Martinez-Abad, A., Fabra, M. J., Olivera, C., Reis, M., & Lagaron, J. M. (2014). Stabilization of antimicrobial silver nanoparticles by a polyhydroxyalkanoate obtained from mixed bacterial culture. *Int J Biol Macromol, 71*, 103-110. doi:10.1016/j.ijbiomac.2014.06.059

Castro-Mayorga, J. L., Martínez-Abad, A., Fabra, M. F., Lagarón, J.M., Ocio, M.J. and. Sánchez, G. Chapter 32 - Silver-Based antibacterial and virucide biopolymers: usage and potential.

Chen, J., Li, S., Luo, J., Wang, R., & Ding, W. (2016). Enhancement of the Antibacterial Activity of Silver Nanoparticles against Phytopathogenic BacteriumRalstonia solanacearumby Stabilization. *Journal of Nanomaterials, 2016*(1), 1-15. doi:10.1155/2016/7135852

Dallas, P., Sharma, V. K., & Zboril, R. (2011). Silver polymeric nanocomposites as advanced antimicrobial agents: classification, synthetic paths, applications, and perspectives. *Adv Colloid Interface Sci, 166*(1-2), 119-135. doi:10.1016/j.cis.2011.05.008

Dapeng, Y., Bin, Z., & Minghuan, L. (2017). It is a kind of to prepare CaCO by template of egg-shell meal3The method of Ag composites.

Dasaradhudu, Y., & Arunachalam Srinivasan, M. (2020). Synthesis and characterization of silver nano particles using co-precipitation method. *Materials Today: Proceedings, 33*, 720-723. doi:10.1016/j.matpr.2020.06.029

Dizaj, S. M., Lotfipour, F., Barzegar-Jalali, M., Zarrintan, M. H., & Adibkia, K. (2014). Antimicrobial activity of the metals and metal oxide nanoparticles. *Mater Sci Eng C Mater Biol Appl, 44*, 278-284. doi:10.1016/j.msec.2014.08.031

Dlugosz, M., Bulwan, M., Kania, G., Nowakowska, M., & Zapotoczny, S. (2012). Hybrid calcium carbonate/polymer microparticles containing silver nanoparticles as antibacterial agents. *J Nanopart Res, 14*(12), 1313-1319. doi:10.1007/s11051-012-1313-7

Du, J., Hu, Z., Yu, Z., Li, H., Pan, J., Zhao, D., & Bai, Y. (2019). Antibacterial activity of a novel Forsythia suspensa fruit mediated green silver nanoparticles against food-borne pathogens and mechanisms investigation. *Mater Sci Eng C Mater Biol Appl, 102*, 247-253. doi:10.1016/j.msec.2019.04.031

Duran, N., Nakazato, G., & Seabra, A. B. (2016). Antimicrobial activity of biogenic silver nanoparticles, and silver chloride nanoparticles: an overview and comments. *Appl Microbiol Biotechnol, 100*(15), 6555-6570. doi:10.1007/s00253-016-7657-7

Dutta, R. K., Nenavathu, B. P., Gangishetty, M. K., & Reddy, A. V. (2012). Studies on antibacterial activity of ZnO nanoparticles by ROS induced lipid peroxidation. *Colloids Surf B Biointerfaces, 94*, 143-150. doi:10.1016/j.colsurfb.2012.01.046

Echegoyen, Y., & Nerin, C. (2013). Nanoparticle release from nano-silver antimicrobial food containers. *Food Chem Toxicol, 62*, 16-22. doi:10.1016/j.fct.2013.08.014

Emamifar, A., Kadivar, M., Shahedi, M., & Soleimanian-Zad, S. (2010). Evaluation of nanocomposite packaging containing Ag and ZnO on shelf life of fresh orange juice. *Innovative Food Science & Emerging Technologies, 11*(4), 742-748. doi:10.1016/j.ifset.2010.06.003

Gnanasekharan, V., & Floros, J. D. (1997). Migration and sorption phenomena in packaged foods. *Crit Rev Food Sci Nutr, 37*(6), 519-559. doi:10.1080/10408399709527788

Gola, D., kriti, A., Bhatt, N., Bajpai, M., Singh, A., Arya, A., . . . Agrawal, Y. (2021). Silver nanoparticles for enhanced dye degradation. *Current Research in Green and Sustainable Chemistry, 4*. doi:10.1016/j.crgsc.2021.100132

Grigor'eva, A., Saranina, I., Tikunova, N., Safonov, A., Timoshenko, N., Rebrov, A., & Ryabchikova, E. (2013). Fine mechanisms of the interaction of silver nanoparticles with the cells of Salmonella typhimurium and Staphylococcus aureus. *Biometals, 26*(3), 479-488. doi:10.1007/s10534-013-9633-3

Haider, A., Haider, S., & Kang, I.-K. (2018). A comprehensive review summarizing the effect of electrospinning parameters and potential applications of nanofibers in biomedical and biotechnology. *Arabian Journal of Chemistry, 11*(8), 1165-1188. doi:10.1016/j.arabjc.2015.11.015

Hassan, T. A., Rangari, V. K., Rana, R. K., & Jeelani, S. (2013). Sonochemical effect on size reduction of CaCO3 nanoparticles derived from waste eggshells. *Ultrason Sonochem, 20*(5), 1308-1315. doi:10.1016/j.ultsonch.2013.01.016

Hincke, M., Gautron, J., Rodriguez-Navarro, A. B. and McKee, M. D. . (2011). Chapter 8 The eggshell: structure and protective function. doi:10.1016/B978-1-84569-754-9.50008-5

Hincke, M. T., Nys, Y., Gautron, J., Mann, K., Rodriguez-Navarro, A.B. and McKee, M.D. (2012). Hinckeetal.the eggshell: structure, composition and mineralization. 2012.pdf.

Humberto H Lara, N. V. A.-N., Liliana Ixtepan-Turrent, Cristina Rodriguez-Padilla. (2010). Mode of antiviral action of silver nanoparticles against HIV-1. *Journal of Nanobiotechnology, 8*(1), 1-10.

Jada, A., & Jradi, K. (2006). Role of Polyelectrolytes in Crystallogenesis of Calcium Carbonate. *Macromolecular Symposia, 233*(1), 147-151. doi:10.1002/masy.200690011

Kalantari, K., Mostafavi, E., Afifi, A. M., Izadiyan, Z., Jahangirian, H., Rafiee-Moghaddam, R., & Webster, T. J. (2020). Wound dressings functionalized with silver nanoparticles: promises and pitfalls. *Nanoscale, 12*(4), 2268-2291. doi:10.1039/c9nr08234d

Kamat, Z. S. P. a. P. V. (2004

). What Factors Control the Size and Shape of Silver Nanoparticles in the Citrate Ion Reduction Method?

. *Journal of Physical Chemistry, 108*(3), 945-951.

Kamat*, Z. S. P. a. P. V. (2004). What Factors Control the Size and Shape of Silver Nanoparticles in the Citrate Ion

Reduction Method? *J. Phys. Chem., 108*.

Kandarp Mavani, M. S. (2013). Synthesis of Silver Nanoparticles by using Sodium Borohydride as a Reducing

Agent. *International Journal of Engineering Research & Technology (IJERT), 2*(3), 1-5. doi:10.13140/2.1.3116.8648

Karunadasa, K. S. P., Manoratne, C. H., Pitawala, H. M. T. G. A., & Rajapakse, R. M. G. (2019). Thermal decomposition of calcium carbonate (calcite polymorph) as examined by in-situ high-temperature X-ray powder diffraction. *Journal of Physics and Chemistry of Solids, 134*, 21-28. doi:10.1016/j.jpcs.2019.05.023

Kayaci, F., Umu, O. C., Tekinay, T., & Uyar, T. (2013). Antibacterial electrospun poly(lactic acid) (PLA) nanofibrous webs incorporating triclosan/cyclodextrin inclusion complexes. *J Agric Food Chem, 61*(16), 3901-3908. doi:10.1021/jf400440b

Kim, J. S., Kuk, E., Yu, K. N., Kim, J. H., Park, S. J., Lee, H. J., . . . Cho, M. H. (2007). Antimicrobial effects of silver nanoparticles. *Nanomedicine, 3*(1), 95-101. doi:10.1016/j.nano.2006.12.001

Kinayturk, N. K., Tunali, B., & Turkoz Altug, D. (2021). Eggshell as a biomaterial can have a sorption capability on its surface: A spectroscopic research. *R Soc Open Sci, 8*(6), 210100. doi:10.1098/rsos.210100

Kumar, R., Howdle, S., & Munstedt, H. (2005). Polyamide/silver antimicrobials: effect of filler types on the silver ion release. *J Biomed Mater Res B Appl Biomater, 75*(2), 311-319. doi:10.1002/jbm.b.30306

Kwiatkowska, A., Drabik, M., Lipko, A., Grzeczkowicz, A., Stachowiak, R., Marszalik, A., & Granicka, L. H. (2022). Composite Membrane Dressings System with Metallic Nanoparticles as an Antibacterial Factor in Wound Healing. *Membranes (Basel), 12*(2), 1-25. doi:10.3390/membranes12020215

Lee, S. H., & Jun, B. H. (2019). Silver Nanoparticles: Synthesis and Application for Nanomedicine. *Int J Mol Sci, 20*(4). doi:10.3390/ijms20040865

Lee, S. M., Song, K. C., & Lee, B. S. (2010). Antibacterial activity of silver nanoparticles prepared by a chemical reduction method. *Korean Journal of Chemical Engineering, 27*(2), 688-692. doi:10.1007/s11814-010-0067-0

Lei, M., Tang, W. H., Cao, L. Z., Li, P. G., & Yu, J. G. (2006). Effects of poly (sodium 4-styrene-sulfonate) on morphology of calcium carbonate particles. *Journal of Crystal Growth, 294*(2), 358-366. doi:10.1016/j.jcrysgro.2006.06.029

Luo, C. J., Nangrejo, M., & Edirisinghe, M. (2010). A novel method of selecting solvents for polymer electrospinning. *Polymer, 51*(7), 1654-1662. doi:10.1016/j.polymer.2010.01.031

Lutpi, H. A., Anuar, H., Samat, N., Surip, S. N., & Bonnia, N. N. (2012). Evaluation of Elastic Modulus and Hardness of Polylactic Acid-Based Biocomposite by Nano-Indentation. *Advanced Materials Research, 576*, 446-449. doi:10.4028/www.scientific.net/AMR.576.446

M., X. (2009). Xanthos M. (ed.) - Functional Fillers for Plastics-Wiley (2009).pdf.

Maliszewska, I., & Czapka, T. (2022). Electrospun Polymer Nanofibers with Antimicrobial Activity. *Polymers (Basel), 14*(9). doi:10.3390/polym14091661

Mamun Ur Rashid, M. K. H. B. a. M. E. Q. (2013). Synthesis of Silver Nano Particles (Ag-NPs) and their uses for Quantitative Analysis of Vitamin C Tablets. *Journal of Pharmaceutical Sciences, 12*(1), 29-33.

Marambio-Jones, C., & Hoek, E. M. V. (2010). A review of the antibacterial effects of silver nanomaterials and potential implications for human health and the environment. *Journal of Nanoparticle Research, 12*(5), 1531-1551. doi:10.1007/s11051-010-9900-y

Matabola, K. P., & Moutloali, R. M. (2013). The influence of electrospinning parameters on the morphology and diameter of poly(vinyledene fluoride) nanofibers-effect of sodium chloride. *Journal of Materials Science, 48*(16), 5475-5482. doi:10.1007/s10853-013-7341-6

Matahwa, H., Ramiah, V., & Sanderson, R. D. (2008). Calcium carbonate crystallization in the presence of modified polysaccharides and linear polymeric additives. *Journal of Crystal Growth, 310*(21), 4561-4569. doi:10.1016/j.jcrysgro.2008.07.089

Maxwell T. Hincke1, Y. N., Joel Gautron2, Karlheinz Mann3, Alejandro B. Rodriguez-Navarro4, Marc D. McKee5. (2012). The eggshell: structure, composition and mineralization

. *Frontiers in Bioscience 17*(1), 1266-1280.

Mensah, K., Abdelmageed, A. M., & Shokry, H. (2022). Effect of eggshell/N,N-dimethylformamide (DMF) mixing ratios on the sonochemical production of CaCO3 nanoparticles. *Journal of Engineering and Applied Science, 69*(1). doi:10.1186/s44147-022-00070-y

Molleman, B., & Hiemstra, T. (2015). Surface Structure of Silver Nanoparticles as a Model for Understanding the Oxidative Dissolution of Silver Ions. *Langmuir, 31*(49), 13361-13372. doi:10.1021/acs.langmuir.5b03686

Morones, J. R., Elechiguerra, J. L., Camacho, A., Holt, K., Kouri, J. B., Ramirez, J. T., & Yacaman, M. J. (2005). The bactericidal effect of silver nanoparticles. *Nanotechnology, 16*(10), 2346-2353. doi:10.1088/0957-4484/16/10/059

Mousavi Khaneghah, A., Hashemi, S. M. B., & Limbo, S. (2018). Antimicrobial agents and packaging systems in antimicrobial active food packaging: An overview of approaches and interactions. *Food and Bioproducts Processing, 111*, 1-19. doi:10.1016/j.fbp.2018.05.001

Nadia Razali1, N. J., 2*, Adlin Yasmin Jalani1, Nurhanim Zulaikha Kamarulzaman1, Khairul Faizal Pa'ee3. (2022). THERMAL DECOMPOSITION OF CALCIUM CARBONATE IN CHICKEN EGGSHELLS: STUDY ON TEMPERATURE AND CONTACT TIME. *Malaysian Journal of Analytical Sciences, 26*.

Nocchetti, M., Donnadio, A., Ambrogi, V., Andreani, P., Bastianini, M., Pietrella, D., & Latterini, L. (2013). Ag/AgCl nanoparticle decorated layered double hydroxides: synthesis, characterization and antimicrobial properties. *J. Mater. Chem. B, 1*(18). doi:10.1039/c3tb00561e

Omerovic, N., Djisalov, M., Zivojevic, K., Mladenovic, M., Vunduk, J., Milenkovic, I., . . . Vidic, J. (2021). Antimicrobial nanoparticles and biodegradable polymer composites for active food packaging applications. *Compr Rev Food Sci Food Saf, 20*(3), 2428-2454. doi:10.1111/1541-4337.12727

Pakolpakçıl, A., Draczyński, Z., Szulc, J., Stawski, D., Tarzyńska, N., Bednarowicz, A., . . . Gutarowska, B. (2021). An In Vitro Study of Antibacterial Properties of Electrospun Hypericum perforatum Oil-Loaded Poly(lactic Acid) Nonwovens for Potential Biomedical Applications. *Applied Sciences, 11*(17). doi:10.3390/app11178219

Pan, S.-F., Ke, X.-X., Wang, T.-Y., Liu, Q., Zhong, L.-B., & Zheng, Y.-M. (2018). Synthesis of Silver Nanoparticles Embedded Electrospun PAN Nanofiber Thin-Film Composite Forward Osmosis Membrane to Enhance Performance and Antimicrobial Activity. *Industrial & Engineering Chemistry Research, 58*(2), 984-993. doi:10.1021/acs.iecr.8b04893

Parvekar, P., Palaskar, J., Metgud, S., Maria, R., & Dutta, S. (2020). The minimum inhibitory concentration (MIC) and minimum bactericidal concentration (MBC) of silver nanoparticles against Staphylococcus aureus. *Biomater Investig Dent, 7*(1), 105-109. doi:10.1080/26415275.2020.1796674

Pillay, V., Dott, C., Choonara, Y. E., Tyagi, C., Tomar, L., Kumar, P., . . . Ndesendo, V. M. K. (2013). A Review of the Effect of Processing Variables on the Fabrication of Electrospun Nanofibers for Drug Delivery Applications. *Journal of Nanomaterials, 2013*, 1-22. doi:10.1155/2013/789289

Pinto, R. J., Fernandes, S. C., Freire, C. S., Sadocco, P., Causio, J., Neto, C. P., & Trindade, T. (2012). Antibacterial activity of optically transparent nanocomposite films based on chitosan or its derivatives and silver nanoparticles. *Carbohydr Res, 348*, 77-83. doi:10.1016/j.carres.2011.11.009

Popescu, M.-A., Isopescu, R., Matei, C., Fagarasan, G., & Plesu, V. (2014). Thermal decomposition of calcium carbonate polymorphs precipitated in the presence of ammonia and alkylamines. *Advanced Powder Technology, 25*(2), 500-507. doi:10.1016/j.apt.2013.08.003

Quintavall, S. (2002). Antimicrobial food packaging in meat industry. *Meat Science, 62*, 373–380. doi:10.1016/S0309-1740(02)00121-3

Radusin. (2013). Actual and future trends in antimicrobial food packaging. *Agro food Industry Hi Tech, 24*, 44-48.

Rahn, H., Paganelli, C. V., & Ar, A. (1987). Pores and gas exchange of avian eggs: a review. *J Exp Zool Suppl, 1*, 165-172.

Ranoszek-Soliwoda, K., Tomaszewska, E., Socha, E., Krzyczmonik, P., Ignaczak, A., Orlowski, P., . . . Grobelny, J. (2017). The role of tannic acid and sodium citrate in the synthesis of silver nanoparticles. *J Nanopart Res, 19*(8), 273. doi:10.1007/s11051-017-3973-9

Rodriguez-Tobias, H., Morales, G., & Grande, D. (2019). Comprehensive review on electrospinning techniques as versatile approaches toward antimicrobial biopolymeric composite fibers. *Mater Sci Eng C Mater Biol Appl, 101*, 306-322. doi:10.1016/j.msec.2019.03.099

Sadasivuni, K. K., Rattan, S., Waseem, S., Brahme, S. K., Kondawar, S. B., Ghosh, S., . . . Mazumdar, P. (2019). Silver Nanoparticles and Its Polymer Nanocomposites—Synthesis, Optimization, Biomedical Usage, and Its Various Applications. In *Polymer Nanocomposites in Biomedical Engineering* (pp. 331-373).

Sato, S., Gondo, D., Wada, T., Kanehashi, S., & Nagai, K. (2013). Effects of various liquid organic solvents on solvent-induced crystallization of amorphous poly(lactic acid) film. *Journal of Applied Polymer Science, 129*(3), 1607-1617. doi:10.1002/app.38833

Silke Megelski, Jean S. Stephens, D. Bruce Chase, & Rabolt, J. F. (2002). Micro- and Nanostructured Surface Morphology on Electrospun Polymer

Fibers. *Macromolecules*(35), 8456-8466.

Sill, T. J., & von Recum, H. A. (2008). Electrospinning: applications in drug delivery and tissue engineering. *Biomaterials, 29*(13), 1989-2006. doi:10.1016/j.biomaterials.2008.01.011

Singh, P., Garg, A., Pandit, S., Mokkapati, V., & Mijakovic, I. (2018). Antimicrobial Effects of Biogenic Nanoparticles. *Nanomaterials (Basel), 8*(12). doi:10.3390/nano8121009

Siracusa, V., Rocculi, P., Romani, S., & Rosa, M. D. (2008). Biodegradable polymers for food packaging: a review. *Trends in Food Science & Technology, 19*(12), 634-643. doi:10.1016/j.tifs.2008.07.003

Sofi, S. A., Singh, J., Rafiq, S., Ashraf, U., Dar, B. N., & Nayik, G. A. (2018). A Comprehensive Review on Antimicrobial Packaging and its Use in Food Packaging. *Current Nutrition & Food Science, 14*(4), 305-312. doi:10.2174/1573401313666170609095732

Storz, H. a. V., K-D. (2013). Bio-based plastics: status, challenges and trends

. *Appl Agric Forestry Res, 4*. doi:10.3220/LBF_2013_321-332

Su, S., Duhme, M., & Kopitzky, R. (2020). Uncompatibilized PBAT/PLA Blends: Manufacturability, Miscibility and Properties. *Materials (Basel), 13*(21). doi:10.3390/ma13214897

Süfer, Ö. (2017). Poly (Lactic Acid) Films in Food Packaging Systems. *Food Science & Nutrition Technology, 2*(4). doi:10.23880/fsnt-16000131

Sutapun, W., Pakdeechote, P., Suppakarn, N., & Ruksakulpiwat, Y. (2013). Application of Calcined Eggshell Powder as Functional Filler for High Density Polyethylene. *Polymer-Plastics Technology and Engineering, 52*(10), 1025-1033. doi:10.1080/03602559.2013.769578

Sutapun, W., Ruksakulpiwat, Y., Suppakarn, N., Jeencham, R., & Aontee, A. (2011). Characterization of Precipitated Calcium Carbonate from Eggshell Powder. *Advanced Materials Research, 410*, 228-231. doi:10.4028/www.scientific.net/AMR.410.228

Taib, N.-A. A. B., Rahman, M. R., Huda, D., Kuok, K. K., Hamdan, S., Bakri, M. K. B., . . . Khan, A. (2022). A review on poly lactic acid (PLA) as a biodegradable polymer. *Polymer Bulletin, 80*(2), 1179-1213. doi:10.1007/s00289-022-04160-y

Talank, N., Morad, H., Barabadi, H., Mojab, F., Amidi, S., Kobarfard, F., . . . Mostafavi, E. (2022). Bioengineering of green-synthesized silver nanoparticles: In vitro physicochemical, antibacterial, biofilm inhibitory, anticoagulant, and antioxidant performance. *Talanta, 243*, 123374. doi:10.1016/j.talanta.2022.123374

Tanase-Opedal, M., Espinosa, E., Rodriguez, A., & Chinga-Carrasco, G. (2019). Lignin: A Biopolymer from Forestry Biomass for Biocomposites and 3D Printing. *Materials (Basel), 12*(18). doi:10.3390/ma12183006

Teamsinsungvon, A., Ruksakulpiwat, C., Amonpattaratkit, P., & Ruksakulpiwat, Y. (2022). Structural Characterization of Titanium-Silica Oxide Using Synchrotron Radiation X-ray Absorption Spectroscopy. *Polymers (Basel), 14*(13). doi:10.3390/polym14132729

Truong, L. B., Medina-Cruz, D., Martínez-Sanmiguel, J. J., Soto-Mendoza, A., Esquivel-López, I. G., Pérez, Y., . . . Mostafavi, E. (2022). Biogenic metal nanomaterials to combat antimicrobial resistance. In *Emerging Nanomaterials and Nano-Based Drug Delivery Approaches to Combat Antimicrobial Resistance* (pp. 261-304).

Tsai, W.-T., Yang, J.-M., Hsu, H.-C., Lin, C.-M., Lin, K.-Y., & Chiu, C.-H. (2008). Development and characterization of mesoporosity in eggshell ground by planetary ball milling. *Microporous and Mesoporous Materials, 111*(1-3), 379-386. doi:10.1016/j.micromeso.2007.08.010

Valodkar, M., Modi, S., Pal, A., & Thakore, S. (2011). Synthesis and anti-bacterial activity of Cu, Ag and Cu–Ag alloy nanoparticles: A green approach. *Materials Research Bulletin, 46*(3), 384-389. doi:10.1016/j.materresbull.2010.12.001

Verma, P., & Maheshwari, S. K. (2018). Preparation of Sliver and Selenium Nanoparticles and Its Characterization by Dynamic Light Scattering and Scanning Electron Microscopy. *J Microsc Ultrastruct, 6*(4), 182-187. doi:10.4103/JMAU.JMAU_3_18

Wang, C., He, C., Tong, Z., Liu, X., Ren, B., & Zeng, F. (2006). Combination of adsorption by porous CaCO3 microparticles and encapsulation by polyelectrolyte

multilayer films for sustained drug delivery. *Int J Pharm, 308*(1-2), 160-167. doi:10.1016/j.ijpharm.2005.11.004

Wang, T., & Kumar, S. (2006). Electrospinning of polyacrylonitrile nanofibers. *Journal of Applied Polymer Science, 102*(2), 1023-1029. doi:10.1002/app.24123

Wang, W., Yu, Z., Alsammarraie, F. K., Kong, F., Lin, M., & Mustapha, A. (2020). Properties and antimicrobial activity of polyvinyl alcohol-modified bacterial nanocellulose packaging films incorporated with silver nanoparticles. *Food Hydrocolloids, 100*. doi:10.1016/j.foodhyd.2019.105411

Wang, X., Zhang, T., Yang, Y., Liu, L., Tian, T., Zhu, D., . . . Xie, S. (2023). Effects of different storage temperatures on microbial spoilage and bacterial community structure of fresh beef by high-throughput sequencing technology. *Food Science and Technology, 43*. doi:10.1590/fst.100522

Wu, J. H., Hu, T. G., Wang, H., Zong, M. H., Wu, H., & Wen, P. (2022). Electrospinning of PLA Nanofibers: Recent Advances and Its Potential Application for Food Packaging. *J Agric Food Chem, 70*(27), 8207-8221. doi:10.1021/acs.jafc.2c02611

Xiu, Z. M., Zhang, Q. B., Puppala, H. L., Colvin, V. L., & Alvarez, P. J. (2012). Negligible particle-specific antibacterial activity of silver nanoparticles. *Nano Lett, 12*(8), 4271-4275. doi:10.1021/nl301934w

Yang, K., Yang, Q., Li, G., Sun, Y., & Feng, D. (2006). Morphology and mechanical properties of polypropylene/calcium carbonate nanocomposites. *Materials Letters, 60*(6), 805-809. doi:10.1016/j.matlet.2005.10.020

Yin, I. X., Zhang, J., Zhao, I. S., Mei, M. L., Li, Q., & Chu, C. H. (2020). The Antibacterial Mechanism of Silver Nanoparticles and Its Application in Dentistry. *Int J Nanomedicine, 15*, 2555-2562. doi:10.2147/IJN.S246764

Zhang, X. F., Liu, Z. G., Shen, W., & Gurunathan, S. (2016). Silver Nanoparticles: Synthesis, Characterization, Properties, Applications, and Therapeutic Approaches. *Int J Mol Sci, 17*(9), 1-34. doi:10.3390/ijms17091534

APPENDIX

Publications

Moe Ei Ei Zin, Pornpimol Moolkaew, Tiraporn Junyusen and Wimonlak Sutapun. Preparation of hybrid particles of Ag nanoparticles and eggshell calcium carbonate and their antimicrobial efficiency against beef- extracted bacteria. **Royal Society of Open Science.**

Moe Ei Ei Zin and Wimonlak Sutapun. Study of parameter affecting morphology of electrospun poly (lactic acid) (PLA) fibers loaded with Ag/$CaCO_3$ filler. **IOP Conf. Series: Materials Science and Engineering.**

Presentation at conferences

Moe Ei Ei Zin and Wimonlak Sutapun. Study of parameter affecting morphology of electrospun poly (lactic acid) (PLA) fibers loaded with Ag/$CaCO_3$ filler. **The 3rd International Conference on Materials Research and Innovation (ICMARI 2021).** 15-17 December 2021 in Bangkok, Thailand. (Oral)

Moe Ei Ei Zin and Wimonlak Sutapun. Electrospun PLA Fibers with Silver Loaded Calcium Carbonate Filler as the Antimicrobial Material: Effect of Solvent Systems and Mechanical Properties. **The 37th International Conference of the Polymer Processing Society.** 11-15 April 2022 in Fukuoka, japan. (Oral)

ROYAL SOCIETY OPEN SCIENCE

royalsocietypublishing.org/journal/rsos

Research

Cite this article: Zin MEE, Moolkaew P, Junyusen T, Sutapun W. 2023 Preparation of hybrid particles of Ag nanoparticles and eggshell calcium carbonate and their antimicrobial efficiency against beef-extracted bacteria. *R. Soc. Open Sci.* **10**: 221197.
https://doi.org/10.1098/rsos.221197

Received: 22 October 2022
Accepted: 17 April 2023

Subject Category:
Chemistry

Subject Areas:
inorganic chemistry/materials science

Keywords:
antimicrobial agent, silver nanoparticles, eggshell calcium carbonate, silver loaded eggshell calcium carbonate, food packaging, co-precipitation

Author for correspondence:
Wimonlak Sutapun
e-mail: wimonlak@sut.ac.th

This article has been edited by the Royal Society of Chemistry, including the commissioning, peer review process and editorial aspects up to the point of acceptance.

Electronic supplementary material is available online at https://doi.org/10.6084/m9.figshare.c.6644155.

ROYAL SOCIETY OF CHEMISTRY

THE ROYAL SOCIETY PUBLISHING

Preparation of hybrid particles of Ag nanoparticles and eggshell calcium carbonate and their antimicrobial efficiency against beef-extracted bacteria

Moe Ei Ei Zin[1,2], Pornpimol Moolkaew[3], Tiraporn Junyusen[3] and Wimonlak Sutapun[1,2]

[1]School of Polymer Engineering, Institute of Engineering, [2]Research Centre for Biocomposite Materials for Medical and Agricultural and Food Industry, and [3]School of Agricultural Engineering, Institute of Engineering, Suranaree University of Technology, Nakhon Ratchasima 30000, Thailand

MEEZ, 0000-0002-8800-481X; PM, 0000-0002-0404-3724; TJ, 0000-0002-8382-1861; WS, 0000-0003-3008-8085

In this study, hybrid particles of AgNPs-loaded eggshell calcium carbonate (AgNPs/eCaCO$_3$) were prepared by co-precipitating the eggshell in the presence of freshly prepared AgNPs with a particle size of 10–30 nm. The hybrid particles were comparatively precipitated at 25°C and 35°C using poly (sodium 4-styrenesulfonate) as a polyelectrolyte. The AgNPs/eCaCO$_3$ particles prepared at 25°C had a spherical morphology with a mean diameter of 3.56 µm, and Brunauer–Emmett–Teller (BET) surface area of 85.08 m^2 g^{-1}. On the other hand, the particles prepared at 35°C had a broader size distribution with a mean diameter of 3.19 µm, and a BET surface area of 79.25 m^2 g^{-1}. AgNPs-loaded commercial calcium carbonate particles (AgNPs/CaCO$_3$) comparatively prepared at 35°C were perfectly spherical with a mean diameter of 5.61 µm. At preparing temperature of 25°C, the hybrid particles contain AgNPs of 0.78 wt% for AgNPs/eCaCO$_3$ and 3.20 wt% for AgNPs/CaCO$_3$. The AgNPs/eCaCO$_3$ and AgNPs/CaCO$_3$ particles exhibited the same efficiency against bacteria extracted from beef with an average inhibition zone diameter of 7–10 mm according to the modified Kirby–Bauer disc diffusion assay depending on their concentration and beef source. Freshly prepared silver colloids showed comparatively poorer antimicrobial efficiency.

1. Introduction

Several types of metal and metal oxide nanoparticles such as Ag, Au, TiO_2, CuO and ZnO, have gained attention owing to their antimicrobial efficiency and high surface area per volume. Ag nanoparticles (AgNPs) are less expensive than Au and TiO_2. The TiO_2 nanoparticles are effective antifungal agents against fluconazole-resistant strains and are suitable for photocatalytic activity. Ag, CuO and ZnO nanoparticles show antibacterial activity against Gram-negative and Gram-positive bacteria. However, Ag nanoparticles (AgNPs) are the most popular antimicrobial agents because of their high activity against drug-resistant bacteria, high stability and non-toxicity [1]. Moreover, AgNPs are highly effective antimicrobial agents against a wide spectrum of Gram-negative and Gram-positive bacteria; fungi such as *Aspergillus niger* and *Candida albicans*; and viruses including HIV-1, hepatitis B virus, respiratory syncytial virus, herpes simplex virus type 1 and monkeypox virus [2–5]. The cytotoxicity of AgNPs is derived from the nanoparticles themselves and Ag^+ released from oxidative dissolution. In aqueous environments, AgNPs suspensions are oxidized in the presence of oxygen and protons, thereby releasing Ag^+ via surface oxidative dissolution [2]. The oxidative dissolution reaction is shown in equation (1.1) [6]. The release rate of Ag^+ depends on the size, shape, surface properties, capping agent and colloidal state of AgNPs [7].

$$Ag^0(s) + (1/4)O_2(aq) + H^+(aq) \leftrightarrow Ag^+(aq) + (1/2)H_2O. \tag{1.1}$$

Although the mechanisms underlying the activity of AgNPs against bacteria have not yet been fully clarified, various antibacterial mechanisms have been proposed. Yin *et al.* proposed the following possible mechanisms: (i) disruption of the cell wall and membrane by Ag^+, (ii) denaturation of ribosomes by Ag^+, (iii) interruption of adenosine triphosphate (ATP) production by Ag^+, (iv) disruption of the cell membrane by reactive oxygen species (ROS), (v) interference of DNA replication by AgNPs, Ag^+ and ROS, (vi) denaturation of the cell membrane by AgNPs, and (vii) perforation of the membrane by AgNPs [8]. A diagram of the antibacterial mechanisms of AgNPs drawn using *BioRender* is shown in figure 1. Durán *et al.* reported that ROS could be a principal agent in the induction of cell membrane disruption and deoxyribonucleic acid (DNA) modification. The interaction of Ag^+ with sulfur and phosphorus, which are important DNA compounds, can cause problems in DNA replication and cell reproduction, or even result in the termination of microorganisms. Furthermore, the synthesis of proteins can be inhibited by Ag^+, causing denaturation of ribosomes in the cytoplasm [9].

The cytotoxicity of AgNPs is highly dependent on several factors such as size, shape, surface chemistry, stability, surface charge, capping agent, pH, ionic strength and degree of agglomeration. Size-dependent cytotoxicity of AgNPs has been demonstrated in many studies. Smaller particles have a larger specific surface area, which can expose a large number of atoms on the surface for redox, photochemical and biochemical reactions, as well as physico-chemical interactions with cells [5]. In addition, the presence of ligands, divalent cations and macromolecules also plays a key role on cytotoxicity [2,5,10].

Silver nanoparticles could be prepared via physical, chemical, green synthetic and biological methods. The physical methods result in low yields. The chemical reduction of a silver salt in aqueous media is a common method for producing AgNPs with reducing compounds such as sodium borohydride ($NaBH_4$) [11,12], trisodium citrate ($Na_3C_6H_5O_7$) [13–15], glucose ($C_6H_{12}O_6$), hydrazine (N_2H_4) and ascorbate ($C_6H_7O_6$) [5]. Trisodium citrate was commonly used as a reducing and stabilizing agent for silver nitrate to produce AgNPs [16]. The citrate reduction of silver colloids serves the dual role of the reductant and stabilizer. The silver particles prepared by the citrate reduction method were relatively large sized (50–100 nm) with well-defined facets [14]. AgNPs can be also green synthesized from plant-extracted chemicals and biologically obtained from yeast extracts [17–19]. Preferred particle size and distribution, and morphology of the AgNPs can be obtained via the chemical techniques with suitable parameters. By utilizing low-toxic chemicals as reducing agent and stabilizing agent in the reduction chemical method, the harmful effects on the environment and hazardous by-products will be reduced.

Owing to growing concerns about antibiotics resistance, incorporating AgNPs into different matrices/supporters/carriers has emerged as an effective way to produce materials with high antimicrobial efficiency. AgNPs incorporated into polymer matrices are currently a popular type of nanocomposite with excellent antimicrobial properties. Antimicrobial polymer composites can be applied in food packaging containers [20], food packaging films [21], wound dressing materials

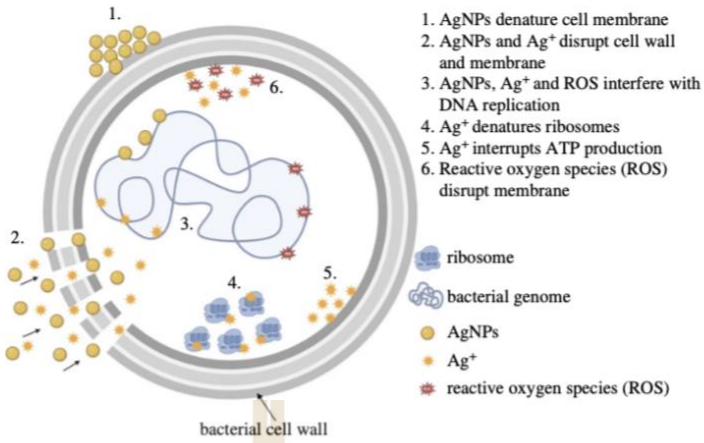

Figure 1. The antibacterial mechanism of silver nanoparticles (AgNPs) [8].

[22,23] and other antimicrobial applications [24,25] owing to their outstanding antimicrobial activity. One of the main challenges in producing this type of antimicrobial is the synthesis of stable nanoparticles, as their antimicrobial effectiveness greatly depends on their size, size distribution and agglomeration state [26]. Notably, the most common application problem involves the agglomeration and diffusion of these nanoparticles into a polymer matrix, which reduces antibacterial activity. To prevent agglomeration and maintain the long-lasting antimicrobial activity of AgNPs, porous micro $CaCO_3$ particles in vaterite polymorph have been used as carriers for metallic nanoparticles [16,27,28]. Lei *et al*. synthesized vaterite $CaCO_3$ in the presence of poly (sodium 4-styrene-sulfonate) of a specific size and morphology [29]. Using porous micro $CaCO_3$ particles as carriers or supporters, the antimicrobial activity of the active AgNPs can be prolonged owing to reduced agglomeration of the nanoparticles as well as limiting contact of AgNPs with the human body [16]. Moreover, chemical and physical techniques for synthesizing $CaCO_3$ containing AgNPs as hybrid particles must be made greener using either low-toxicity chemicals or raw materials from bioresources for sustainability.

Chicken eggshells from household waste are extensively used as a replacement for mineral calcium carbonate in several applications such as plastic and elastomer fillers, heavy metal absorbents, dye removal bio-calcium supplements, concrete replacement and biodiesel oil catalysts [30]. Eggshells are readily available with a high $CaCO_3$ content (94 wt%), in the form of calcite polymorph [31,32] with 7000 and 17 000 pores [33,34] and the smallest pore size of 3–13 µm [33,34]. In addition, chicken eggshells contain other inorganic compounds including magnesium carbonate (1%), calcium phosphate (1%) and organic matter (4%) [35]. Eggshell waste can be used as an alternative and green precursor for hybrid particles of AgNPs and $CaCO_3$.

The number of patents on eggshell applications has increased exponentially in the last 7 years, from 150 in 2014 to 250 in 2020, emphasizing biotechnological applications involving biomedical, chemical, engineering and environmental technology [36]. One of the biotechnological applications of eggshell calcium carbonate is as a hybrid particle. The ceramic–ceramic and ceramic–metal hybrid particles exploit the advantages of the synergistic function of the compositions of the hybrid particles. For example, TiO_2/SiO_2, a ceramic–ceramic hybrid particle, can be applied as a functional filler for elastomers and possesses the advantages of photocatalytic properties and antimicrobial biomaterials by TiO_2, as well as high thermal stability and excellent mechanical strength by SiO_2 [37]. For ceramic–metal hybrid particles, AgNPs/$CaCO_3$ could be used as an antimicrobial agent, with $CaCO_3$ acting as an AgNPs carrier and AgNPs as an active antimicrobial agent. The $CaCO_3$ carrier also improves the distribution and distributive properties of AgNPs [16,28].

The patent filed by Yang *et al*. disclosed a method to produce hybrid particles of AgNPs and $CaCO_3$ using eggshells as a template. Eggshells were pulverized and loaded with Ag^+, followed by heating at 400–600°C. The resultant hybrid particles can be used for various applications including catalysis, tissue engineering, coatings and the production of antibacterial agents, pigments and ceramics [38]. Nevertheless, the proposed method consumes a large amount of energy while heating up to 600°C. Hassan *et al*. prepared eggshell $CaCO_3$ platelets using a combination of mechanochemical and

sonochemical techniques. The obtained $CaCO_3$ platelets had particle sizes, Brunauer–Emmett–Teller (BET) surface areas and pore volumes of 10 nm, 43.69 $m^2\ g^{-1}$ [32] and 0.164 $cm^3\ g^{-1}$ [39], respectively. Apalangya *et al*. employed a mechanochemical milling technique to deposit spherical AgNPs with a diameter of 5–20 nm onto the surface of micrometre-sized ground eggshells with crystal polymorphs of calcite [28]. They also mentioned that macromolecular proteins and functional groups in the eggshells, such as hydroxyl, carboxyl and amino functional groups could stabilize and immobilize AgNPs onto the surfaces of eggshell particles. However, the morphology of the ground eggshells obtained using the mechanochemical milling technique is platelet-shaped, resulting in the anisotropic properties for the hybrid particles. Zapotoczny *et al*. prepared hybrid particles of AgNPs and $CaCO_3$, for sustained release applications, using a calcium nitrate and sodium carbonate solution for co-precipitation in the presence of freshly prepared silver colloids [16]. The particle size of the AgNPs was 10–30 nm. However, crystal polymorphs of the co-precipitated $CaCO_3$ have not yet been reported.

In addition to the above-mentioned techniques involving the preparation of ground eggshell powders, hybrid particles of AgNPs and eggshell $CaCO_3$, and AgNPs and mineral $CaCO_3$, this article proposes a two-step method using the green raw material of bio-eggshell waste to prepare hybrid particles of AgNPs and $CaCO_3$ as antimicrobial agents. The two-step method comprising silver colloids preparation and silver colloids/eggshell $CaCO_3$ co-precipitation. Using the two-step method, the specific particle size, size distribution and morphology of the hybrid particles of AgNPs and eggshell $CaCO_3$ were chemically controllable with a higher BET specific surface area and pore volume.

In this study, AgNPs were used as an active agent against the growth of bacteria contaminating fresh beef. Due to their highly effective antimicrobial activity against a wide spectrum of Gram-negative and Gram-positive bacteria, biocompatibility and low production cost. Veterite calcium carbonate was prepared from eggshell and functioned as the AgNPs carrier due to its porous structure, isotropic property and non-toxicity. To prepare the hybrid particles of AgNPs and vaterite calcium carbonate (AgNPs/e$CaCO_3$), AgNPs were freshly synthesized by a chemical reduction method using trisodium citrate, a low toxicity chemical, and then deposited *in situ* into micro-sized eggshell calcium carbonate particles during precipitation. In addition, hybrid particles of AgNPs loaded with commercial calcium carbonate (AgNPs/$CaCO_3$) were comparatively prepared. Furthermore, the effect of precipitation temperature on the particles size and size distribution of AgNPs/e$CaCO_3$ was investigated. The hybrid particles were characterized using field emission scanning electron microscopy (FESEM), transmission electron microscopy (TEM) and energy dispersive X-ray spectroscopy (EDS, EDX) to monitor particle size and size distribution; particle morphology; and silver content, respectively. Dynamic light scattering (DLS) technique was also employed to study the hydrodynamic radius of the AgNPs. BET analysis was used to determine the specific surface area, pore volume and pore diameter of the particles. Finally, the antimicrobial activities of silver colloids, AgNPs/e$CaCO_3$ particles, AgNPs/$CaCO_3$ particles and precipitated e$CaCO_3$ particles against beef-extracted bacteria were compared using a modified Kirby–Bauer disc diffusion assay. Soon, AgNPs/e$CaCO_3$ particles will be incorporated into a biodegradable poly (lactic acid) using the electrospinning method for antimicrobial food packaging. Using eggshell as a precursor for preparing $Ca(NO_3)_2$ in precipitating vaterite calcium carbonate for carrying AgNPs has not been previously reported. Effect of the eggshell precipitation temperature has not been studied, as well. This study offers the novel co-precipitation technique for preparing hybrid particles of AgNPs and micrometre-sized vaterite calcium carbonate using bio-green source chicken eggshell with the determined mixing step and temperature to control the size of AgNPs, and morphology and size of vaterite calcium carbonate. For the hybrid particles aiming as antimicrobial agents in beef packaging, AgNPs function as active antimicrobial agents and vaterite calcium carbonate as carriers or supporters.

2. Materials and methods

2.1. Materials

Chicken eggshells (ES) were obtained from household waste, and commercial calcium carbonate particles were obtained from Sand and Soil Industry Co., Ltd. Silver nitrate (≥99.0%, ACS reagent), sodium carbonate (≥99.5%, ACS reagent), sodium citrate tribasic dihydrate (trisodium citrate) (≥99.0%, ACS reagent) and poly (sodium 4-styrenesulphonate) (PSS, average M_w~70 000 g $mole^{-1}$) were obtained from Sigma Aldrich. Nitric acid (65%, AR grade) was purchased from ANaPURE. Plate count agar (PCA) and peptone were purchased from HiMedia Laboratories Pvt. Ltd and Sisco Research

Laboratories Pvt. Ltd, respectively. Unpacked fresh beef and vacuum-packed fresh beef (MAX BEEF) were purchased from a local fresh market and a Home-Fresh Mart supermarket, respectively.

2.2. Preparation of eggshell powder

Household waste eggshells were washed with tap water and boiled in a rice cooker at 100°C for 4 h. Subsequently, eggshell membranes were peeled off. The eggshells were crushed into small pieces and dried at room temperature for 24 h. To obtain fine eggshells pieces, a grinding machine (Retsch, SR300) was used to reduce the initial size of the dried eggshells. To remove all the remaining biomacromolecules, such as the eggshell membrane, the eggshell powder was washed with water at least five times and then dried in an oven at 60°C for 24 h. Ball milling with different ball sizes was used for further size reduction. After 24 h of ball milling, the eggshell powder was sieved through No. 500 and No. 450 sieves, to obtain particle size of 25–32 µm.

2.3. Preparation of calcium nitrate solution

To prepare the calcium nitrate solution, 102 g of eggshell powder (ESP) was dissolved in 1000 ml of 2 M nitric acid solution. After the ESP was completely dissolved, titration was performed with a 0.5 M sodium hydroxide solution using phenolphthalein as an indicator to determine the exact molarity of the calcium nitrate solution, after which the pH of the solution was adjusted to neutral using a 0.50 M sodium hydroxide solution. To obtain a molarity equivalent to that of sodium carbonate solution, the calcium nitrate solution was diluted to 0.03 M concentration.

For comparison, 100 g of commercial calcium carbonate was dissolved in a 2 M nitric acid solution. To get 0.03 M calcium nitrate solution from commercial calcium carbonate, the same procedure mentioned in the previous paragraph was performed.

2.4. Preparation of silver nanoparticles deposited on eggshell $CaCO_3$ and commercial calcium carbonate

Hybrid particles of silver nanoparticles (AgNPs) deposited on eggshell $CaCO_3$ and commercial calcium carbonate were prepared using a co-precipitation method, as described by Zapotoczny *et al*. [16]. First, to prepare the silver colloids, 45 mg of silver nitrate was dissolved in 250 ml of deionized (DI) water, and then 5 ml of 1 w/v% trisodium citrate was added. The reaction mixture was placed in an ultrasonic bath and heated at 70–72°C for 60 min.

At the same time, PSS was dissolved in DI water to get a 4.8 g l^{-1} PSS solution, and a 0.03 M sodium carbonate solution was prepared. Then, 20 ml of the freshly prepared silver colloids was simultaneously mixed with 50 ml of 0.03 M $Ca(NO_3)_2$ solution prepared from either eggshell calcium carbonate or commercial calcium carbonate and 50 ml of 0.03 M Na_2CO_3 solution with the addition of 15 ml of PSS (4.8 g l^{-1}). The mixture was then sonicated for 5 min at 25°C. The obtained particles were washed with DI water and centrifuged at 4000 r.p.m. for 5 min to remove the excess silver. The washing process was repeated thrice, and the obtained particles were dried under vacuum at 40°C for 24 h. AgNPs/e$CaCO_3$ and precipitated e$CaCO_3$ were also prepared at a sonication temperature of 35°C via the same procedure.

2.5. Sample characterization

The particle morphology and size of AgNPs, precipitated e$CaCO_3$, AgNPs/e$CaCO_3$ and AgNPs/$CaCO_3$ were determined using a field emission scanning electron microscope (FESEM, JEOL JSM 7800F) with an accelerating voltage of 3.0 kV. Prior to observation, each sample was coated using a gold sputter coater (Neo-Coater, MP-19020NCTR) for 2 min. The diameter of the particles was measured from the SEM micrographs using an analysis software (ImageJ) and calculated by randomly selecting 200 particles. Matlab R2022a was used to obtain the mean diameter, size distribution and histogram.

Moreover, the morphology and elemental composition of the AgNPs, precipitated e$CaCO_3$, AgNPs/e$CaCO_3$ and AgNPs/$CaCO_3$ were investigated using a transmission electron microscope (TEM, Thermo Scientific Talos F200X) coupled with energy dispersive X-ray spectroscopy (EDX). The morphology and size distribution of the nanoparticles from the TEM micrographs were recorded digitally, and the elemental composition of the particles was determined by EDS in the mapping mode using Velox

software. Samples for TEM were prepared by depositing a drop of each sample in distilled water on a carbon-coated standard copper grid (200 meshes) and allowed to dry before investigation.

The crystal polymorphs of the ground eggshells, precipitated $eCaCO_3$ and hybrid particles were determined by an X-ray diffraction analyser (XRD, Bruker D8 ADVANCE). The study was carried out in a 2θ range of 5–80° with a voltage of 40 kV, current of 40 mA and a Cu Kα (1.5606 Å) radiation source.

To study the decomposition temperature of ground eggshells and precipitated $eCaCO_3$ prepared at 35°C, a thermogravimetric analyser (TGA, Mettler Toledo, TGA/DSC1) was employed. The samples were heated from 35 to 1000°C at a heating rate of 10°C min^{-1} under nitrogen atmosphere.

The hydrodynamic particle size and polydispersity index (PDI) of silver colloids and AgNPs, was determined by dynamic light scattering analyser (DLS, Malvern Instruments Zetasizer Nano ZS). The measurements were carried out in triplicate at 25°C with laser wavelength of 633 nm, beam back-scattering angle of 173° and DI water's refractive index of 1.330.

The BET surface area and porosity of all particles were measured using a BET analyser (Micromeritics 3Flex). All samples were degassed at 40°C for 24 h under vacuum before examination.

2.6. Antimicrobial test

To examine the antimicrobial efficiency of the hybrid silver nanoparticles/calcium carbonate particles on beef-extracted bacteria, a modified Kirby–Bauer disc diffusion assay was performed as follows. Bacteria were extracted from two types of beef, unpacked beef available at a local market and vacuum-packed beef available at a supermarket ('MAX BEEF' brand). The beef loaf was cut into small pieces and kept at room temperature for 18 h. The powdered forms of precipitated $eCaCO_3$, AgNPs/$eCaCO_3$ and AgNPs/$CaCO_3$ were dispersed in sterile DI water and kept at 4°C overnight. Then, 2.35 g of plate count agar (PCA) powder was completely dissolved in 100 ml sterile DI water using a hot plate. Next, the PCA solution was sterilized, and then poured into sterile Petri dishes after the solution and the dishes were cool down to 45–50°C. Approximately 25 g of spoiled beef was blended with 225 ml of 0.10% sterile peptone water using a Stomacher laboratory blender for 6 min. The obtained beef extract was smeared onto plate count agar using a sterile cotton swab. Four sterile circular Whatman filter paper discs (6 mm diameter) were placed onto the smeared agar plate and impregnated with 5 µl of precipitated $eCaCO_3$, freshly prepared silver colloids (silver colloids at 0 h), AgNPs/$eCaCO_3$ and AgNPs/$CaCO_3$. The test was performed at particle concentrations of 500, 250 and 125 mg ml^{-1}. The plates were incubated at 37°C for 24 h. After that, each inhibition zone diameter was monitored, and digital images of the antimicrobial zone were taken. The diameters were averaged from the three measurements. The antimicrobial test was performed in triplicate and the average diameter of the inhibition zone with standard deviation was calculated.

3. Results and discussion

3.1. Characteristic of silver nanoparticles

The optical micrographs in figure 2*a*,*b* show images of the silver colloids over time. Freshly prepared silver colloids are clear and light-yellow, resulting in both large and exceedingly small silver nanoparticles (AgNPs) of approximately 100–200 nm and 1 nm, respectively, as shown in figure 2*a*1,*a*2. However, after being left at room temperature for 24 h, the silver colloids became dark brown (figure 2*b*) because the small nanoparticles became larger. The AgNPs began to grow over time, as confirmed by the SEM micrographs shown in figure 2*b*1,*b*2. Agglomeration can also be observed in the SEM micrograph shown in figure 2*b*2.

TEM micrographs, EDS mapping images and EDX spectrum of AgNPs obtained from freshly prepared silver colloids are shown in figure 3. The TEM micrographs show the spherical morphology of AgNPs, as observed from SEM in figure 2, and the average size of the individual particles was approximately 10–30 nm. Particles with diameters of less than 10 nm were observed as small dots. The EDS image mapping and EDX spectrum in figure 3*c*–*g* illustrate that the particles were mainly composed of silver. Large-sized (50–100 nm) silver crystallites were found using trisodium citrate as a reducing and stabilizing agent [14]. Arif *et al*. also studied the synthesis of silver nanoparticles in the presence of trisodium citrate, resulting in diameters of approximately 40 nm AgNPs [40]. According to the smaller particle size and lesser agglomeration, the freshly prepared silver colloids were further used to prepare AgNPs-loaded calcium carbonate particles as antimicrobial agents.

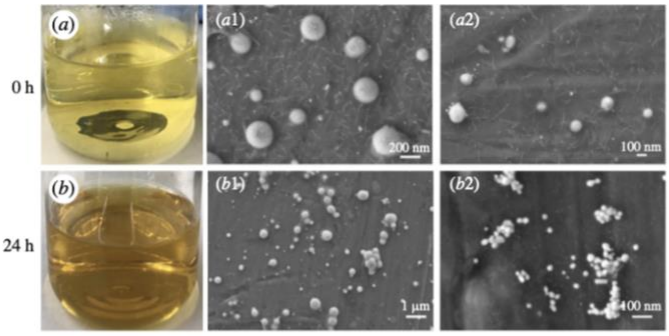

Figure 2. The image of freshly prepared silver colloids (silver colloids at 0 h) (*a*) and SEM micrographs of AgNPs obtained from the silver colloids at 0 h with a magnification of 50k× (*a*1) and 50k× (*a*2). The image of silver colloids at 24 h (*b*) and SEM micrographs of AgNPs obtained from the silver colloids at 24 h with a magnification of 10k× (*b*1) and 100k× (*b*2).

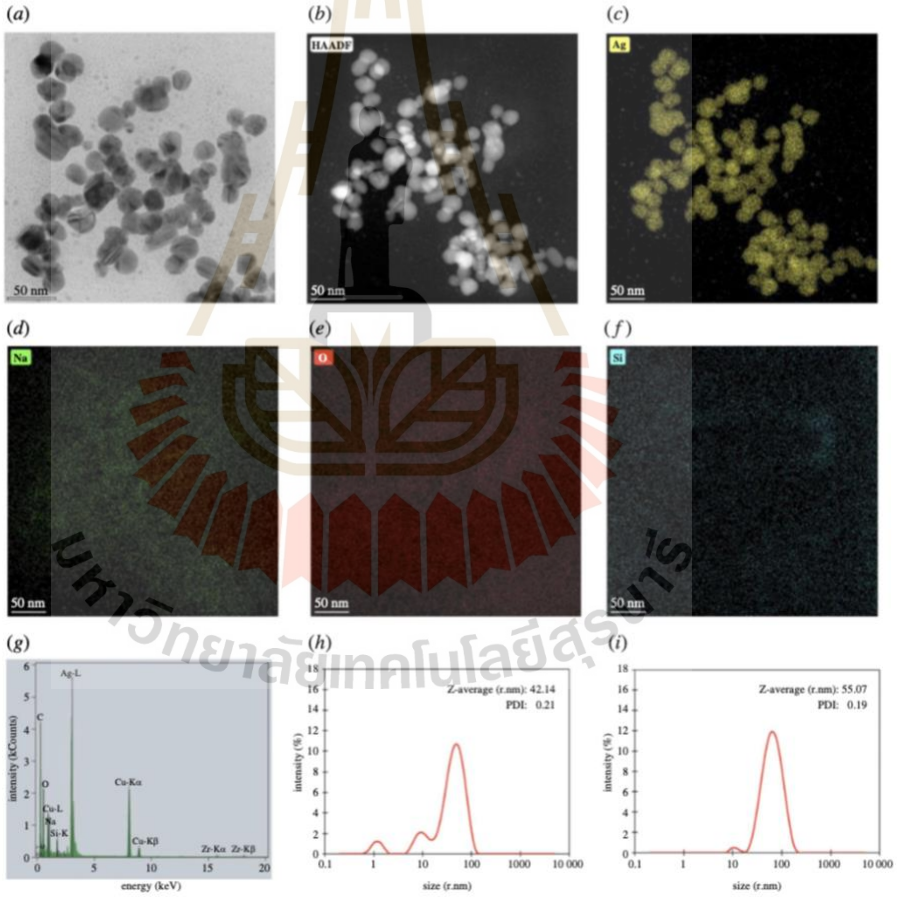

Figure 3. TEM micrograph (*a*), high-angle annular dark-field imaging (HAADF) (*b*), Silver (Ag) EDS image mapping (*c*), Sodium (Na) EDS image mapping (*d*), Oxygen (O) EDS image mapping (*e*), Silicon (Si) EDS image mapping (*f*) and EDX spectrum (*g*) of AgNPs obtained from freshly prepared silver colloids, and the hydrodynamic size distribution curves of (*h*) and AgNPs obtained from (*i*) freshly prepared silver colloids.

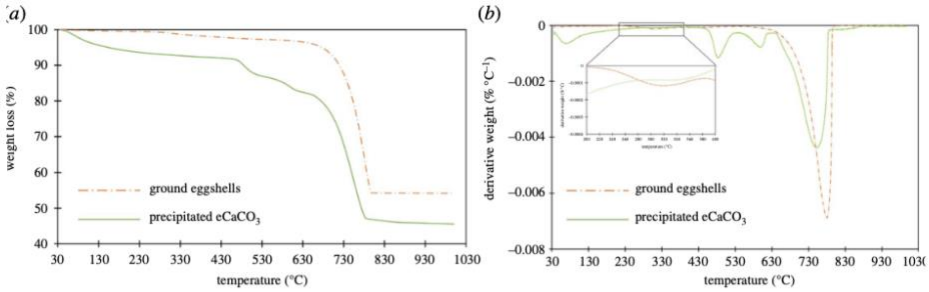

Figure 4. TGA curves (*a*) and DTGA curves (*b*) of ground eggshells and precipitate $eCaCO_3$ prepared at 35°C.

The freshly prepared silver colloids contained the Z-average (r.nm) of 42.1 nm and PDI of 0.2, as observed from figure 3*h*. The hydrodynamic size distribution curve of freshly prepared silver colloids, shown in figure 3*h*, shows three peaks at 50.0, 10.3 and 1.2 nm. This distribution curve corresponded well with their TEM micrograph in figure 3*a*, showing three different sizes of the particles. In addition, the Z-average size (r.nm) and PDI of AgNPs, obtained from the freshly prepared silver colloids, were 55.1 and 0.2, with two peaks at 69.6 and 11.0 nm as illustrated by the hydrodynamic size distribution curve in figure 3*i*. The 1 nm AgNPs might be extracted out during the centrifugal separation; as a result, there are two particle size ranges observed from the distribution curve. Ranoszek-Soliwoda *et al*. [41] prepared AgNPs at 100°C using trisodium citrate as a capping agent. They reported hydrodynamic size (d.nm) of the prepared AgNPs in ranges of 9 ± 2 nm and 58 ± 20 nm, with PDI of 0.5, and the particle size of the AgNPs observed from scanning transmission electron microscopy (STEM) in ranges of 5–45 nm and larger than 100 nm.

3.2. Characteristic of precipitated eggshell calcium carbonate ($eCaCO_3$) particles

The TGA and differential thermogravimetric analysis (DTGA) curves of the ground eggshells and precipitated $eCaCO_3$ prepared at 35°C are shown in figure 4*a*,*b*. Ground eggshells exhibited three thermal transitions of mass loss. The first thermal decomposition occurred in the temperature range of 35–110°C due to the evaporation of physically adsorbed water. The second transition in the range of 240–350°C caused by thermal decomposition of the eggshell matrix left in the ground eggshell. The TGA curve shows overall mass loss of 1.9% from water evaporation and eggshell matrix decomposition. Castro *et al*. also reported that natural eggshells showed a mass loss of 1.9% between 30 and 400°C [42]. The third mass loss occurred between 400 and 800°C, with a DTGA peak at 783°C and a mass loss of 45.8%. This loss is related to the CO_2 released from $CaCO_3$ decomposition. Decarbonization of chicken eggshells has been reported to occur in the temperature range of 600–850°C [43,44].

In the case of precipitated $eCaCO_3$ prepared at 35°C, the TGA and DTGA curves show four regions of thermal decomposition with an overall weight loss of approximately 46.2%. The first weight loss at 35–180°C was due to the evaporation of physically adsorbed water from $CaCO_3$. The second and third decompositions in the temperature range of 430–520°C and 550–650°C, were derived from the thermal degradation of PSS in precipitated $eCaCO_3$. These two thermal decomposition ranges were also reported by Bahrom *et al*. [45]. They reported that the thermal decomposition of precipitated $CaCO_3$ using PSS as an organic additive at 430–520°C and 550–650°C was due to the decomposition of PSS. The fourth thermal decomposition at 790°C corresponded to the decarbonization of vaterite $CaCO_3$. It could be concluded that there was no organic matter left in the precipitated $eCaCO_3$, and vaterite polymorph precipitated from eggshell absorbed more water than calcite polymorph of eggshell.

SEM micrographs in figure 5*a–c* show spherical morphology and a broad particle size distribution of precipitated $eCaCO_3$ particles prepared at 35°C, with a mean diameter of 3.55 ± 1.32 µm. The mechanism of $CaCO_3$ formation involves the creation of nanometre-sized crystallites in the first stage which later aggregate to form micrometre-sized superstructures [16]. According to the XRD pattern in figure 5*d*, crystal polymorphs of the precipitated $eCaCO_3$ prepared at 35°C was vaterite, whereas that of the ground eggshells was calcite. Sutapun *et al*. also reported that ground eggshells were mainly composed of a calcite crystal structure [43]. The vaterite crystal structure is formed when $CaCO_3$ is

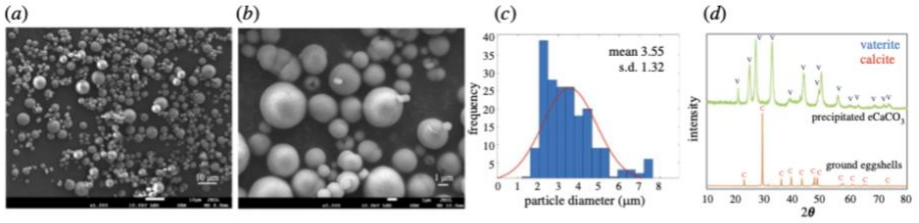

Figure 5. SEM micrographs with magnification of 1k× (*a*) and 5k× (*b*), and a particle size distribution curve (*c*) of precipitated $eCaCO_3$ particles prepared at 35°C, and XRD patterns of the precipitated $eCaCO_3$ particles and ground eggshells (*d*).

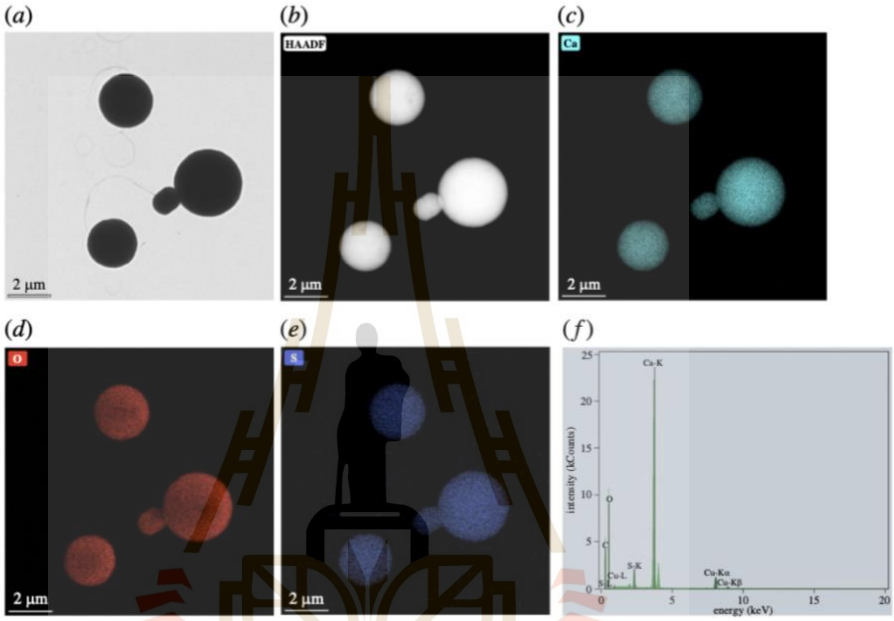

Figure 6. TEM micrograph (*a*), high-angle annular dark-field imaging (HAADF) (*b*), calcium (Ca) EDS image mapping (*c*), oxygen (O) EDS image mapping (*d*), sulfur (S) EDS image mapping (*e*) and EDX spectrum (*f*) of precipitated $eCaCO_3$ particles prepared at 35°C.

precipitating in the presence of poly (sodium 4-styrenesulfonate) (PSS) as a polyelectrolyte. Lei *et al.* studied precipitating vaterite $CaCO_3$ from 0.5 M $CaCl_2$ and 0.5 M Na_2CO_3 and 70 000 g mole^{-1} and 1 g l^{-1} PSS at pH 10 and the obtained $CaCO_3$ particles were vaterite polymorph with micrometre-sized spherical shapes. It was deduced that PSS initiated vaterite nucleation through the binding of calcium ions to anionic sulfonate groups, and stabilized the vaterite during crystal growth [29]. Azarian also found that the crystal structure of precipitated calcium carbonate from calcium nitrate and sodium carbonate in the presence of polyelectrolytes was vaterite with a spherical morphology [46]. The TEM micrographs in figure 6*a*,*b* also show a broad particle size distribution. The EDS image mapping and EDX spectrum in figure 6*c*–*f* illustrated that the particles were rich in calcium carbonate.

3.3. Characteristic of silver nanoparticles / eggshell calcium carbonate (AgNPs/$eCaCO_3$) particles

Figure 7*a*–*d* show the particle morphology, histogram plot of particle diameter versus frequency and XRD spectrum for AgNPs/$eCaCO_3$ particles prepared at 35°C. The spherical morphology of AgNPs/$eCaCO_3$ particles with a particle size distribution ranging from 1.44 to 7.38 µm and a mean diameter of 3.19 ± 1.20 µm was obtained. Figure 7*e*–*h* show the morphology, histogram plot of particle diameter versus frequency and XRD spectrum for AgNPs/$eCaCO_3$ particles prepared at 25°C. The XRD patterns in figure 7*d*,*h* confirm that the particles prepared at 25°C and 35°C were mainly composed of vaterite crystal

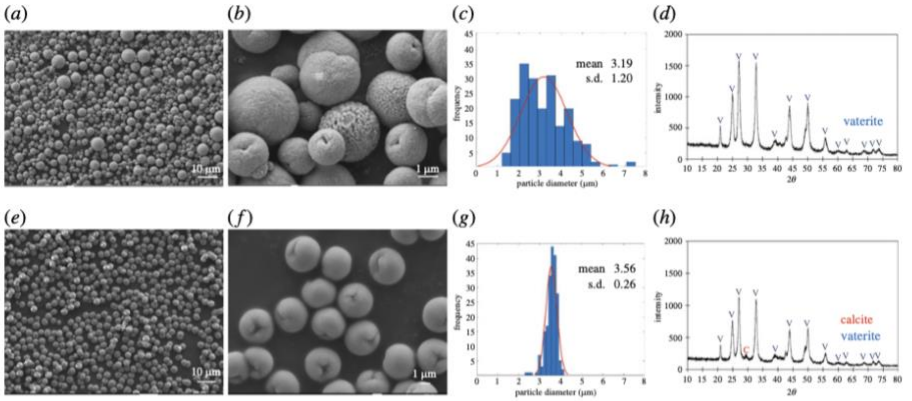

Figure 7. SEM micrographs with magnification of 1k× (*a*) and 10k× (*b*), a particle size distribution curve (*c*) and an XRD pattern (*d*) of AgNPs/eCaCO$_3$ particles prepared at 35°C. SEM micrographs with magnification of 1k× (*e*) and 5k× (*f*), a particle size distribution curve (*g*) and an XRD pattern (*h*) of AgNPs/eCaCO$_3$ particles prepared at 25°C.

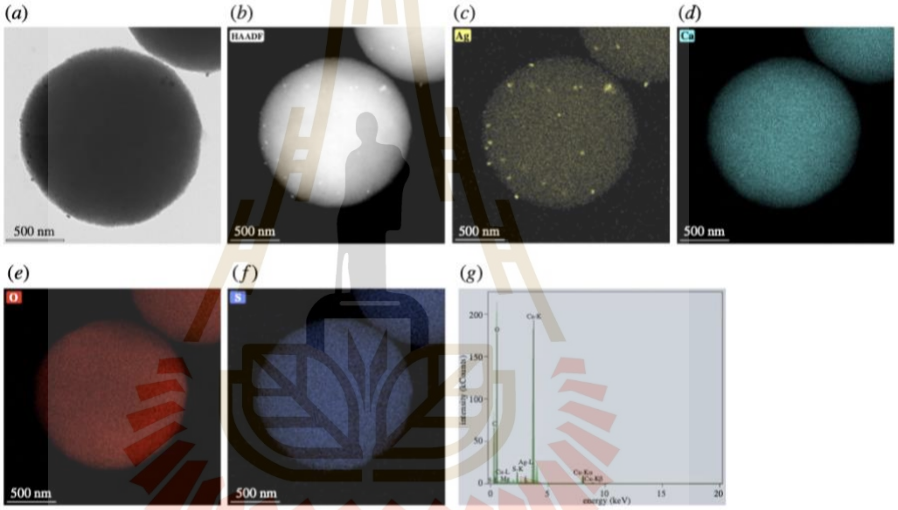

Figure 8. TEM micrograph (*a*), high-angle annular dark-field imaging (HAADF) (*b*), silver (Ag) EDS image mapping (*c*), calcium (Ca) EDS image mapping (*d*), oxygen (O) EDS image mapping (*e*), sulfur (S) EDS image mapping (*f*) and EDX spectrum (*g*) of AgNPs/eCaCO$_3$ particles prepared at 25°C.

structures. The obtained AgNPs/eCaCO$_3$ particles also showed a spherical morphology with a narrow size distribution ranging from 2.39 to 4.15 µm and a mean diameter of 3.56 ± 0.26 µm. One of the factors affecting particle size and distribution of precipitated CaCO$_3$ is crystallization temperature. At high temperature, the crystallization is governed by kinetic factors. Mathawa *et al*. studied crystallization of CaCO$_3$ at 25 and 80° C using polyacrylic acid (PAA) as a stabilizing agent. They stated that when the crystallization was carried out at high temperature, the dissolution of CaCO$_3$ from the surface of growing particles might have occurred, and the secondary crystallization might then be formed. This secondary crystallization resulted in smaller CaCO$_3$ crystals compared with the larger primary crystals [47].

At an ambient temperature of 25°C, the precipitated eCaCO$_3$ particles crystallized homogeneously with a narrow particle size distribution, and they did not form perfect spherical structure like precipitated commercial calcium carbonate particles as shown in figure 9. This is because other compositions of chicken eggshells such as magnesium carbonate (1%) and calcium phosphate (1%) might disturb the crystallization [35].

TEM micrographs, EDS image mapping and EDX spectrum of AgNPs/eCaCO$_3$ prepared at 25°C in figure 8 show that AgNPs are attached to the eggshell calcium carbonate particles. The TEM micrographs

and EDS image mapping in figure 8*a–c* confirm the presence of AgNPs on both the surface and inside of $eCaCO_3$. AgNPs are attached to the whole particle of calcium carbonate resulting in silver content of 0.78 wt% confirmed through EDS mapping element analysis. According to the EDX spectrum shown in figure 8*g*, the particles were composed solely of silver and calcium carbonate and no other impurities were observed. So, AgNPs/$eCaCO_3$ particles prepared at 25°C were further used as antimicrobial agents against food-related bacteria due to their smaller size and narrow distribution.

3.4. Characteristic of silver nanoparticles / commercial calcium carbonate (AgNPs/$CaCO_3$) particles

The morphology, size distribution and XRD pattern of the AgNPs/$CaCO_3$ particles are shown in figure 9*a–d*. According to the SEM micrographs, the AgNPs/$CaCO_3$ particles prepared at 25°C were spherical microparticles with a particle size distribution ranging from 4.15 to 6.95 µm and a mean diameter of 5.61 ± 0.66 µm (figure 9*c*). The particles are dominant in the vaterite crystal structure, as shown in the XRD pattern in figure 9*d*. The spherical shape of the precipitated commercial calcium carbonate was loaded with AgNPs on both the surface and inside of the calcium carbonate particles as shown by the TEM micrographs and EDS image mapping in figure 10*a–c* with a silver content of 3.20 wt%. The EDX spectrum in figure 10*g* confirms that the particles contain only silver and calcium carbonate. Zapotoczny *et al*. prepared AgNPs loaded calcium carbonate particles at 25°C using calcium nitrate and sodium carbonate, resulting in a particle size of 2 µm, in approximation [16]. In this study, AgNPs/$eCaCO_3$ and AgNPs/$CaCO_3$ prepared at 25°C using eggshell and commercial calcium carbonate as a precursor had a mean particle size of 3.56 ± 0.26 µm and 5.61 ± 0.66 µm, respectively.

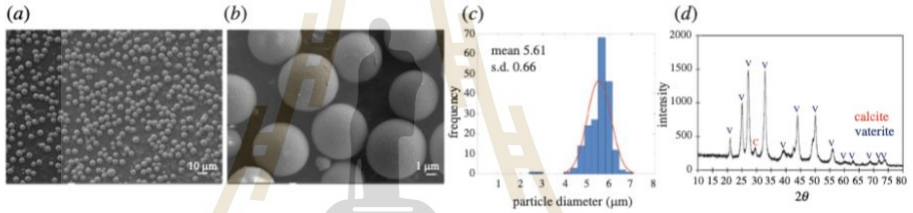

Figure 9. SEM micrographs with magnification of 500× (*a*) and 5k× (*b*), a particle size distribution curve (*c*) and an XRD pattern (*d*) for AgNPs/$CaCO_3$ particles prepared at 25°C.

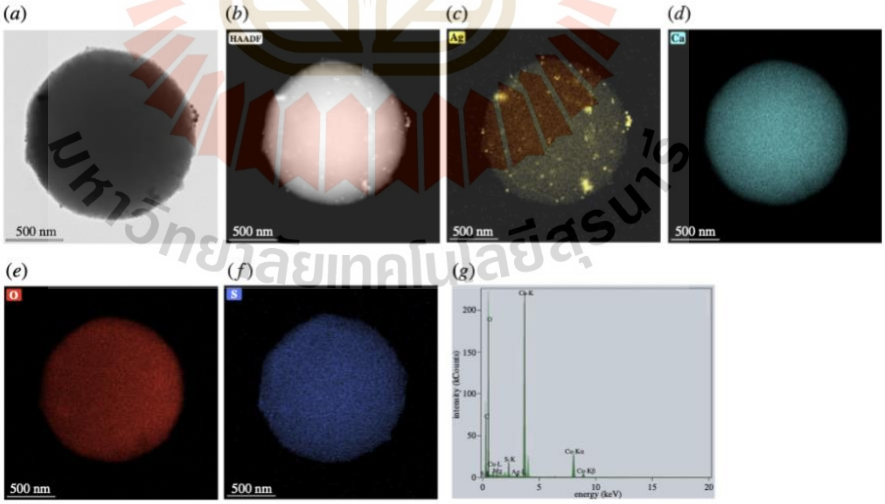

Figure 10. TEM micrograph (*a*), high-angle annular dark-field imaging (HAADF) (*b*), silver (Ag) EDS image mapping (*c*), calcium (Ca) EDS image mapping (*d*), oxygen (O) EDS image mapping (*e*), sulfur (S) EDS image mapping (*f*) and EDX spectrum (*g*) of AgNPs/$CaCO_3$ particles.

Table 1. Silver content, BET specific surface area (S_{BET}), total pore volume (V), and mean pore diameter (d_p) of precipitated $eCaCO_3$, $AgNPs/eCaCO_3$ and $AgNPs/CaCO_3$.

particles	silver content (wt%)	S_{BET} ($m^2\ g^{-1}$)	V ($m^3\ g^{-1}$)	d_p (nm)
precipitated $eCaCO_3$ prepared at 35°C	—	79.77	0.07	3.72
$AgNPs/eCaCO_3$ prepared at 35°C	—	79.25	0.07	3.78
$AgNPs/eCaCO_3$ prepared at 25°C	0.78	85.08	0.07	3.26
$AgNPs/CaCO_3$ prepared at 25°C	3.20	85.85	0.07	3.39

Table 2. Inhibition zone diameter against extracted bacteria from unpacked and vacuum-packed beef using precipitated $eCaCO_3$, freshly prepared silver colloids, $AgNPs/eCaCO_3$ and $AgNPs/CaCO_3$ as antimicrobial agents.

	inhibition zone diameter (mm)					
	unpacked beef-extracted bacteria			vacuum-packed beef extracted bacteria		
samples	500 mg ml^{-1}	250 mg ml^{-1}	125 mg ml^{-1}	500 mg ml^{-1}	250 mg ml^{-1}	125 mg ml^{-1}
precipitated $eCaCO_3$	no effect	no effect	no effect	no effect	no effect	no effect
freshly prepared silver colloids	6.99 ± 0.12	6.77 ± 0.12	6.57 ± 0.19	7.38 ± 0.50	7.17 ± 0.58	7.13 ± 0.33
$AgNPs/eCaCO_3$	8.76 ± 0.26	8.24 ± 0.67	8.98 ± 0.47	10.52 ± 1.06	8.56 ± 0.22	7.44 ± 0.47
$AgNPs/CaCO_3$	8.97 ± 0.49	8.09 ± 0.31	8.27 ± 0.31	10.16 ± 0.80	7.89 ± 0.81	7.45 ± 0.38

The specific surface area, total pore volume and mean pore diameter of precipitated $eCaCO_3$ and $AgNPs/eCaCO_3$ prepared at 35°C were remarkably similar, as shown in table 1. The specific area of the hybrid particles of AgNPs and $CaCO_3$ prepared at 25°C was higher than that prepared at 35°C. At co-precipitation temperature of 25°C, the specific area of $AgNPs/eCaCO_3$ was approximately the same as that of $AgNPs/CaCO_3$. However, the mean pore diameter of the hybrid particles of AgNPs and $CaCO_3$ prepared at 25°C was slightly smaller than that of the particles prepared at 35°C. All particles mentioned in table 2 have the same total pore volume (V) of around 0.07 $m^3\ g^{-1}$ and a mean pore diameter (d_p) in a range of 3.3–3.8 nm.

3.5. Antimicrobial efficiency

As shown in figures 11*a–c* and 12*a–c*, precipitated $eCaCO_3$ (disc 'a') showed no inhibitory effect against bacteria extracted from unpacked beef purchased from the fresh market and vacuum-packed beef of 'MAX BEEF' brand. The freshly prepared silver colloids showed slight antimicrobial activity against the bacteria extracted from the unpacked beef and the vacuum-packed beef with inhibition zone diameters of approximately 7 mm, as observed from disc 'b' in figures 11*a–c* and 12*a–c*, respectively. The antimicrobial efficiency of the silver colloids was lower than that of $AgNPs/eCaCO_3$ and $AgNPs/CaCO_3$. This might be caused by the agglomeration of the silver colloids within the disc, in which the dissolution of Ag^0 or Ag^+ was slower than that of the hybrid particles of $AgNPs/eCaCO_3$ and $AgNPs/CaCO_3$ [26]. Lee *et al*. investigated the antimicrobial activity of AgNPs prepared at different molar ratios using the Kirby–Bauer disc diffusion assay and demonstrated a good inhibitory effect against *Escherichia coli* (*E. coli*) and *Staphylococcus aureus* [48]. The antimicrobial efficiency depends on the particle size, particle size and concentration [18,19], and the degree of agglomeration of nanoparticles [26]. Therefore, the superior antimicrobial activity of $AgNPs/eCaCO_3$ and $AgNPs/CaCO_3$ particles compared with that of the silver colloid was attributed to the reduced agglomeration of AgNPs, giving rise to a better stabilized and sustained release of AgNPs from the $eCaCO_3$ and

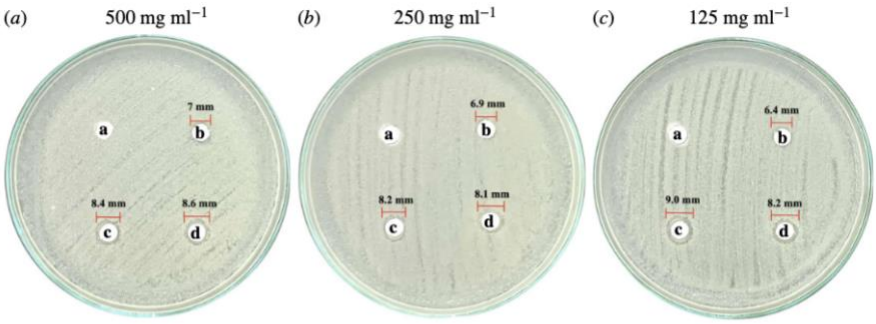

Figure 11. Antimicrobial activity against bacteria extracted from unpacked raw beef from a local fresh market. The discs were impregnated with precipitated $eCaCO_3$ (a), freshly prepared silver colloids (b), AgNPs/$eCaCO_3$ (c), and AgNPs/$CaCO_3$ (d), at concentrations of 500 mg ml^{-1} (*a*), 250 mg ml^{-1} (*b*), and 125 mg ml^{-1} (*c*).

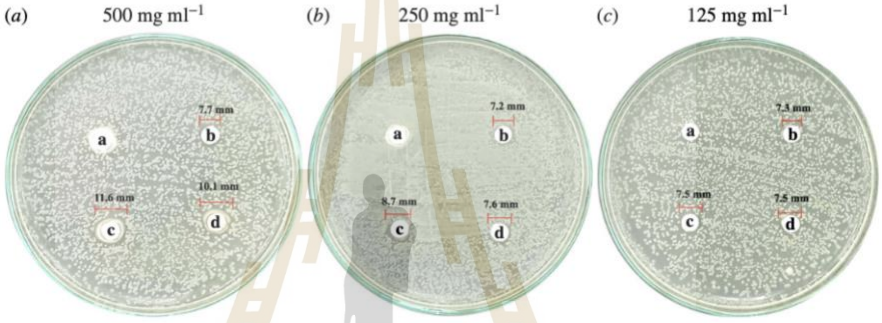

Figure 12. Antimicrobial activity against bacteria extracted from vacuum-packed beef ('MAX BEEF' brand). The discs were impregnated with precipitated $eCaCO_3$ (a), freshly prepared silver colloids (b), AgNPs/$eCaCO_3$ (c), and AgNPs/$CaCO_3$ (d), at concentrations of 500 mg ml^{-1} (*a*), 250 mg ml^{-1} (*b*) and 125 mg ml^{-1} (*c*).

$CaCO_3$ carriers [28]. It was reported that 20 nm AgNPs showed antimicrobial against *Escherichia coli* at MIC (minimum inhibitory concentration) of 0.621 mg ml^{-1} [49]. In addition, 5 nm and 10 nm AgNPs exhibited MIC at 0.625 mg ml^{-1} and 1.35 mg ml^{-1}, respectively, against *Staphylococcus aureus* [50].

In addition, AgNPs/$eCaCO_3$ and AgNPs/$CaCO_3$ showed concentration-independent antimicrobial activity against bacteria extracted from unpacked beef. The diameters of the inhibition zones at 125, 250, and 500 mg ml^{-1} were not significantly different, with an average diameter of 8–9 mm. This suggested that the optimum concentration of AgNPs/$eCaCO_3$ and AgNPs/$CaCO_3$ for inhibiting bacteria growth was 125 mg ml^{-1}. By contrast, AgNPs/$eCaCO_3$ and AgNPs/$CaCO_3$ showed concentration-dependent antimicrobial activity against bacteria extracted from vacuum-packed beef. The average inhibition diameter tended to increase with increasing the hybrid particle concentration.

The Laboratory of Cell-Based Assay and Innovation (CBAI), Suranaree University of Technology, reported that the extract from the unpacked beef contained two types of Gram-negative and one type of Gram-positive bacteria, whereas the extract from the vacuum-packed beef contained one type of Gram-negative and one type of Gram-positive bacteria. The lesser types of extracted bacteria from vacuum-packed beef might be the main effect of concentration-dependent antimicrobial activity against the bacteria of the hybrid particles. However, it could be concluded that the antimicrobial efficiencies of AgNPs/$eCaCO_3$ and AgNPs/$CaCO_3$ against bacteria extracted from unpacked and vacuum-packed beef were comparable.

For the case of AgNPs/$CaCO_3$, Zapotoczny *et al*. studied the antimicrobial activity of AgNPs/$CaCO_3$ microparticles against *Staphylococcus* and *Candida* species and reported that the AgNPs/$CaCO_3$ showed inhibitory effects for those species [16]. Apalangya *et al*. reported that AgNPs/eggshell particles exhibited

superior antimicrobial activity against *Escherichia coli* compared with that of AgNPs [28]. The mentioned reports were in good agreement with the inhibitory effect of the hybrid particles of AgNPs/eCaCO$_3$ and AgNPs against bacteria extracted from beef, as shown in table 2. In addition, Wang *et al*. mentioned that *Pseudomonas fragi*, *Myroides phaeus* and *Brochothrix thermosphacta* were bacteria found in beef [51], and it was reported that *E. coli* was found in raw beef, as well [52].

The summary of the average inhibition zone diameter with standard deviation obtained from precipitated eCaCO$_3$, freshly prepared silver colloids, AgNPs/eCaCO$_3$ and AgNPs/CaCO$_3$, against extracted bacteria from the unpacked and vacuum-packed beef versus testing concentrations are shown in table 2.

4. Conclusion

Spherical AgNPs with an average size of 10–30 nm were successfully prepared by reducing an AgNO$_3$ aqueous solution at 70°C in the presence of trisodium citrate as a reducing agent and stabilizer. The Z-average (r.nm) and PDI are 42.1 nm and 0.2, respectively for freshly prepared silver colloids, and 55.1 and 0.2, respectively for AgNPs. Novel hybrid antimicrobial microspherical particles of AgNPs/eCaCO$_3$ and AgNPs/CaCO$_3$ were successfully prepared via aqueous precipitation in the presence of freshly prepared silver colloids using poly (sodium 4-styrenesulfonate) as a polyelectrolyte. TEM, EDS and EDX confirmed that AgNPs were incorporated into the spherical precipitated CaCO$_3$ from eggshells and commercial calcium carbonate. The crystal polymorph of the precipitated eCaCO$_3$ was vaterite. The hybrid AgNPs/eCaCO$_3$ particles prepared at 25°C had a spherical morphology and a narrow size distribution, with a mean diameter of 3.56 ± 0.26 µm. By contrast, AgNPs/eCaCO$_3$ prepared at 35°C showed a broader size distribution with a mean diameter of 3.19 ± 1.20 µm. In addition, 0.78 wt% and 3.20 wt% AgNPs were deposited onto and inside the microspherical particles of precipitated eggshells and commercial calcium carbonate, respectively. AgNPs/CaCO$_3$ particles prepared at 25°C also had a spherical morphology and a narrow size distribution with a mean diameter of 5.61 ± 0.66 µm. Therefore, eggshells and commercial calcium carbonate can be applied as carriers or supporters for the nanoparticles.

Antimicrobial test showed that both AgNPs/eCaCO$_3$ and AgNPs/CaCO$_3$ particles exhibited the same antimicrobial activity. The hybrid microspherical AgNPs/eCaCO$_3$ and AgNPs/CaCO$_3$ particles inhibited the growth of bacteria extracted from both unpacked and vacuum-packed beef. However, AgNPs/eCaCO$_3$ and AgNPs/CaCO$_3$ showed concentration-dependent antimicrobial activity against bacteria extracted from vacuum-packed beef.

Data accessibility. The supplements supporting this article are available from the Dryad Digital Repository: https://doi.org/10.5281/zenodo.7080849 [53]. The datasets supporting this article are available from the Dryad Digital Repository: https://doi.org/10.5061/dryad.kd51c5b8w [54].

The data are provided in electronic supplementary material [55].

Authors' contributions. M.E.E.Z.: data curation, investigation, visualization, writing—original draft; P.M.: data curation, validation; T.J.: data curation, validation; W.S.: funding acquisition, project administration, supervision, validation, writing—review and editing.

All authors gave final approval for publication and agreed to be held accountable for the work performed therein.

Conflict of interest declaration. We have no competing interests.

Funding. This research was supported by Suranaree University of Technology, Thailand Science Research and Innovation (TSRI) and the National Science, Research, and Innovation Fund (NSRF) for research funding. The grant no. was NRIIS 160344.

Acknowledgements. The authors gratefully acknowledge the Thailand Government Scholarship and the SUT Graduate International Students Scholarship (Vithedbundit). We would also like to thank Suranaree University of Technology, Thailand Science Research, and Innovation (TSRI) and the National Science, Research, and Innovation Fund (NSRF) for research funding. We would like to express our gratitude to Thae Thae Min for her suggestion regarding antimicrobial testing.

References

1. Dizaj SM, Lotfipour F, Barzegar-Jalali M, Zarrintan MH, Adibkia K. 2014 Antimicrobial activity of the metals and metal oxide nanoparticles. *Mater. Sci. Eng. C Mater. Biol. Appl.* **44**, 278–284. (doi:10.1016/j.msec.2014.08.031)
2. Chen J, Li S, Luo J, Wang R, Ding W. 2016 Enhancement of the antibacterial activity of silver nanoparticles against phytopathogenic bacterium *Ralstonia solanacearum* by stabilization. *J. Nanomater.* **2016**, 1–15. (doi:10.1155/2016/7135852)

3. Lara HH, Ayala-Nuñez NV, Ixtepan-Turrent L, Rodriguez-Padilla C. 2010 Mode of antiviral action of silver nanoparticles against HIV-1. *J. Nanobiotechnol.* **8**, 1–10. (doi:10.1186/1477-3155-8-1)
4. Beaudrie CEH, Kandlikar M, Ramachandran G. 2011 Using expert judgment for risk assessment. In *Assessing nanoparticle risks to human health*, 1st edn (ed. G Ramachandran), pp. 109–138. Norwich, NY: William Andrew Publishing. (doi:10.1016/B978-1-4377-7863-2.00005-4)
5. Marambio-Jones C, Hoek EMV. 2010 A review of the antibacterial effects of silver nanomaterials and potential implications for human health and the environment. *J. Nanopart. Res.* **12**, 1531–1551. (doi:10.1007/s11051-010-9900-y)
6. Molleman B, Hiemstra T. 2015 Surface structure of silver nanoparticles as a model for understanding the oxidative dissolution of silver ions. *Langmuir* **31**, 13 361–13 372. (doi:10.1021/acs.langmuir.5b03686)
7. Lee SH, Jun BH. 2019 Silver nanoparticles: synthesis and application for nanomedicine. *Int. J. Mol. Sci.* **20**, 1–24. (doi:10.3390/ijms20040865)
8. Yin IX, Zhang J, Zhao IS, Mei ML, Li Q, Chu CH. 2020 The antibacterial mechanism of silver nanoparticles and its application in dentistry. *Int. J. Nanomedicine.* **15**, 2555–2562. (doi:10.2147/IJN.S246764)
9. Durán N, Nakazato G, Seabra AB. 2016 Antimicrobial activity of biogenic silver nanoparticles, and silver chloride nanoparticles: an overview and comments. *Appl. Microbiol. Biotechnol.* **100**, 6555–6570. (doi:10.1007/s00253-016-7657-7)
10. Xiu ZM, Zhang QB, Puppala HL, Colvin VL, Alvarez PJJ. 2012 Negligible particle-specific antibacterial activity of silver nanoparticle. *Nano Lett.* **12**, 4271–4275. (doi:10.1021/nl301934w)
11. Mavani K, Shah M. 2013 Synthesis of silver nanoparticles by using sodium borohydride as a reducing agent. *Int. J. Eng. Res. Technol.* **2**, 1–5. (doi:10.13140/2.1.3116.8648)
12. Bannea SV, Patil MS, Kulkarni RM, Patil SJ. 2017 Synthesis and characterization of silver nano particles for EDM applications. *Mater. Today: Proc.* **4**, 12 054–12 060. (doi:10.1016/j.matpr.2017.09.130)
13. Ahari H, Karim G, Anvar AA, Pooyamanesh M, Sajadi A, Mostaghim A, Heydari S. 2018 Synthesis of the silver nanoparticle by chemical reduction method and preparation of nanocomposite based on AgNPs\n. In *Proc. of the 4th World Congress on Mechanical, Chemical, and Material Engineering, Madrid, Spain, 16–18 August*.
14. Pillai ZS, Kamat PV. 2003 What factors control the size and shape of silver nanoparticles in the citrate ion reduction method? *J. Phys. Chem.* **108**, 945–951. (doi:10.1021/jp037018r)
15. Rashid MU, Bhuiyan MKH, Quayum ME. 2013 Synthesis of silver nano particles (Ag-NPs) and their uses for quantitative analysis of vitamin C tablets. *J. Pharm. Sci.* **12**, 29–33. (doi:10.3329/dujps.v12i1.16297)
16. Długosz M, Bulwan M, Kania G, Nowakowska M, Zapotoczny S. 2012 Hybrid calcium carbonate/polymer microparticles containing silver nanoparticles as antibacterial agents. *J. Nanopart. Res.* **14**, 1313–1319. (doi:10.1007/s11051-012-1313-7)
17. Truong LB *et al.* 2022 Chapter 8 - Biogenic metal nanomaterials to combat antimicrobial resistance. In *Emerging nanomaterials and nano-based drug delivery approaches to combat antimicrobial resistance* (eds M Saravanan, H Barabadi, E Mostafavi, T Webber), pp. 261–304. Amsterdam, The Netherlands: Elsevier.
18. Barabadi H, Mohammadzadeh A, Vahidi H, Rashedi M, Saravanan M, Talank N, Alizadeh A. 2021 Penicillium chrysogenum-derived silver nanoparticles: exploration of their antibacterial and biofilm inhibitory activity against the standard and pathogenic *Acinetobacter baumannii* compared to tetracycline. *J. Cluster Sci.* **33**, 1929–1942. (doi:10.1007/s10876-021-02121-5)
19. Talank N *et al.* 2022 Bioengineering of green-synthesized silver nanoparticles: *in vitro* physicochemical, antibacterial, biofilm inhibitory, anticoagulant, and antioxidant performance. *Talanta* **243**, 123 374–123 389. (doi:10.1016/j.talanta.2022.123374)
20. Echegoyen Y, Nerín C. 2013 Nanoparticle release from nano-silver antimicrobial food containers. *Food Chem. Toxicol.* **62**, 16–22. (doi:10.1016/j.fct.2013.08.014)
21. Omerović N, Djisalov M, Živojević K, Mladenović M, Vunduk J, Milenković I, Knežević NŽ, Gadjanski I, Vidić J. 2021 Antimicrobial nanoparticles and biodegradable polymer composites for active food packaging applications. *Compr. Rev. Food Sci. Food Saf.* **20**, 2428–2454. (doi:10.1111/1541-4337.12727)
22. Kwiatkowska A, Stachowiak R, Drabik M, Lipko A, Grzeczkowicz A, Marszalik A, Granicka LH. 2022 Composite membrane dressings system with metallic nanoparticles as an antibacterial factor in wound healing. *Membranes* **12**, 1–25. (doi:10.3390/membranes12020215)
23. Kalantari K, Mostafavi E, Afifi AM, Izadiyan Z, Jahangirian H, Rafiee-Moghaddam R, Webster TJ. 2020 Wound dressings functionalized with silver nanoparticles: promises and pitfalls. *Nanoscale* **12**, 2268–2291. (doi:10.1039/c9nr08234d)
24. Dallas P, Sharma VK, Zboril R. 2011 Silver polymeric nanocomposites as advanced antimicrobial agents: classification, synthetic paths, applications, and perspectives. *Adv. Colloid Interface Sci.* **166**, 119–135. (doi:10.1016/j.cis.2011.05.008)
25. Zhang XF, Liu ZG, Shen W, Gurunathan S. 2016 Silver nanoparticles: synthesis, characterization, properties, applications, and therapeutic approaches. *Int. J. Mol. Sci.* **17**, 1–34. (doi:10.3390/ijms17091534)
26. Castro-Mayorga JL, Martínez-Abad A, Fabra MJ, Olivera C, Reis M, Lagarón JM. 2014 Stabilization of antimicrobial silver nanoparticles by a polyhydroxyalkanoate obtained from mixed bacterial culture. *Int. J. Biol. Macromol.* **71**, 103–110. (doi:10.1016/j.ijbiomac.2014.06.059)
27. Wang C, He C, Tong Z, Liu X, Ren B, Zeng F. 2006 Combination of adsorption by porous $CaCO_3$ microparticles and encapsulation by polyelectrolyte multilayer films for sustained drug delivery. *Int. J. Pharm.* **308**, 160–167. (doi:10.1016/j.ijpharm.2005.11.004)
28. Apalangya V, Rangari V, Tiimob B, Jeelani S, Samuel T. 2014 Development of antimicrobial water filtration hybrid material from bio source calcium carbonate and silver nanoparticles. *Appl. Surf. Sci.* **295**, 108–114. (doi:10.1016/j.apsusc.2014.01.012)
29. Lei M, Tang WH, Cao LZ, Li PG, Yu JG. 2006 Effects of poly (sodium 4-styrene-sulfonate) on morphology of calcium carbonate particles. *J. Crystal Growth.* **294**, 358–366. (doi:10.1016/j.jcrysgro.2006.06.029)
30. Boyjoo Y, Pareek VK, Liu J. 2014 Synthesis of micro and nano-sized calcium carbonate particles and their applications. *J. Mater. Chem. A* **2**, 14 270–14 288. (doi:10.1039/c4ta02070g)
31. Hincke MT, Nys Y, Gautron J, Mann K, Rodriguez-Navarro AB, McKee MD. 2012 The eggshell: structure, composition and mineralization. *Front Biosci.* **17**, 1266–1280. (doi:10.2741/3985)
32. Hassan TA, Rangari VK, Rana RK, Jeelani S. 2013 Sonochemical effect on size reduction of $CaCO_3$ nanoparticles derived from waste eggshells. *Ultrason. Sonochem.* **20**, 1308–1315. (doi:10.1016/j.ultsonch.2013.01.016)
33. Kinayturk NK, Tunali B, Altug DT. 2021 Eggshell as a biomaterial can have a sorption capability on its surface: a spectroscopic research. *R. Soc. Open Sci.* **8**, 210100. (doi:10.1098/rsos.210100)
34. Rahn H, Paganelli CV, Ar A. 1987 Pores and gas exchange of avian eggs: a review. *J. Exp. Zool. Suppl.* **1**, 165–172.
35. Tsai WT, Yang JM, Hsu HC, Lin CM, Lin KY, Chiu CH. 2008 Development and characterization of mesoporosity in eggshell ground by planetary ball milling. *Micropor. Mesopor. Mater.* **111**, 379–386. (doi:10.1016/j.micromeso.2007.08.010)
36. Ahmed TAE, Wu L, Younes M, Hincke M. 2021 Biotechnological applications of eggshell: recent advances. *Front. Bioeng. Biotechnol.* **9**, 675364. (doi:10.3389/fbioe.2021.675364)
37. Teamsinsungvon A, Ruksakulpiwat C, Amonpattaratkit P, Ruksakulpiwat Y. 2022 Structural characterization of titanium-silica oxide using synchrotron radiation x-ray absorption spectroscopy. *Polymers (Basel)* **14**, 1–27. (doi:10.3390/polym14132729)
38. Yang D, Zhang B, Liu MH. 2017 A kind of to prepare $CaCO_3$ by template of eggshell meal. The method of Ag composites. State Intellectual Property Office of the People's Republic of China. CN106862585A.
39. Mensah K, Abdelmageed AM, Shokry H. 2022 Effect of eggshell/N,N-dimethylformamide (DMF) mixing ratios on the sonochemical production of $CaCO_3$ nanoparticles. *J. Eng. Appl. Sci.* **69**, 1–12. (doi:10.1186/s44147-022-00070-y)
40. Arif MS, Ulfiya R, Erwin, Panggabean AS. 2021 Synthesis silver nanoparticles using trisodium citrate and development in analysis method. *AIP Conf. Proc.* **2360**, 050007. (doi:10.1063/5.0059493)
41. Ranoszek-Soliwoda K, Tomaszewska E, Socha E, Krzyczmonik P, Ignaczak A, Orlowski P, Krzyzowska M, Celichowski G, Grobelny J. 2017 The role of tannic acid and sodium citrate in the synthesis of silver nanoparticles. *J. Nanopart.*

Res. **19**, 273–288. (doi:10.1007/s11051-017-3973-9)

42. Castro LS, Barañano AG, Pinheiro CJG, Menini L, Pinheiro PF. 2019 Biodiesel production from cotton oil using heterogeneous CaO catalysts from eggshells prepared at different calcination temperatures. *Green Process. Synth.* **8**, 235–244. (doi:10.1515/gps-2018-0076)
43. Sutapun W, Ruksakulpiwat Y, Suppakarn N, Jeencham R, Aontee A. 2011 Characterization of precipitated calcium carbonate from eggshell powder. *Adv. Mater. Res.* **410**, 228–231. (doi:10.4028/www.scientific.net/AMR.410.228)
44. Razali N, Jumadi N, Jalani AY, Kamarulzaman NZ, Pa'ee KF. 2022 Thermal decomposition of calcium carbonate in chicken eggshells: study on temperature and contact time. *Malays. J. Anal. Sci.* **26**, 347–359.
45. Bahrom H *et al.* 2019 Controllable synthesis of calcium carbonate with different geometry: comprehensive analysis of particle formation, cellular uptake, and biocompatibility. *ACS Sustain. Chem. Eng.* **7**, 19 142–19 156. (doi:10.48550/arXiv.2106.15974)
46. Azarian MH, Sutapun W. 2022 Tuning polymorphs of precipitated calcium carbonate from discarded eggshells: effects of polyelectrolyte and salt concentration. *RSC Adv.* **12**, 14 729–14 739. (doi:10.1039/d2ra01673g)
47. Matahwa H, Ramiah V, Sanderson RD. 2008 Calcium carbonate crystallization in the presence of modified polysaccharides and linear polymeric additives. *J. Crystal Growth* **310**, 4561–4569. (doi:10.1016/J.JCRYSGRO.2008.07.089)
48. Lee SM, Song KC, Lee BS. 2010 Antibacterial activity of silver nanoparticles prepared by a chemical reduction method. *Korean J. Chem. Eng.* **27**, 688–692. (doi:10.2478/s11814-010-0067-0)
49. Ashmore D'A *et al.* 2018 Evaluation of E. coli inhibition by plain and polymer-coated silver nanoparticles. *Rev. Inst. Med. Trop. São. Paulo.* **60**, 1–11. (doi:10.1590/s1678-9946201860018)
50. Parvekar P, Palaskar J, Metgud S, Maria R, Dutta S. 2020 The minimum inhibitory concentration (MIC) and minimum bactericidal concentration (MBC) of silver nanoparticles against *Staphylococcus aureus*. *Biomater. Investig. Dent.* **7**, 105–109. (doi:10.1080/26415275.2020.1796674)
51. Wang X, Zhang T, Yang Y, Liu L, Tian T, Zhu D, Ma M, Xie S. 2022 Effects of different storage temperatures on microbial spoilage and bacterial community structure of fresh beef by high-throughput sequencing technology. *Food Sci. Technol.* **43**, 1–5. (doi:10.1590/fst.100522)
52. US Department of Agriculture. 2019 What bacteria are associated with beef?. See https://ask.usda.gov/s/article/What-bacteria-are-associated-with-beef.
53. Zin MEE, Moolkaew P, Junyusen T, Sutapun W. 2023 Code for: Hybrid AgNPs/eggshell calcium carbonate particles and their antimicrobial efficiency. *Zenodo*. (doi:10.5281/zenodo.7080849)
54. Zin MEE, Moolkaew P, Junyusen T, Sutapun W. 2023 Data from: Hybrid AgNPs/eggshell calcium carbonate particles and their antimicrobial efficiency. Dryad Digital Repository. (doi:10.5061/dryad.kd51c5b8w).
55. Zin MEE, Moolkaew P, Junyusen T, Sutapun W. 2023 Preparation of hybrid particles of Ag nanoparticles and eggshell calcium carbonate and their antimicrobial efficiency against beef-extracted bacteria. Figshare. (doi:10.6084/m9.figshare.c.6644155)

IOP Conference Series: Materials Science and Engineering

PAPER · OPEN ACCESS

Study of parameter affecting morphology of electrospun poly (lactic acid) (PLA) fibers loaded with Ag/$CaCO_3$ filler

To cite this article: M E Zin and W Sutapun 2022 *IOP Conf. Ser.: Mater. Sci. Eng.* **1234** 012009

The International Conference on Materials Research and Innovation (ICMARI 2021) IOP Publishing
IOP Conf. Series: Materials Science and Engineering 1234 (2022) 012009 doi:10.1088/1757-899X/1234/1/012009

Study of parameter affecting morphology of electrospun poly (lactic acid) (PLA) fibers loaded with $Ag/CaCO_3$ filler

M E Zin[1,2] and W Sutapun[1,2,*]

[1] School of Polymer Engineering, Institute of Engineering, Suranaree University of Technology, Nakhon Ratchasima 30000, Thailand.
[2] Research Center for Biocomposite Materials for Medical Industry and Agricultural and Food Industry, Suranaree University of Technology, Nakhon Ratchasima 30000, Thailand.

*Corresponding author: wimonlak@sut.ac.th

Silver nanoparticles (AgNPs) are widely used as antimicrobial agent in commercial products like textiles, cosmetics and drugs. AgNPs deposited on the surface of calcium carbonate ($CaCO_3$) particles, serve as sustained release of antimicrobial activity. The silver nanoparticles embedded calcium carbonate particles ($Ag/CaCO_3$) are prepared by a precipitation method. In this study, precipitated ($Ag/CaCO_3$) filler will be used for preparation of $Ag/CaCO_3$-poly(L-lactic acid) ($Ag/CaCO_3$-PLA) nanofibers by electrospinning. Polymer concentration and functional filler amount in binary solvent system will be studied. The condition for fabricating electrospun PLA and $Ag/CaCO_3$-PLA was a 15 cm of collection distance and 15 kV of working voltage. Morphology of $Ag/CaCO_3$ loaded PLA electrospun fibers will be investigated by the field emission scanning electron microscope (FE-SEM). The electrospun fibers will be further applied as the antimicrobial material.

Keywords: PLA, $Ag/CaCO_3$ filler, Electrospinning, Antimicrobial Applications

1. Introduction

Silver nanoparticles (AgNPs) are widely used as antimicrobial agent in health care, food and commercial products like textiles. AgNPs have now been established as an effective biocidal agent and act on a wide range of both gram-negative and gram-positive bacteria [1]. AgNPs incorporated into polymer matrix are currently a popular type of nanocomposite that can provide excellent antimicrobial properties. Antimicrobial nano polymer composite could be applied as packaging films [2]. wound dressing materials [3] and other antimicrobial applications [4,5] according to their outstanding antimicrobial activity. To reduce agglomeration and maintain the nano size of Ag particles, calcium carbonate is one of a good choice as AgNPs carrier for incorporation into polymer matrix [6]. Polylactic acid (PLA) has been widely used in various applications including biomedical applications and packaging because of its biodegradability, biocompatibility and ability to be dissolved in common solvents for processing [7].

Electrospinning is simple and efficient for the fabrication of nano to microscale fibers. The morphology and diameter of the electrospun fibers depend on solution properties, processing and ambient factors [8]. In this research work, the electrospinning was employed to prepare mat of PLA and PLA loading with $Ag/CaCO_3$. Then, effects of PLA solution concentration, applied voltage, solution flow rate and $Ag/CaCO_3$ filler content on morphology of electrospun fibers and distribution of fiber diameter were studied. This research work is preliminary work for further study on application of $Ag/CaCO_3$ for food packaging.

The International Conference on Materials Research and Innovation (ICMARI 2021) IOP Publishing
IOP Conf. Series: Materials Science and Engineering 1234 (2022) 012009 doi:10.1088/1757-899X/1234/1/012009

2. Experimental

The commercial PLA grade (4043D) was purchased from NatureWorks. Chloroform RPE was purchased form Carlo Erba Reagents and acetone was purchased from Thermo Fisher Scientific. Silver nanoparticles loaded calcium carbonate particles ($Ag/CaCO_3$) were prepared by a coprecipitation method mentioned by *S. Zapotoczny* (2012) [6]. The particle size range of the $Ag/CaCO_3$ is around 2 to 5 μm with D(v,0.9) of 4.66 μm. Various concentrations of PLA were prepared with a binary solvent system of chloroform and acetone (chloroform: acetone = 2:1 in volume). The PLA solution with concentrations of 7.5%, 10%, 12.5% and 15% w/v were prepared by stirring at room temperature for 24 hrs using a magnetic stirrer. For preparing $Ag/CaCO_3$ filled PLA nanofibers, only 10% w/v PLA solution with the binary solvent system of chloroform and acetone was employed. Firstly, 3.00 g of PLA was dissolved in 20 mL of chloroform for 22 h and different $Ag/CaCO_3$ contents which were dispersed in 10 mL of acetone were added to the dissolved PLA solution. Then, the mixtures were magnetically stirred at room temperature for 2 h.

Each PLA solution, unfilled and filled, was loaded into a 10 mL plastic syringe (NIPRO syringe), and the needle (inner diameter 0.9 mm) was used for electrospinning. Two flow rates (1 mL/h and 1.5 mL/h) were varied and high voltage of up to 15 kV were applied. Electrospun fibers were collected on a grounded aluminum collector at a distance of 15 cm from the needle tip. The spinning time for pure PLA solutions and $Ag/CaCO_3$ loaded PLA solutions was 30 min and 15 min, respectively. All experiments were performed at about 30°C and relative humidity around 60%. Morphology of electrospun fibers made of pure PLA and $Ag/CaCO_3$ loaded PLA were investigated by the field emission scanning electron microscope (Carl Zeiss, Auriga) using an accelerating voltage of 3.0 kV. Before observation, each sample was coated with a gold sputter coater for 2 min (Neo Coater).

3. Results and Discussion

SEM micrographs in Figure 1 show morphology of the nanofibers electrospun with different PLA concentrations, flow rates and applied voltages. The SEM micrographs show characteristic of porous structure of PLA fibers electrospun from PLA solution with the binary solvent system of chloroform:acetone. The concentration of PLA solution does affect PLA nanofiber morphology and diameter. The micrographs show that smaller fibers with beads were collected from 7.5% w/v PLA solution (Figure 1A-D). The formation of beads indicates insufficient chain entanglements [9]. On increasing PLA concentration to 10%w/v, continuous fibers with various diameter fibers were produced (Figure 1E-H) and uniform fibers were collected at 12.5%w/v PLA solution (Figure 1I-L). At the highest PLA concentration of 15%w/v, electrospun fibers were folded back and forth not randomly oriented as observed from electrospun fiber with lower concentration of PLA solution (Figure 1M-P). Casasola *et al.* [9] have mentioned that increasing polymer concentration results in more chain entanglements, an increase in the solution viscosity. As a result, hence an increase in the viscoelastic force will be increased and will counterbalance the Coulombic stretching force. Therefore, it results in continuous fibers with fewer beads.

Uniform electrospun nanofibers in size could be prepared via a critical flow rate of a polymeric solution. At higher flow rate of 1.5 mL/h, fibers with larger diameter were produced comparing to the prepared fiber with lower flow rate of 1 mL/h. Increasing flow rate beyond a critical value not only leads to increase in the pore size and fiber diameter but also bead formation. This might be due to incomplete drying of the nanofiber jet during the flight between the needle tip and metallic collector [10]. Upon concerning applied voltage, smaller diameter of fibers was produced at higher applied voltage of 18kV compared to produced fibers at 15kV, as shown in Figure 1. The formation of smaller diameter nanofibers with an increase in the applied voltage is attributed to the stretching of the polymer solution in correlation with the charge repulsion within the polymer jet [10].

SEM micrographs in Figure 2 show electrospun fibers obtained from PLA solutions filled with 1 and 3% w/v $Ag/CaCO_3$ using 1 mL/h flow rate, and 18 and 20 kV applied voltages. At 1%w/v $Ag/CaCO_3$ loading, the electrospun filled PLA fibers contained some particles blooming along the fiber, as shown in Figure 2(A) and 2(B). However, with 3%w/v $Ag/CaCO_3$ loading, the electrospun fiber comparatively contained more particle blooming along the fiber due to higher degree of the local particle agglomeration

The International Conference on Materials Research and Innovation (ICMARI 2021) IOP Publishing
IOP Conf. Series: Materials Science and Engineering 1234 (2022) 012009 doi:10.1088/1757-899X/1234/1/012009

during electrospinning process, as illustrated in Figure 2(C) and 2(D). The local particle agglomeration might be caused by heterogeneous distribution of the particles in PLA solutions during electrospinning.

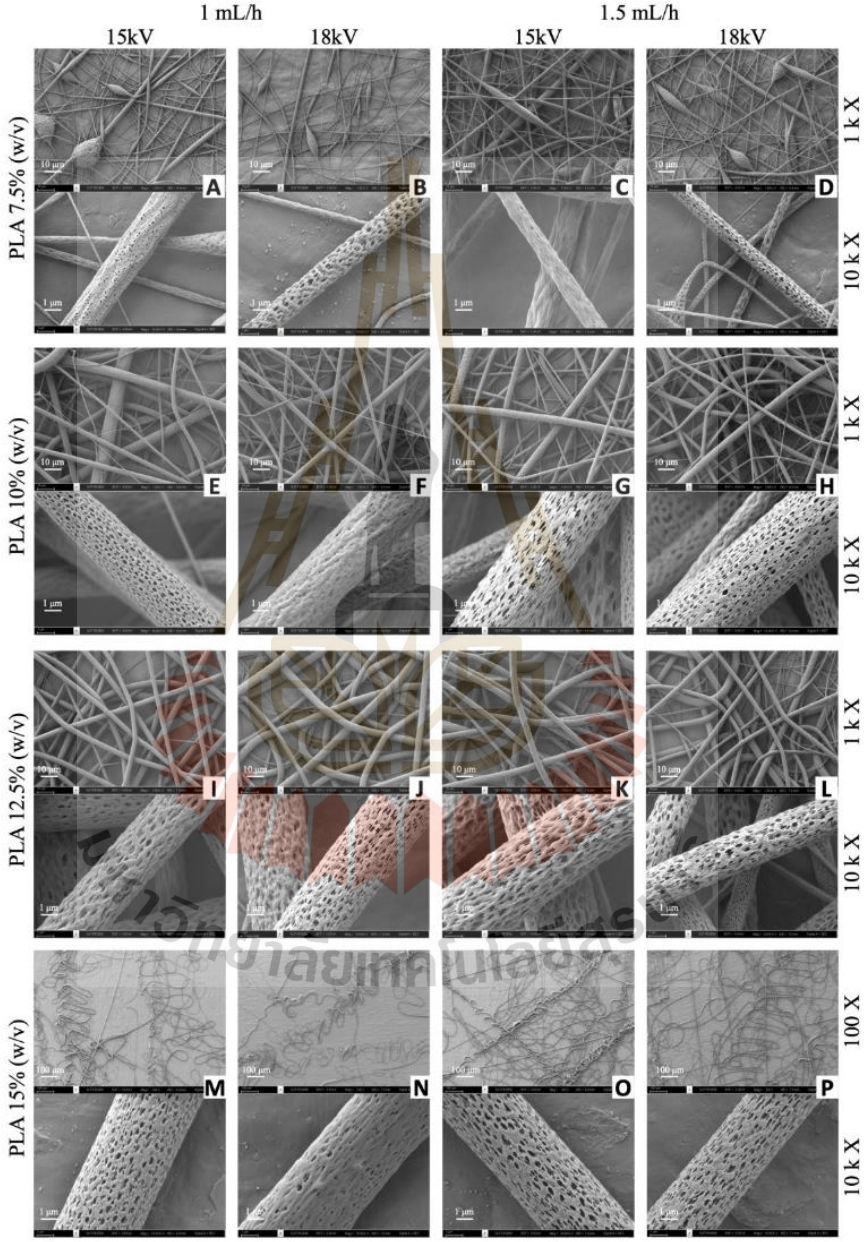

Figure 1. SEM micrographs of electrospun PLA fiber prepared from various concentrations, flow rates of 1 and 1.5 mL/h, and applied voltages of 15 and 18 kV.

The International Conference on Materials Research and Innovation (ICMARI 2021) IOP Publishing
IOP Conf. Series: Materials Science and Engineering 1234 (2022) 012009 doi:10.1088/1757-899X/1234/1/012009

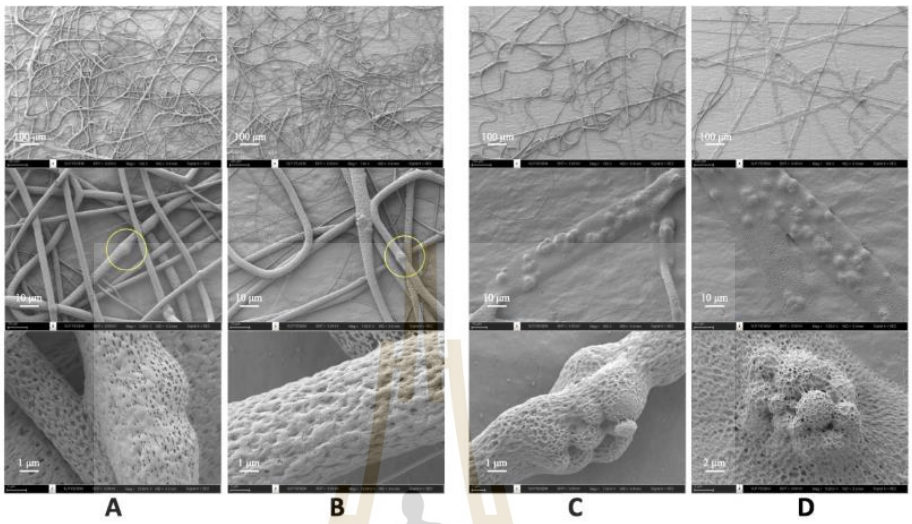

Figure 2. SEM micrographs of the electrospun filled PLA fiber with 1% (w/v) $Ag/CaCO_3$ at 1 mL/h and 18 kV (A), and 1mL/h and 20 kV (B); and 3% (w/v) $Ag/CaCO_3$ at 1 mL/h and 18 kV (C), and 1mL/h and 20 kV (D).

4. Conclusions

Highly porous fibers were prepared by electrospinning from pure PLA solution. PLA solutions of 10 and 15%w/v concentrations would give rise to electrospun continuous fibers without beads. Larger diameter electrospun fibers were obtained at higher flow rate of 1.5 mL/h and applying higher voltage of 18 kV resulted in smaller diameter fibers than applying lower voltage. PLA electrospun fibers filled with 1%w/v $Ag/CaCO_3$ contained some particles blooming along the fiber however, more particle blooming and nonuniform shape were observed from the electrospun fibers filled with 3%w/v $Ag/CaCO_3$. The electrospun fibers obtained from 1%w/v $Ag/CaCO_3$ loading with applied voltage of 20 kV were more uniform in shape.

Acknowledgement

The authors gratefully acknowledge the financial support from Thailand Government Scholarship, SUT Graduate International Students Scholarship (Vithedbundit), and Thailand Science Research and Innovation (TSRI). In addition, we would like to express our gratitude to Associate Prof. Yupaporn Ruksakulpiwat and Assistant Prof. Piya-on Numpaisal for providing electrospinning instrument.

References

[1] Alven, S., Buyana, B., Feketshane, Z., & Aderibigbe, B. A. (2021).*Pharmaceutics, 13*(7). doi:10.3390/pharmaceutics13070964
[2] Casasola, R., Thomas, N. L., Trybala, A., & Georgiadou, S. (2014). *Polymer, 55*(18), 4728-4737. doi:10.1016/j.polymer.2014.06.032
[3] Dlugosz, M., Bulwan, M., Kania, G., Nowakowska, M., & Zapotoczny, S. (2012). *J Nanopart Res, 14*(12), 1313. doi:10.1007/s11051-012-1313-7
[4] Gu, Shu-Ying, & Ren, Jie. (2005). *Macromolecular Materials and Engineering, 290*(11), 1097-1105. doi:10.1002/mame.200500215
[5] Haider, Adnan, Haider, Sajjad, & Kang, Inn-Kyu. (2018). *Arabian Journal of Chemistry, 11*(8), 1165-1188. doi:10.1016/j.arabjc.2015.11.015
[6] Mahapatra, A., Garg, Nidhi, Nayak, B. P., Mishra, B. G., & Hota, G. (2012). *Journal of Applied Polymer Science, 124*(2), 1178-1185. doi:10.1002/app.35076

[7] Pan, Shu-Fang, Ke, Xiao-Xue, Wang, Ting-Yu, Liu, Qing, Zhong, Lu-Bin, & Zheng, Yu-Ming. (2018). *Industrial & Engineering Chemistry Research, 58*(2), 984-993. doi:10.1021/acs.iecr.8b04893
[8] Promnil, Siripanyo, Numpaisal, Piya-on, & Ruksakulpiwat, Yupaporn. (2021). *Materials Today: Proceedings, 47*, 3496-3499. doi:10.1016/j.matpr.2021.03.504
[9] Sadasivuni, Kishor Kumar, Rattan, Sunita, Waseem, Sadiya, Brahme, Snehal Kargirwar, Kondawar, Subhash B., Ghosh, S., Mazumdar, Payal. (2019). In *Polymer Nanocomposites in Biomedical Engineering* (pp. 331-373).
[10] Wang, Wei, Yu, Zhilong, Alsammarraie, Fouad K., Kong, Fanbin, Lin, Mengshi, & Mustapha, Azlin. (2020). *Food Hydrocolloids, 100*. doi:10.1016/j.foodhyd.2019.105411

BIOGRAPHY

Miss Moe Ei Ei Zin was born on August 6, 1995 in Mandalay, Union of Myanmar. She obtained Bachelor of Engineering in Materials and Metallurgy from University of Technology (Yatanarpon Cyber City), Myanmar in 2016. She has continued her study for master degree in Materials Engineering at School of Polymer Engineering, Institute of Engineering, Suranaree University of Technology (SUT), Thailand, since 2018. During her master study at SUT, she attended as oral presenter 2 International Conferences, 3rd International Conference on Materials Research and Innovation (ICMARI 2021) and, 37th International Conference of the Polymer Processing Society. Furthermore, she has published with her thesis adviser 1 article entitled "Preparation of hybrid particles of Ag nanoparticles and eggshell calcium carbonate and their antimicrobial efficiency against beef- extracted bacteria" in Tier 1 journal, Royal Society of Open Science.